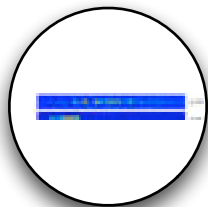
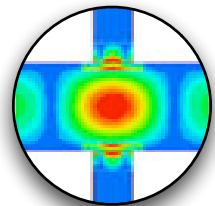
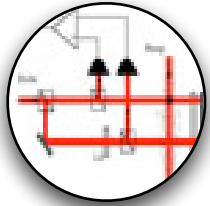


CHAPTER 4
LASER-COOLED
ATOM PHYSICS



Electrostatic Focusing of Laser-Cooled Atoms

Juris G. Kalnins, Glen Lambertson, and Harvey Gould
Lawrence Berkeley National Laboratory
Berkeley, CA 94720

Neutral atoms can be transported and focused by a sequence of electric fields having gradients that alternately focus in one transverse direction while defocusing in the other. Efficient electrostatic transport and focusing of atoms has been difficult to realize in practice because commonly used cylindrical lenses contain strong electric multipoles of all odd orders. This limits the linear region of the lens to a small fraction of the available area. Nonlinearities result in loss of beam, generation of beam halo, and growth in the transverse emittance producing larger beam sizes.

We show how to design electrostatic lenses containing only dipole and sextupole components (and a small decapole contribution) resulting in lenses that have a large linear region [1]. These lenses can be combined to transport laser-cooled atoms over nearly unlimited distances and to focus them.

The applications are in atomic clocks in space, manipulating Bose Einstein condensates, and electron electric dipole moment experiments.

Work supported by the U.S. DOE under contract DE-AC-76SF00098.

[1] J.G. Kalnins, G. Lambertson, and H. Gould, "Improved alternating gradient transport and focusing of neutral molecules," accepted for publication in Rev. Sci. Instr. (<http://arXiv.org/abs/physics/0112073>).

Measurement of G
with an atom interferometer based gravity gradiometer

Greg Foster

Jeff Fixler

Mark Kasevich

Yale University

G Motivation

Scientific:

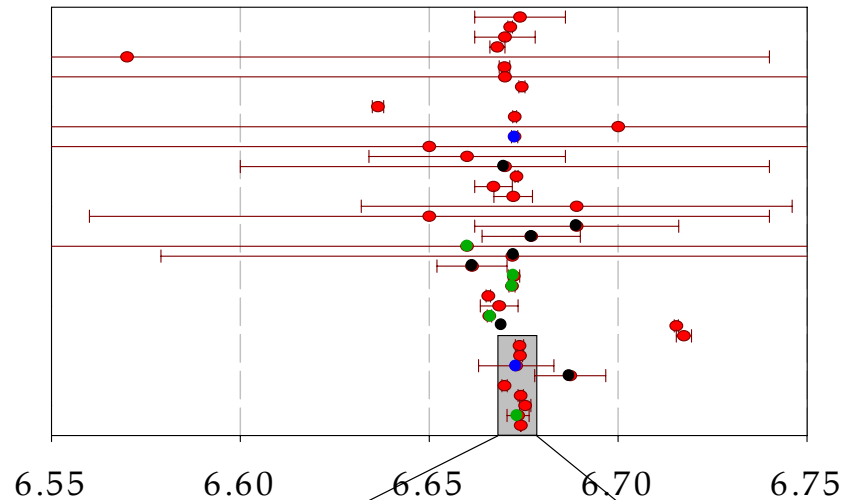
- Newtonian gravitational constant not well known.
- Probe gravity with quantum mechanical system.
- Verify atom interferometry theory

Technical:

- Establish laboratory measurement of instrument accuracy
- Characterize instrument systematic responses

Recent G measurements

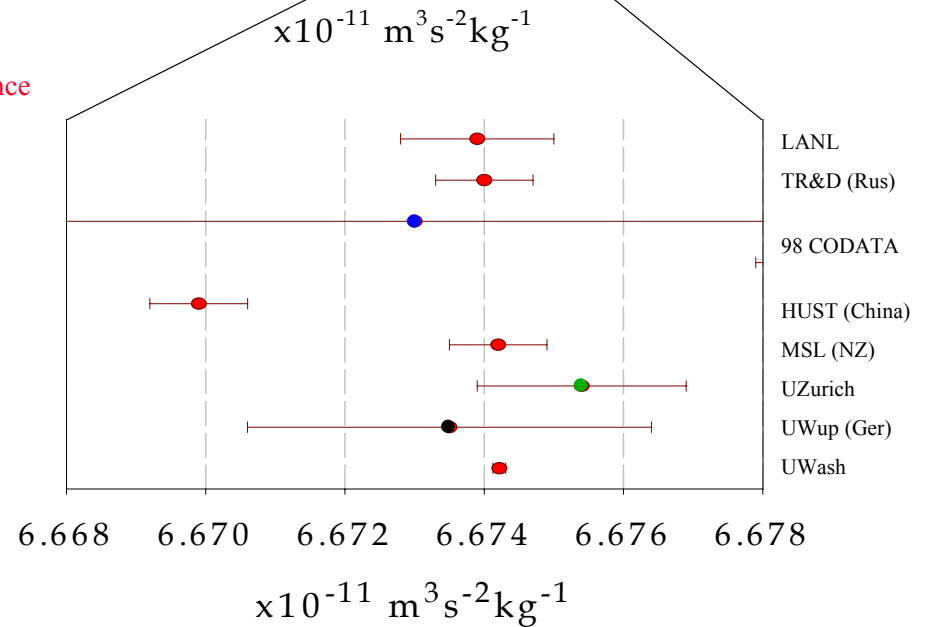
G measurements since 1969



- CODATA
- Torsion Balance
- Fabry-Perot
- Other

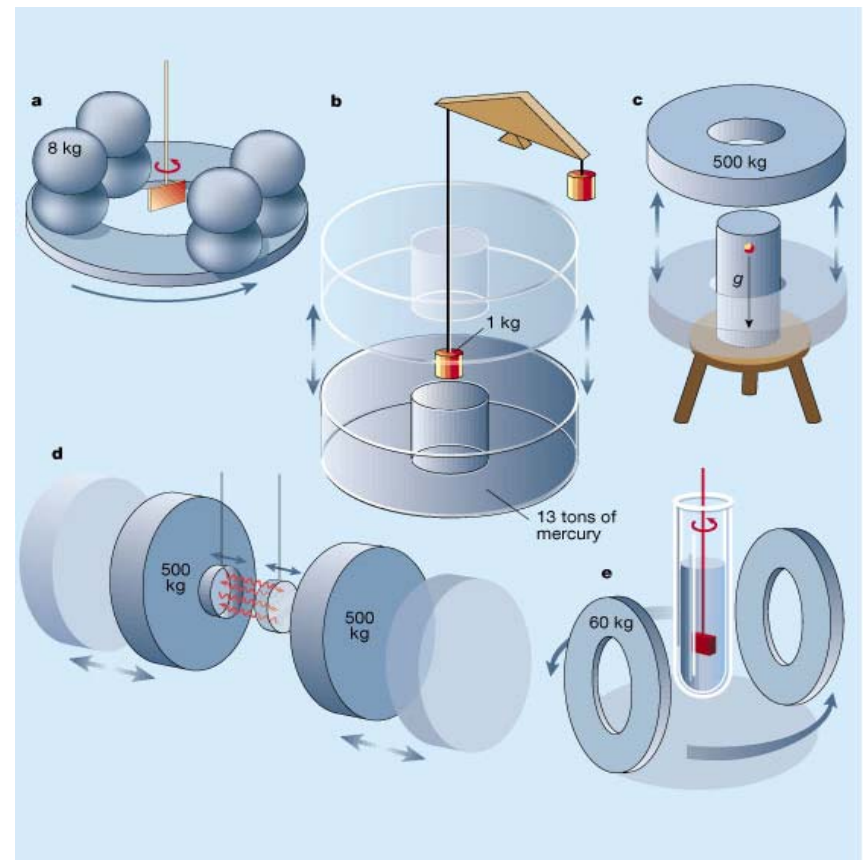
CODATA G =

$$(6.673 \pm 0.010) \times 10^{-11} \text{ m}^3 \text{ kg}^{-1} \text{ s}^{-2}$$



G measurements

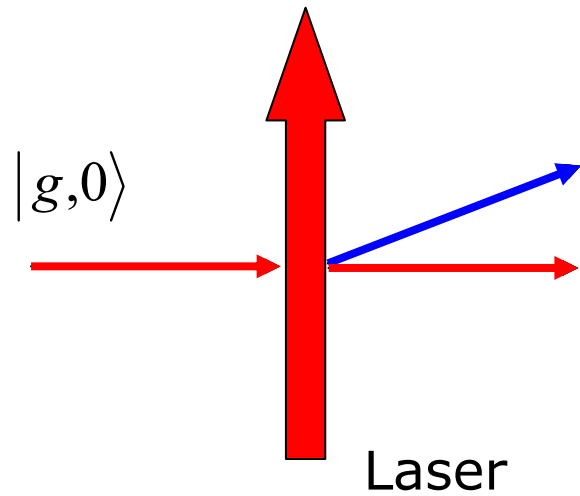
- Classical Techniques:
 - Macroscopic/Mechanical Test Mass
 - Torsion Balance
 - Optical Resonator
 - Falling Cornercube
- Atom Interferometer
 - Microscopic test mass
 - Quantum mechanical system
 - Absolute accuracy
 - Different Systematics



Nature **408**, 920 (2000)

Light Pulse Atom optics

Photon recoil for atom optical elements.



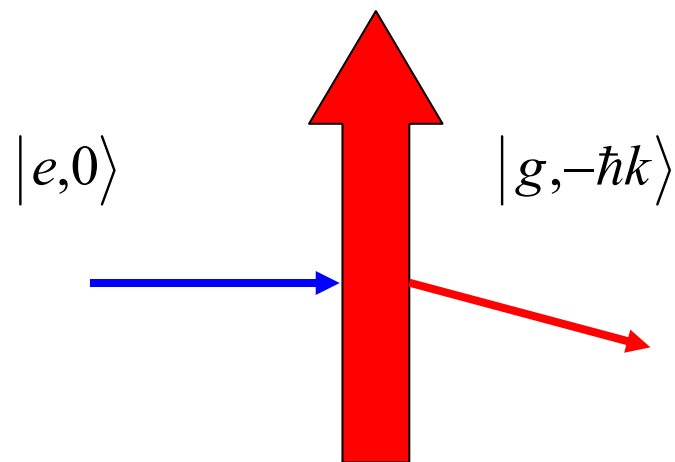
$$\left(|g,0\rangle + |e,\hbar k\rangle \right) / \sqrt{2}$$

Beam Splitter

$|e\rangle$ —————

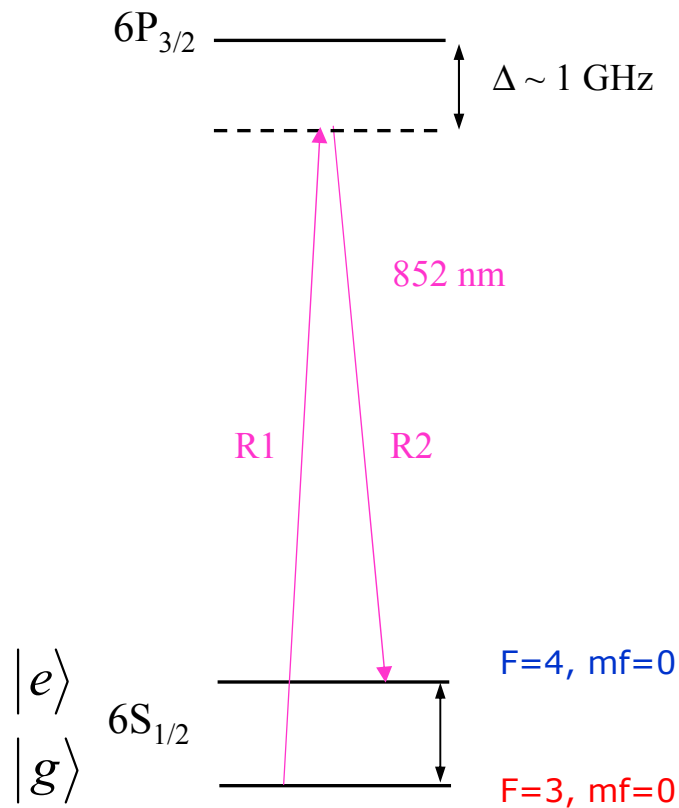
$|g\rangle$ —————

Mirror



Atom Optics Implementation

Connect Cs hyperfine ground states with two photons



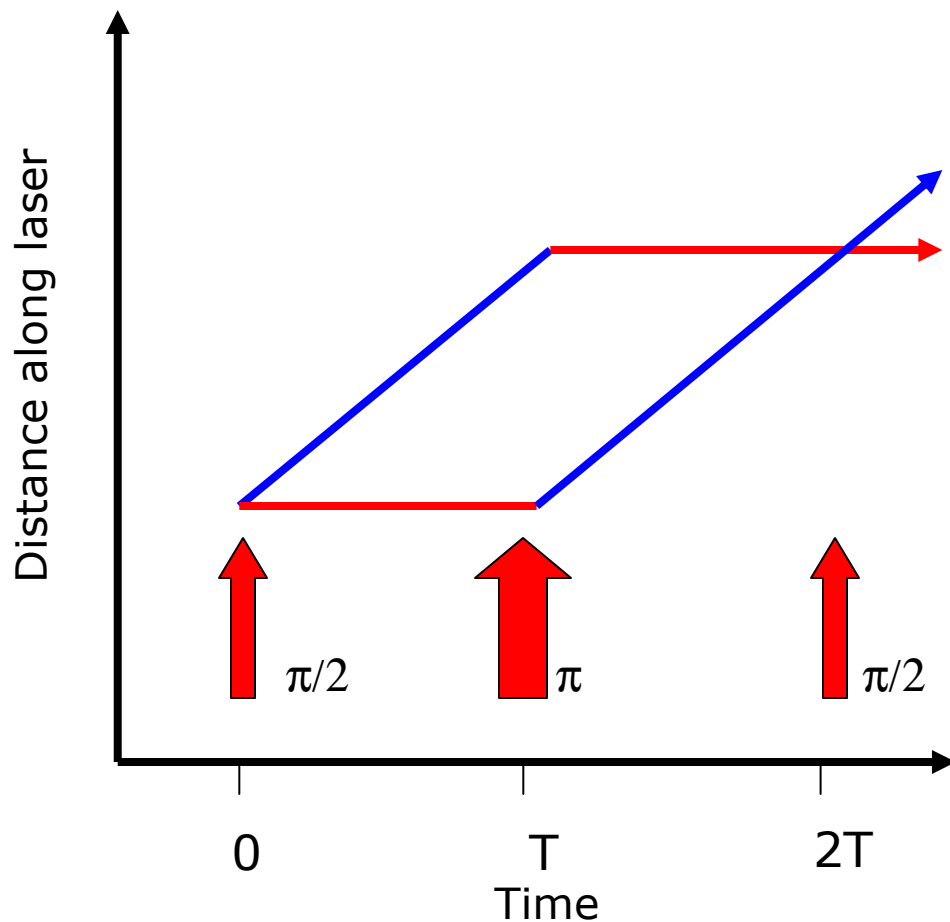
Atom/Light interaction encodes light phase:

$$|g\rangle \rightarrow e^{i\phi} |e\rangle \quad |e\rangle \rightarrow e^{-i\phi} |g\rangle$$

$$\phi = \vec{k} \cdot \vec{r}$$

Atom Interferometer

$\pi/2 - \pi - \pi/2$ light pulse sequence:



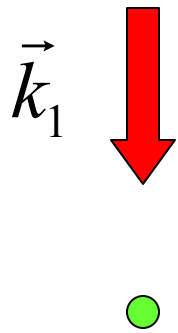
$$\Delta\Phi = \phi_1 - 2\phi_2 + \phi_3$$

Readout:

Phase shift of atomic internal state population fringe.

Gravimeter

Uniform acceleration

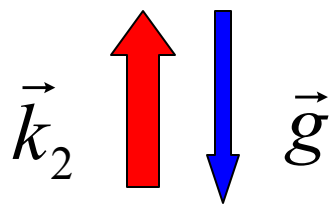


$$\Delta\Phi_{total} = \vec{k}_{eff} \cdot \vec{g} T^2$$

$$k_{eff} = k_1 - k_2 \approx 2(2\pi/\lambda)$$

Gravity gradients -

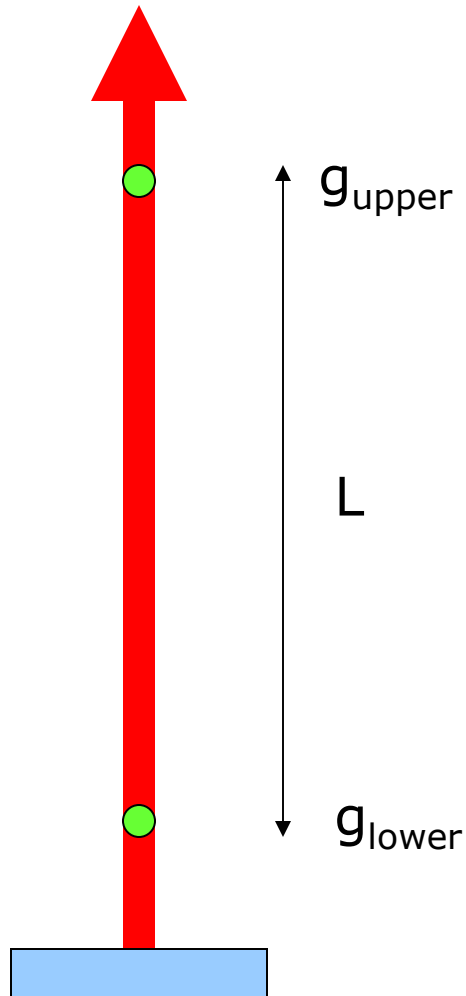
Consider wave packet propagation.



gravimeter

Absolute accuracy λ_{Cs}

Gradiometry



Equivalence Principle \rightarrow
Cannot distinguish between
platform vibrations and gravity.

Make differential acceleration
measurements to resolve
gravity gradient T_{ij} and reject
vibrations.

$$T_{zz} = (g_{\text{upper}} - g_{\text{lower}}) / L$$

\rightarrow *Gradiometers are of high interest for moving platform applications.*

Applications

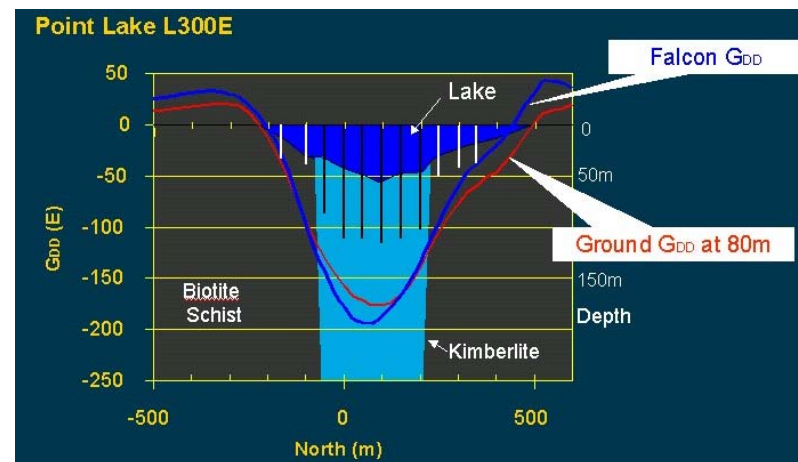
- Gravity-assisted navigation
 - Map-matching
 - Terrain estimation
 - INS limited by gravitational uncertainties
- Remote sensing



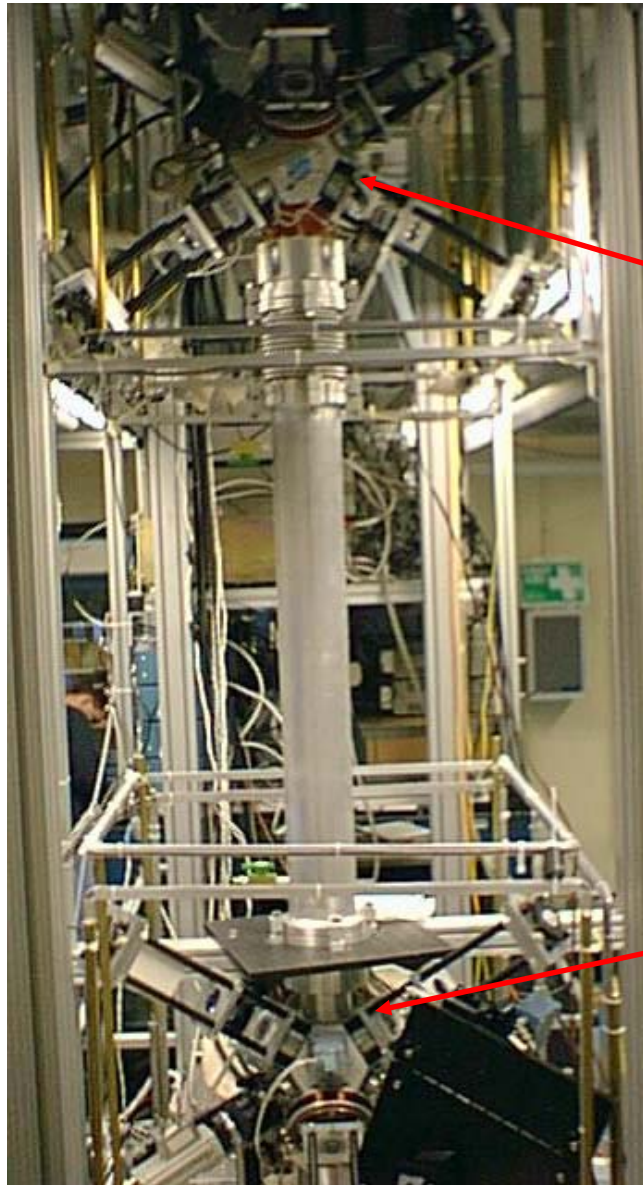
SSBN US Navy



BHP Falcon GG

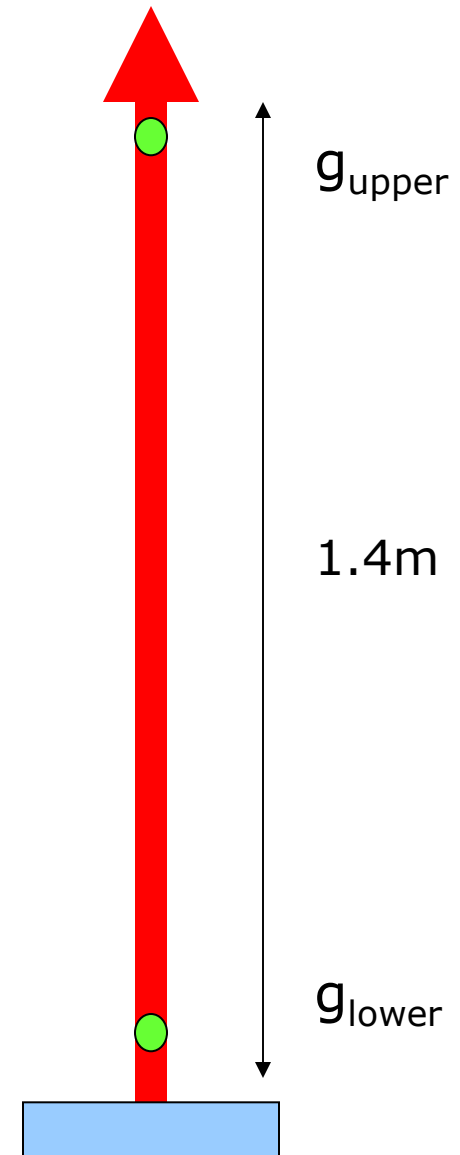


Yale Gradiometer



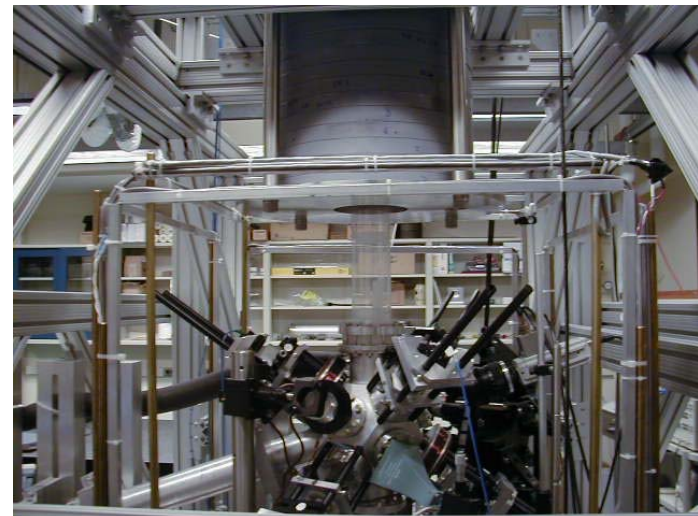
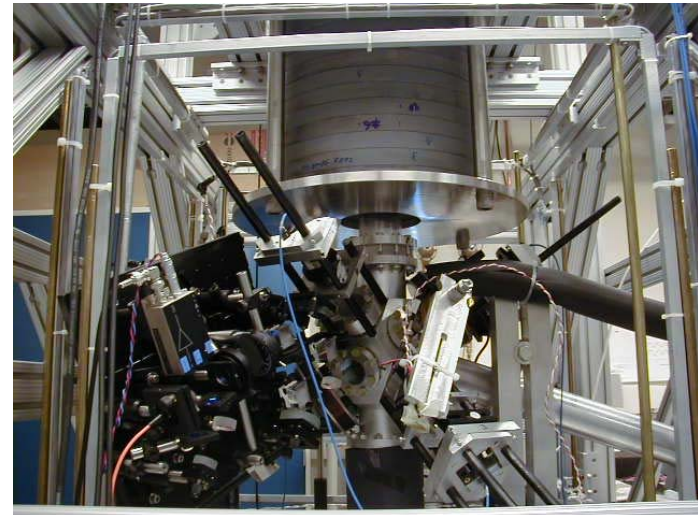
Upper
Magneto-Optical
Trap (MOT)

Lower MOT



Measurement

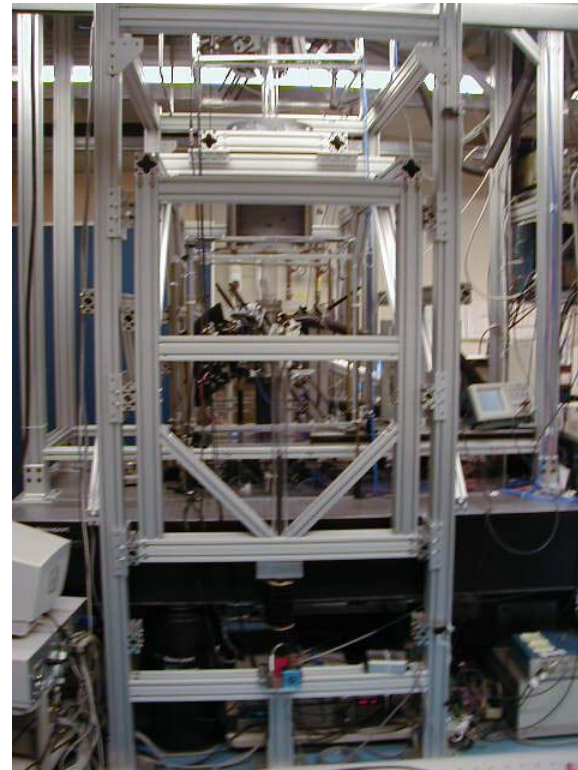
- Measure gravity gradient from 530 kg Pb source mass.
- Calculate gradient signal from measured source geometry and atomic trajectories.
- Determine G from fit of model to measured phase shifts.
- Exploit differential measurements.



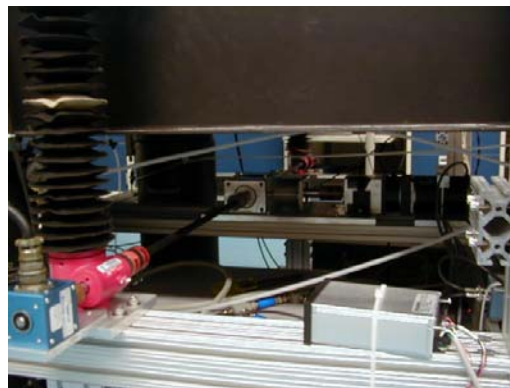
Lifter assembly



Testing

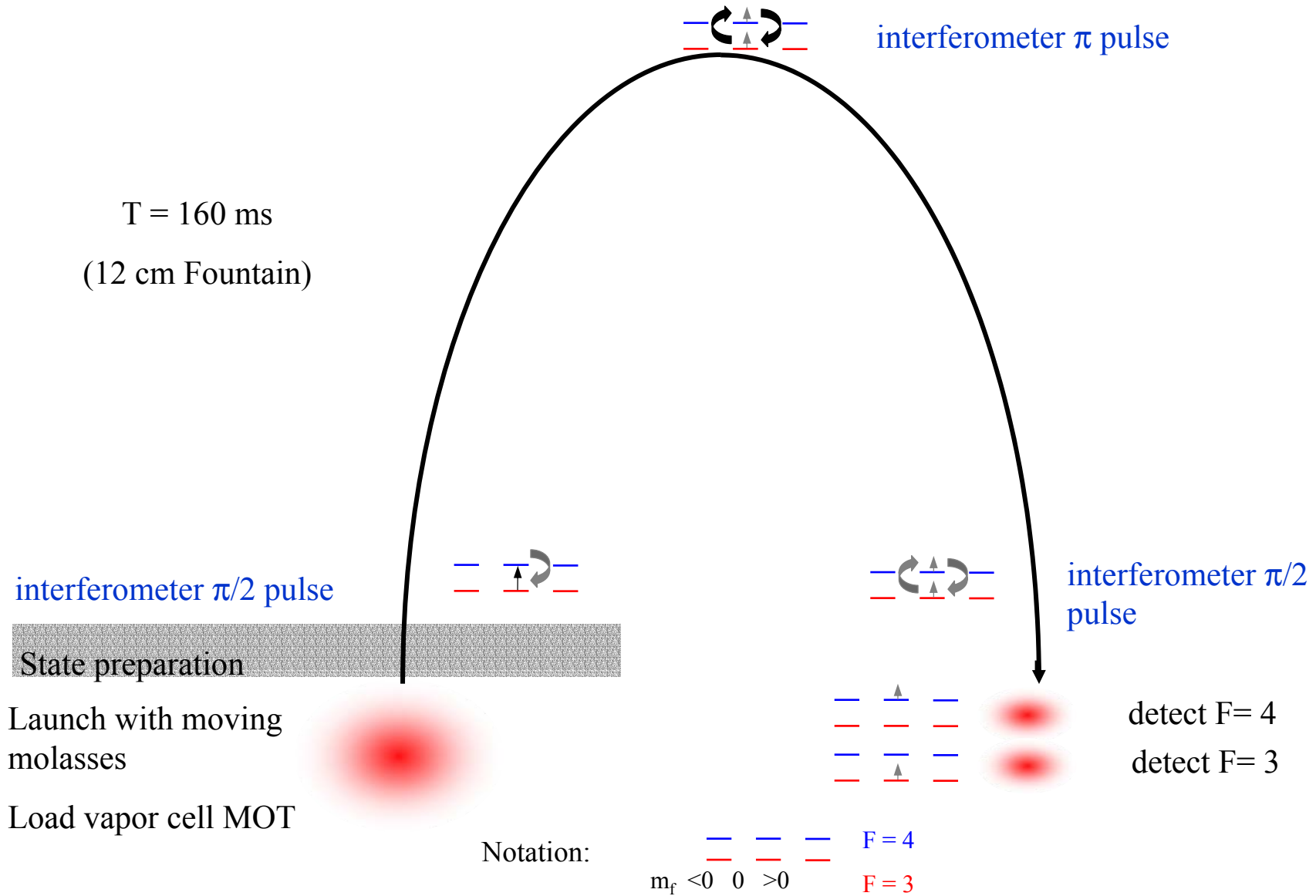


Operation



Lifter Drive

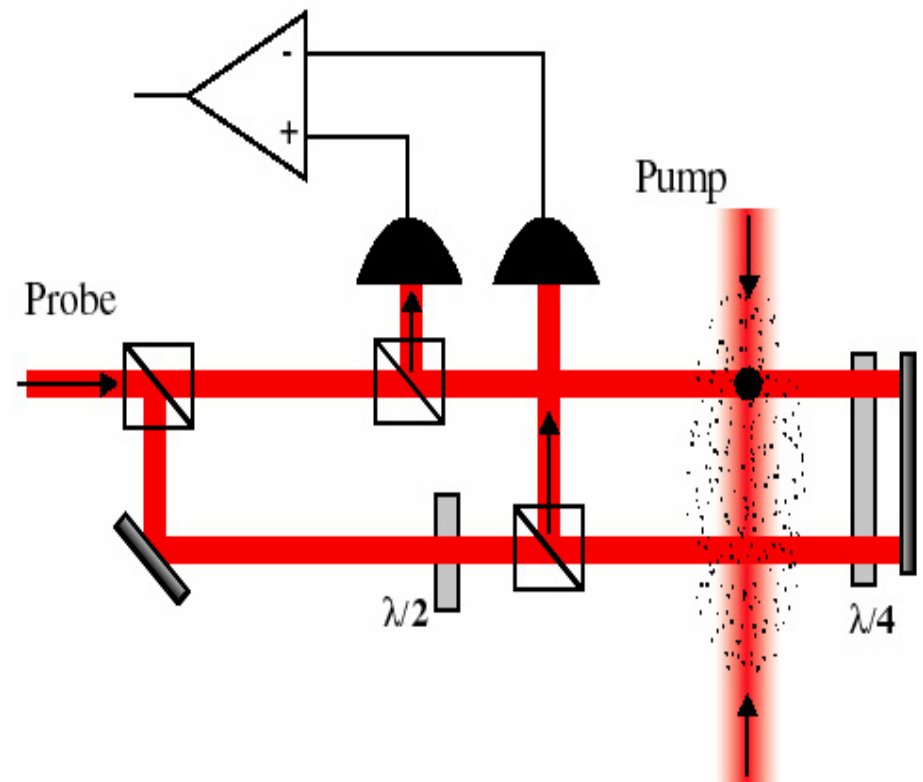
Experimental Sequence



Detection

- Balanced modulation spectroscopy
- Normalize atom number fluctuations by detecting both states.
- Atom Shot noise limited detection demonstrated

$$P_{(F=4)} = \frac{1}{2} (1 - \cos \Delta\Phi_{tot})$$



Ellipse Analysis

- 3×10^{-7} g acceleration of reference mirror will cause ~ 1 rad phase noise
- Take advantage of common mode gravimeter signals:

$$X = A \sin(\theta) + C$$

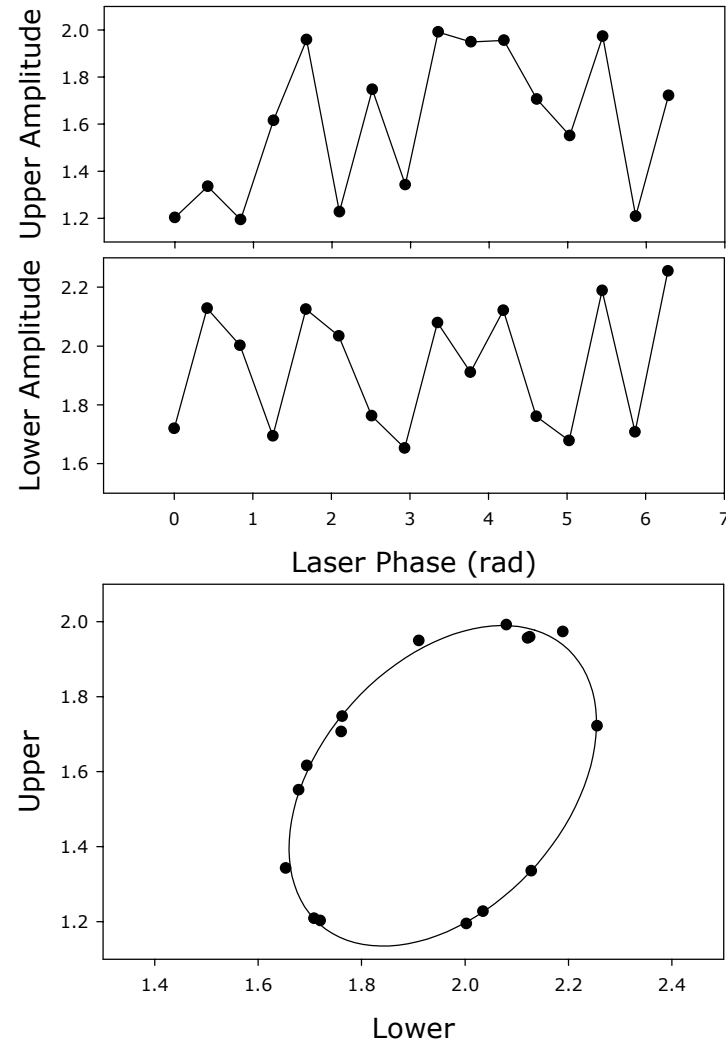
$$Y = B \sin(\theta + d\phi) + D$$

→ Describes an ellipse

$$A'x^2 + B'xy + C'y^2 + D'x + E'y + F' = 0 \quad d\phi = \cos^{-1}\left(\frac{-B'}{2\sqrt{A'C'}}\right)$$

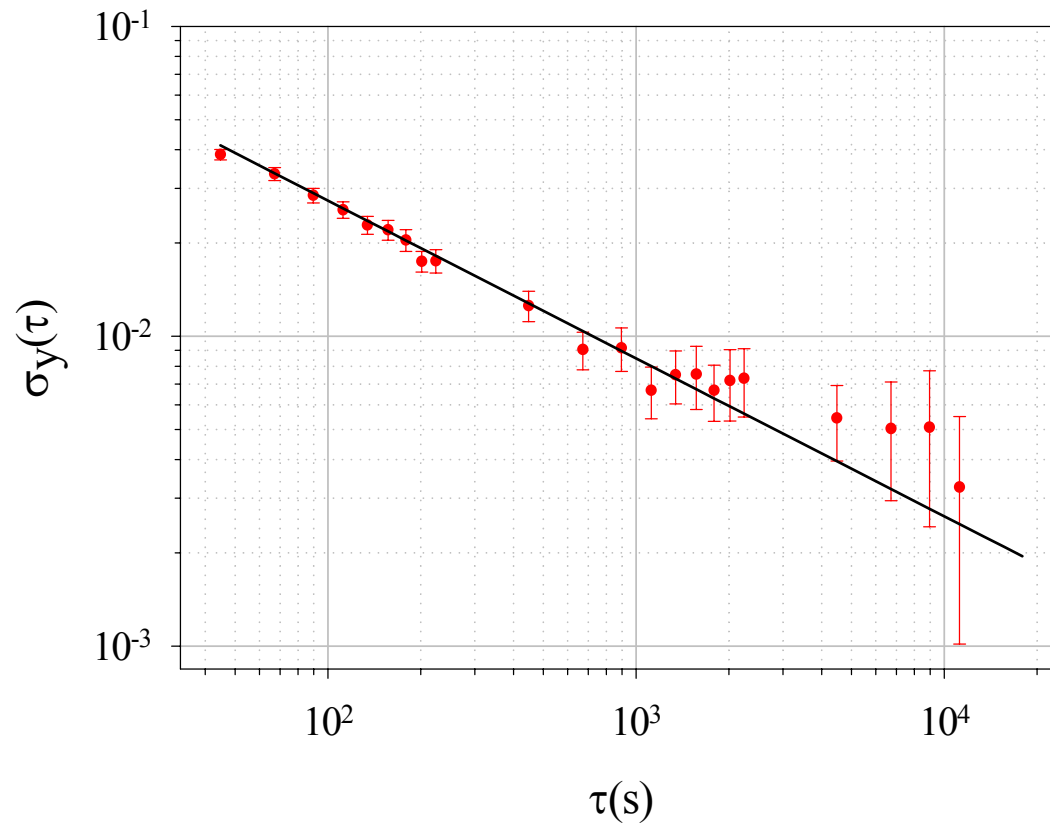
Use ellipse-specific fitting routine

Immunity to common mode phase noise for measuring gradient.



Stability

Measuring Earth gradient



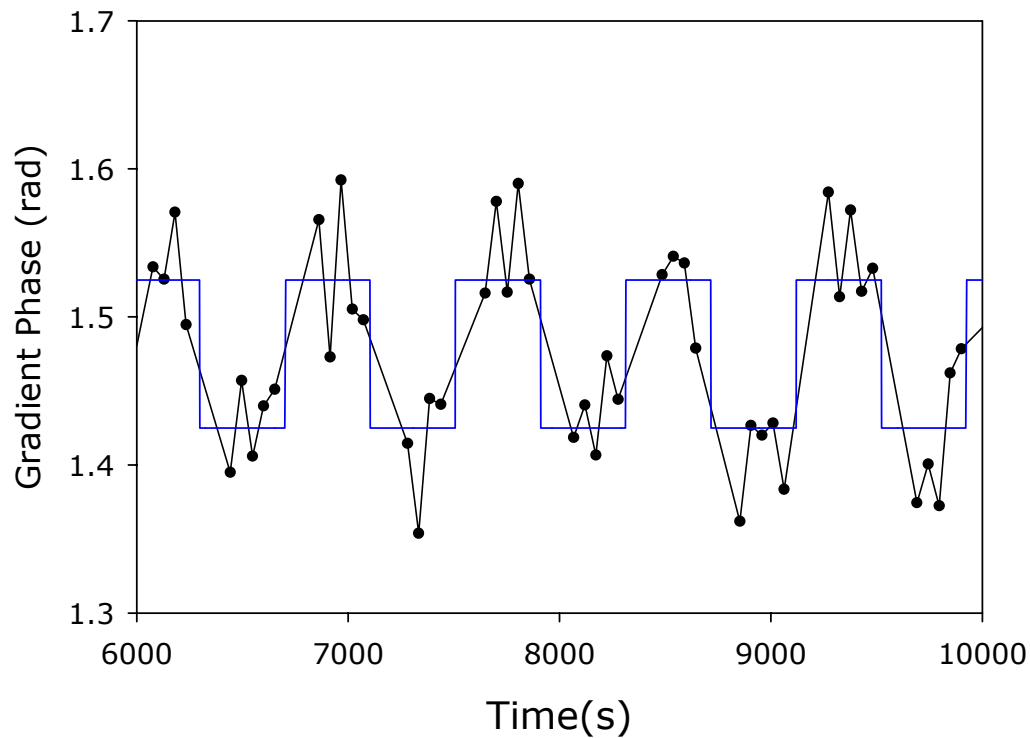
*Typical differential
acceleration sensitivity:*

$$\sim 1.8 \times 10^{-8} \text{ g/Hz}^{1/2}$$

*$\sim 1.3 \times 10^{-8} \text{ g/Hz}^{1/2}$ per
accelerometer*

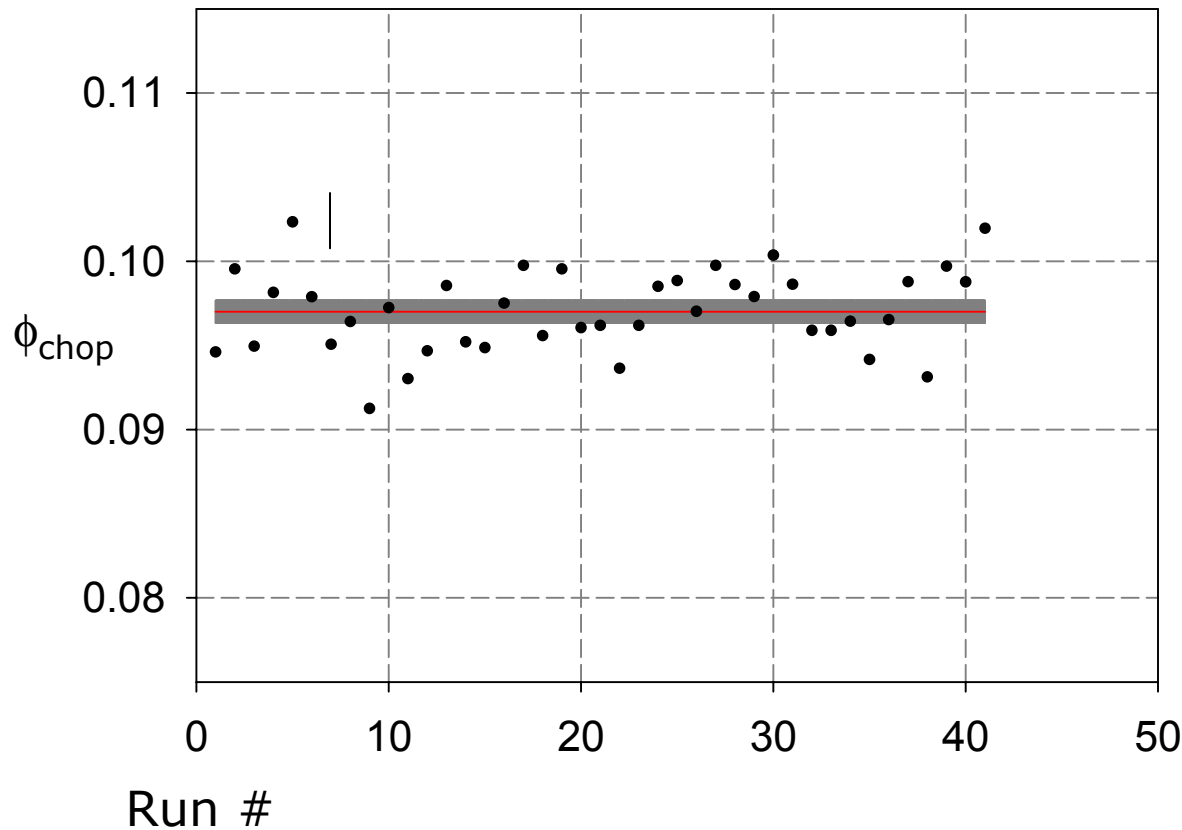
Typical Data

- Translate Pb Source vertically to modulate signal



*Typical chop signal:
~ 3×10^{-8} g change in
acceleration due to
gravitational forces for
different Pb positions*

Measurement of G



41 data sets
~ 1 Month

$$\delta G = 3.7 \times 10^{-3} \text{ G}$$

*Measurement
consistent with
accepted value*

$$(6.657 \pm 0.025) \times 10^{-11} \text{ m}^3 \text{ kg}^{-1} \text{ s}^{-2}$$

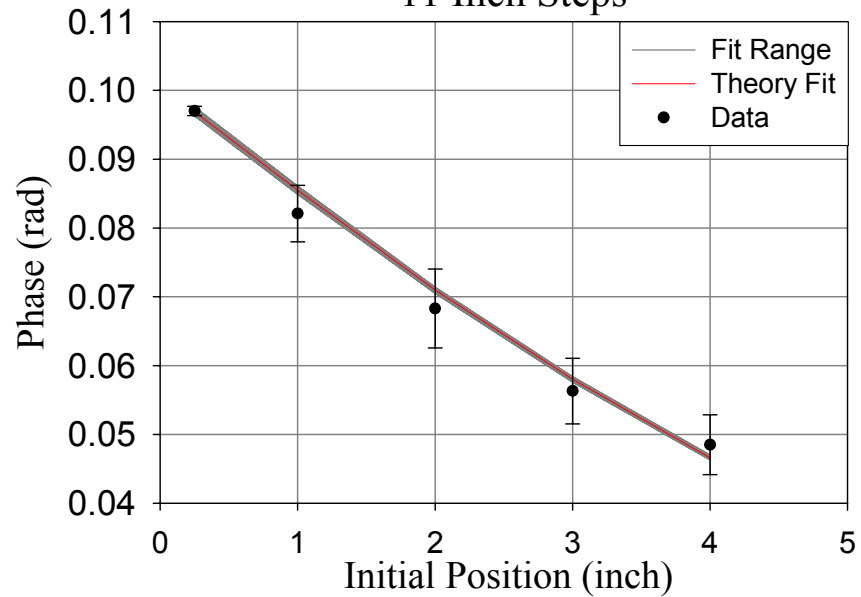
$$(6.673 \pm 0.010) \times 10^{-11} \text{ m}^3 \text{ kg}^{-1} \text{ s}^{-2}$$

Position Dependence

Measured phase shift vs. mass displacement (reference to top of chamber)

Consistent with Newtonian theory

Pb Phase Shift vs. Initial Distance
11 Inch Steps

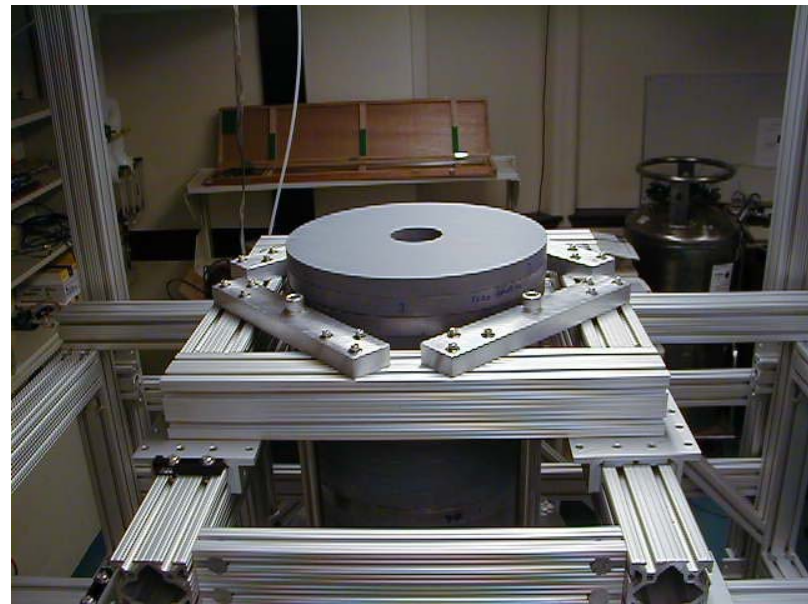


Systematics

- Source mass geometry/density
- Atomic Trajectory
- Source mass positioning
- Magnetic Fields
- Rotations
- Laser parameters/AC Stark shifts

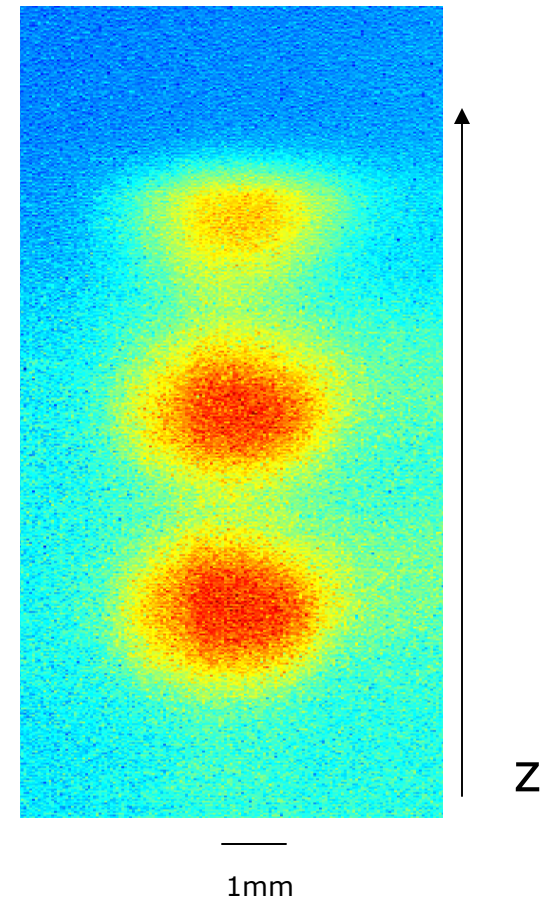
Source Mass

- Measure dimensions → Volume
- Mass of each Pb disc measured to $5 \times 10^{-3} \%$
 - 20 discs (530 kg)
- $\rho = M/V$
 - Density determined to $\sim 0.1\%$.
- Pycnometer method in agreement.



Atomic trajectory

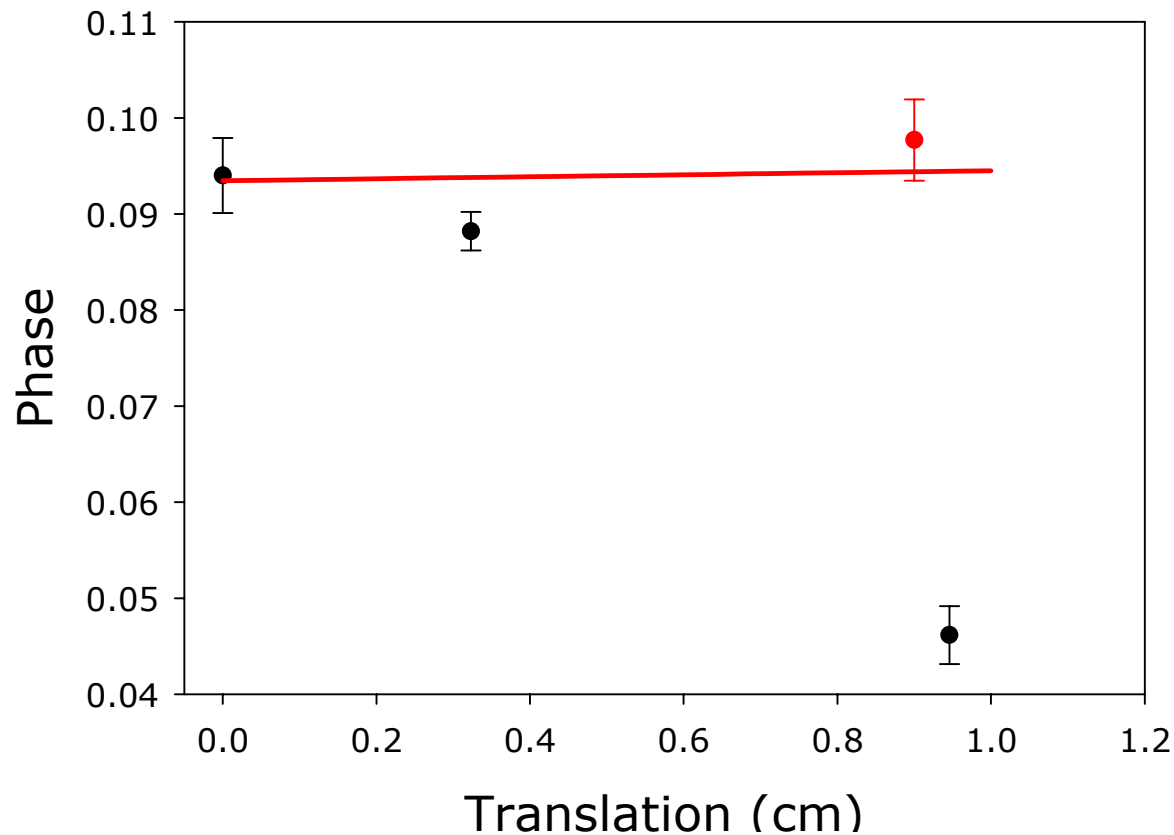
- To calculate gradient phase, need to measure v_0, z_0 for each gravimeter:
 - Atom velocity at start of interferometer
 - CCD camera images TOF
 - Doppler sensitive spectroscopy
 - Atom distance to Source Mass.
 - CCD camera images
- Linear dependence of phase on initial position and velocity.



Source Positioning

Horizontal positioning sensitivity:

~ Flat potential, but measured large fall off.



Culprit:

Induced Eddy current
B-fields during
launch.

Solution:

**Control ramp-off of
MOT quadrupole.**

Magnetic Fields

Magnetic insensitive $m_F = 0$ atoms

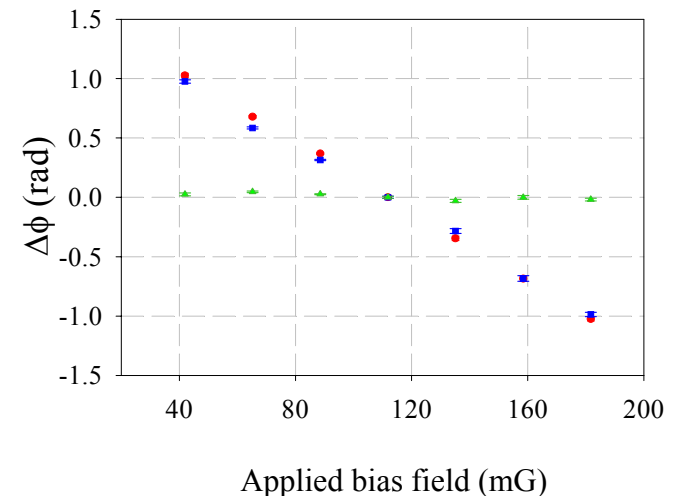
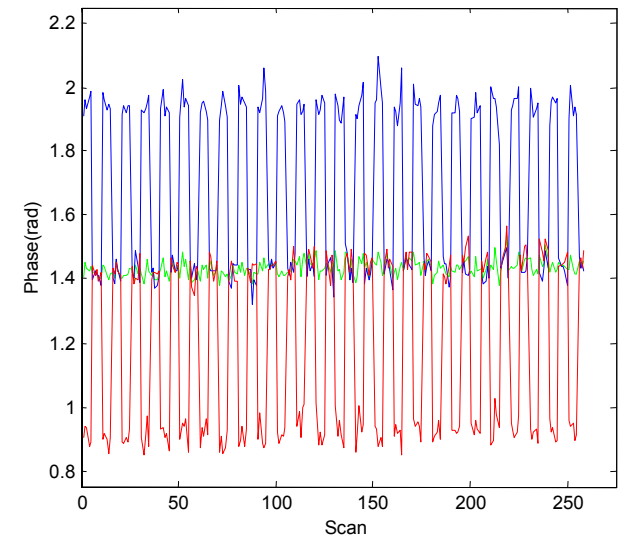
- Insensitive to 1st order Zeeman shift.
- 2nd Order Zeeman shift

$$U = h\alpha B^2 \quad \alpha = 427.5 \text{ Hz} / G^2$$

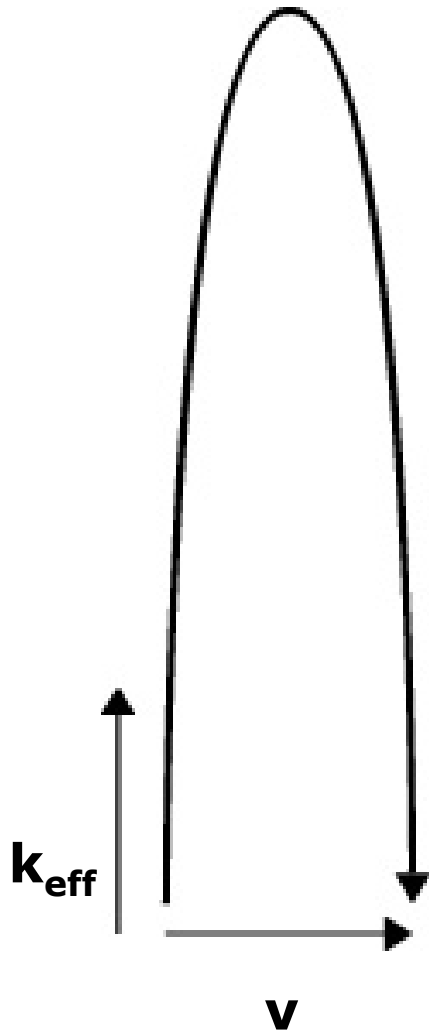
- Interferometer sensitive to B gradients.
 - Propagation reversal / Pb Chop rejects.
 - Measured change in B from Pb source over fountain
 $\sim 0.3 \text{ mG} \rightarrow < 0.1 \%$ effect on chop phase

Propagation Reversal

- Reverse direction of laser
 $k_{\text{eff}} = k_1 - k_2$ relative to g .
 - Gravitational signals change sign ($\delta\phi \sim k \cdot g$)
 - Magnetic and AC Stark shifts remain unchanged and cancel in propagation difference.
- Rejection:
 - Magnetic pulse during interferometer: reduced by at least 100.
 - Rejects change in DC bias



Rotations



- Transverse velocity component will cause AI to enclose a physical area A .
- Sagnac effect.

$$\Delta\phi = \frac{2m}{\hbar} \vec{\Omega} \cdot \vec{A} = 2\vec{\Omega} \cdot (\vec{v} \times \vec{k}_{eff}) T^2$$

Gradiometer and Pb chop reject systematic rotational shift due to launch alignment.

Transverse B-field during launch can induce transverse velocity.

$$\Delta\phi_{rot} < 0.3\%$$

Systematics (Preliminary)

% Uncertainty G

- Source mass geometry/density 0.1 **X**
- Atomic Trajectory 0.5 **X**
- Source mass positioning In progress
- Magnetic Fields 0.1 **X**
- Rotations 0.3 In progress
- Laser parameters/AC Stark shifts <0.1 In progress

Summary: Preliminary Result

$$G = (6.657 \pm 0.025) \times 10^{-11} \text{ m}^3 \text{ kg}^{-1} \text{ s}^{-2}$$

<1% systematic uncertainty

CODATA 98 $(6.673 \pm 0.010) \times 10^{-11} \text{ m}^3 \text{ kg}^{-1} \text{ s}^{-2}$

< 0.3 nG differential accuracy.

Measured with quantum mechanical system

Different Systematics

First precision AI measurement of localized source mass.

Equivalence Principle Test

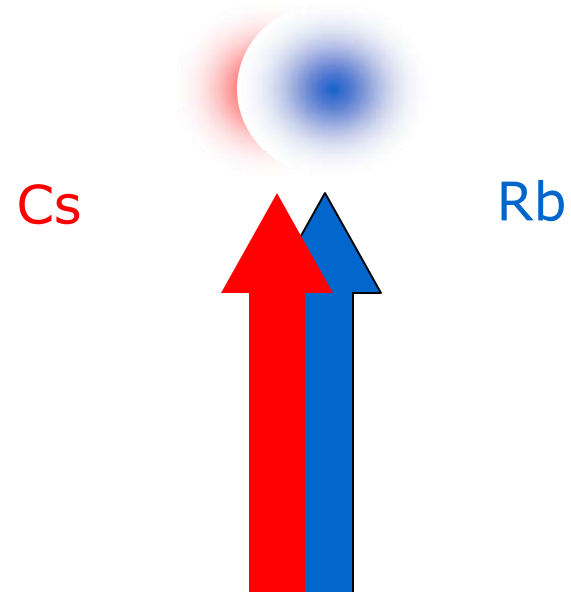
Equivalence Principle:

All objects accelerate at the same rate in gravitational field.

Test: Measure acceleration of different atoms.

String theories predict EP violations at $10^{-12} - 10^{-21} g$

Current Limit: $10^{-12} g$ (UWash)



Future Measurements

- Tests of Equivalence Principle (Cs-Rb)
- Spin-gravity coupling
- Time varying gravitational fields
- Probe higher order AI theory
- Orbiting sensors ($\Delta\phi \sim T^2$)

Possibility to place constraints on string theories

- Sensing/Navigation Applications
- Portable instrument

Experiment to Measure the Electric Dipole Moment of the Electron

Daniel Heinzen
University of Texas at Austin
Austin, TX 78712

The electric dipole moment (edm) of the electron d_e is known from previous measurements to be smaller in magnitude than $1.6 \cdot 10^{-27}$ e cm [1]. This result follows from a measurement of the electric dipole moment of paramagnetic Tl atoms using conventional atomic beam techniques. A nonzero value of d_e can exist only if time reversal symmetry (T) is violated. T-violation within the standard model is far too small to allow for a measurable value of d_e , but extensions of the standard model, such as low-energy supersymmetry, do allow for a value of d_e that could be as large as about ten times the current experimental bound. More sensitive experiments might therefore detect a nonzero value of the electron edm, and provide unambiguous evidence for new physics beyond the standard model. Alternatively, a more sensitive null result would provide further significant constraints on new models of physics. In this talk, we will describe the design of our new experiment to measure the electric dipole moment of the electron using laser cooled Cs atoms. The atoms will be trapped in a far-off resonance optical dipole force trap between electric field plates, and placed within magnetic shields. This experiment has the advantages of long coherent interaction times, resulting in very narrow transition line-widths, and of suppression of velocity dependent errors. Crucial issues include AC Stark shifts induced by the trapping laser fields, and the high degree of magnetic shielding required. This experiment has the potential to yield a sensitivity to a nonzero d_e of the order of $1.0 \cdot 10^{-29}$ e cm, which would represent an advance in sensitivity of about two orders of magnitude.

[1] B. C. Regan et al, Phys. Rev. Lett. **88**, 071805 (2002).

RACE, DISTRIBUTED CAVITY PHASE SHIFTS, AND MICROWAVE PHOTON RECOILS

Chad Fertig, Ruoxin Li, J. Irfon Rees, and Kurt Gibble, The Pennsylvania State University, State College, PA

1. ABSTRACT

The design for RACE, a Rb clock flight experiment for the ISS, is described. The cold collision shift and multiple launching (*juggling*) have important implications for the design and the resulting clock accuracy and stability. We present and discuss the double clock design for RACE. This design reduces the noise contributions of the local oscillator and simplifies and enhances an accuracy evaluation of the clock.

As we try to push beyond the current accuracies of clocks, new systematic errors become important. Here, we study two new potential sources of systematic errors. First, we examine cylindrical TE_{011} microwave cavities and find large phase shifts of the microwave field near the edges of the cut-off waveguide apertures, where there are nodes in the field. The phase shifts lead to a potential distributed cavity phase shift for atomic clocks. Using an additional larger diameter cut-off waveguide section can effectively exclude the nodes and the large phase shifts from the atomic trajectories. Second, it has been suggested that recoils from the absorption of microwave photons lead to frequency shift and also a loss of fringe contrast. We present measurements of the contrast for up to $2 \cdot 19\pi/2$ pulses and find no loss of contrast beyond that expected from measuring microwave field inhomogeneities with up to 19π Rabi pulses.

2. INTRODUCTION

The principal advantage of microgravity for atomic clocks is interrogation times longer than 1 s. With a 10 s interrogation time, a clock has a 50 mHz linewidth suggesting that accuracies may approach 10^{-17} . However, to achieve greater accuracy within the same averaging time, greater stability is needed. RACE is based on Rb to avoid the large cold collision shift of Cs.[1,2] This may allow simultaneously high short-term stability and accuracy. We have three primary goals: (1) Demonstrate new clock techniques for laser-cooled atoms to enable frequency comparisons with accuracies of 1 part in 10^{17} . (2) Significantly improve the classic clock tests of general relativity. (3) Distribute accurate time and frequency from the ISS. We review the design constraints and discuss the double clock design for RACE.

Current atomic fountain clocks have inaccuracies near 10^{-15} . Losses in the microwave cavities lead to small traveling wave components that deliver the power from the cavity feed to the walls of the cavity.[3] The small traveling wave components produce a microradian distribution of phases throughout the cavities, and therefore distributed cavity phase shifts need to be considered. LeMonde *et al.* have shown that there are large phase shifts in multi-Rabi TE_{013} cavities due to the traveling wave component near the nodes of the standing wave.[4] These phase shifts produce large frequency shifts of order 10^{-13} for $\pi/2$ excitation and 10^{-11} for $3\pi/2$ pulses.

Here, we use finite element analysis to study the TE₀₁₁ microwave cavity and find nodes of the cavity field. Hence one might expect large phase shifts due to traveling wave components. The nodes occur in the cut-off waveguide sections used to prevent microwave leakage from the cavity. By symmetry, the lowest coupled mode is the TE₀₁. The longitudinal magnetic field in the TE₀₁ waveguide mode reverses between the center and the copper boundary. Therefore, there must be a node in the time-dependent field the atoms experience as they pass through the cavity with trajectories near the waveguide wall.

In high resolution optical spectroscopy, the energy or frequency shift due to the recoil of an atom when it absorbs a photon is large compared to clock accuracies.[5] Using the same argument, the frequency shift when conserving momentum and energy when absorbing a microwave photon should be of order:[6]

$$\frac{\delta\nu}{\nu} = \frac{\hbar^2 k^2}{2m\hbar\omega} = \frac{\hbar\omega}{2mc^2} = 1.7 \times 10^{-16} \quad (1.1)$$

Wolf et al. have also calculated that there should be a significant loss of contrast, of order 50% for excitations 2 $11\pi/2$ pulses.[6] This should occur due to the spreading of the wave packet during the interrogation time so that, at the second $\pi/2$ pulse, the various parts of the atomic wavefunction do not fully overlap.[7] For higher powers, more photons are absorbed and reemitted leading to a wider spread in the final wave function. Here, we measure the contrast as a function of power but find no detectable loss of contrast due to the microwave photon recoils.

3. DESIGN OF JUGGLING CLOCKS AND RACE

To achieve the potential accuracy of laser-cooled microgravity clocks with reasonable integration times, atoms must be multiply launched (juggled). Juggling imposes several constraints on the design of a microgravity clock. Shutters are needed to block the light scattered from trapping, state preparation, and detection from the interrogation region. In Figure 1, we show a design for a juggling microgravity clock that has a pair of shutters surrounding the Ramsey cavity. This is a design for our Rb microgravity clock, RACE. First we discuss the laser trapping and cooling techniques and then the advantages of having 2 clock cavities.

The double-MOT[8,9] allows a high throughput of cold atoms and therefore a high short-term stability. The high throughput is possible because the double-MOT can rapidly capture many cold atoms and then efficiently launch them through the Ramsey cavity. The “upper” vapor cell trap in Fig. 1 essentially continuously traps atoms and then launches them at 5-10 m/s to the UHV trap “below.” Because of the high launch velocity from the vapor cell trap, the atoms pass quickly through the shutter separating the 2 traps. This implies that the shutter only needs to open for the short time that the ball of atoms flies through, and only during that time must the lasers for the vapor-cell trap be extinguished to prevent light from entering the interrogation region.

The real advantage of the double-MOT design comes from the fact that the UHV trap can capture and launch a ball of atoms in as little as 5 ms. This implies that the shutter separating the UHV trap and interrogation region only has to close for 5 ms for each launch and therefore is nearly always open. This allows a high throughput since, if the shutter is ~10 cm from the center of the UHV trap, the ball of atoms will have expanded considerably before reaching the shutter. For our juggling Cs experiment,[9] it was crucial to reduce the trapping and cooling time of the UHV trap be able to study collisions at low energies (corresponding to juggling rates as high as 140 s⁻¹).

One also has to worry about the effect of the trapping light on the previously launched ball of atoms from the 2nd trap. Again, this was a crucial step in our Cs juggling experiment. By “hiding” the

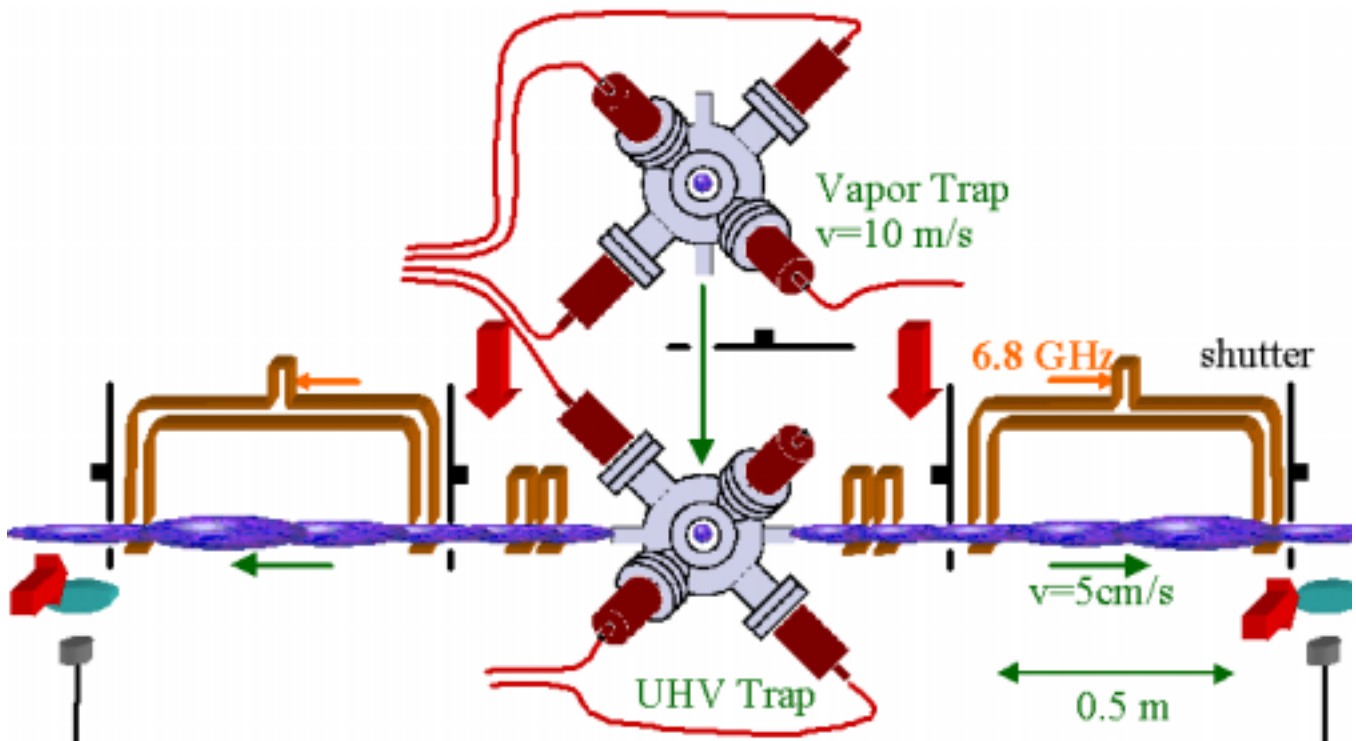


Figure 1. Schematic for juggling microgravity Rb clock RACE. The double MOT launches atoms at high speed from the (upper) vapor trap to the (lower) UHV trap so that the shutter between the traps can be nearly always closed. The shutters between the UHV trap and the cavities are nearly always open except during the ≈ 5 ms that the light for the UHV trap is turned on. The atoms are alternately launched left or right to go through one clock cavity or the other.

ball in the lower hyperfine state immediately after the launch, and by carefully controlling the low intensity repumping light to the 2nd trap, we can capture and launch balls of atoms almost on top of one another.[9]

The RACE schematic in Fig. 1 shows 2 clock cavities. After atoms are collected in the lower laser trap, they are launched either through one cavity or the other. Having 2 cavities is important for a number of reasons. One advantage is that it greatly reduces the requirements for the local oscillator. Few oscillators can perform at the $\sigma_y(\tau) = 3 \times 10^{-15} \tau^{-1/2}$ level and there would be significant work required to develop their flight worthiness. The essential problem with only a single cavity results from the fact that the microwave frequency fed to the cavity must be changed from one side of the transition to the other. During the switch-over, all of the atoms must be cleared from the cavity and this means the oscillator is not tracked for about 10 s when $T = 10$ s. With 2 cavities, we can do the switch-over for one cavity while still monitoring the oscillator with the other cavity and therefore the stability of the clock is so affected by the local oscillator instability.

Vibrations on the ISS in the direction of the launch velocity cause a noise in the interrogation time. With 2 cavities, the 2 detected signals will behave oppositely so that the effects of vibrations can be identified, correlated with an accelerometer, and removed. Furthermore, one of the largest systematic errors is the AC Stark shift due to blackbody radiation at 300K. A measurement of the red shift and time dilation with frequency inaccuracies of 10^{-17} demands absolute knowledge of the average temperature in the clock cavity at the 0.01K level. Having 2 cavities will allow a critical check on our accuracy evaluation. In addition, having 2 cavities gives important redundancy. For example, if a shutter fails in the closed position, we will still be able to achieve mission success goals (although requiring longer averaging times).

4. DISTRIBUTED CAVITY PHASE SHIFTS NEAR NODES IN A TE_{011} CAVITY

In Figures 2 and 3, we show contours of the magnitude of the longitudinal magnetic field (H_z) in a TE_{011} cavity. As shown in Figure 4, those atoms that are near the wall of the waveguide when they enter and exit the cavity first see a field that is reversed (180 degrees phase shifted) relative to that at the center of the cavity. Therefore there are nodes for atoms passing near the walls and, from [4], one would expect large phase errors for atoms passing through these regions. In fact, atoms going through nearly half of the area of the aperture on each pass see a field reversal and therefore a node in the field.

In Figure 5, we show a calculation of the phase as a function of distance from a node for both the TE_{013} cavity and the TE_{011} cavity. The TE_{013} cavity is fed by a single port, which produces much larger phase shifts than for a symmetric feed, and the TE_{011} cavity is taken to be azimuthally symmetric. The phase variation for the TE_{011} is about 20 times less than that for the TE_{013} cavity. Therefore, one might expect errors of order 10^{-15} to 10^{-14} . However, preliminary integrations of the atomic wavefunctions through the cavity suggest the errors may only be of order 10^{-16} . The preliminary calculations also suggest the phase shift becomes very large very near the cavity walls so atomic fountain clocks using such a cavity may be especially sensitive to tilts. Given that, for the TE_{013} cavity, a single feed dramatically increases the phase errors, one should also expect a single feed to lead to larger errors here. It may also be that

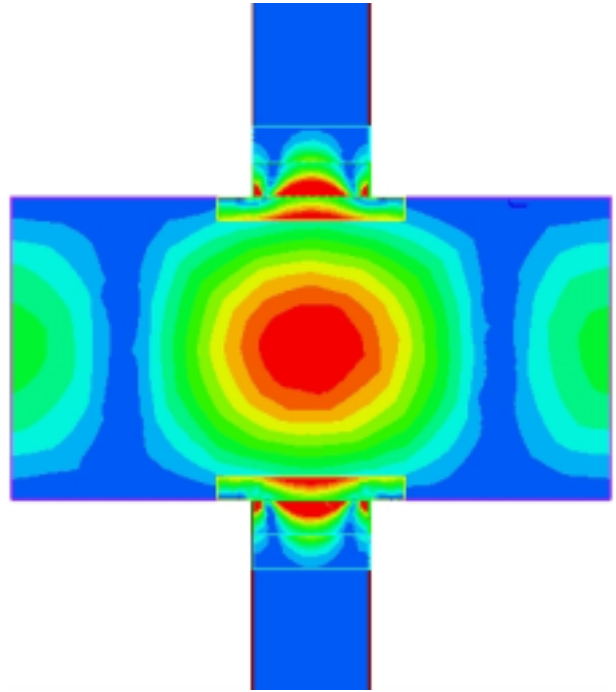


Figure 2. Contours of the magnitude of the longitudinal magnetic field, H_z , in a cylindrical TE_{011} cavity. The cavity radius is 25.5 mm, the height 26.075 mm, the apertures have a 1cm diameter, and the cavity is fed by 4 feeds around the mid-section circumference. The field near and in the cut-off waveguide sections are magnified by 4, 16, and 64 times. The line of field nodes in the below cut-off waveguide sections which extend into the cavity can be clearly seen.

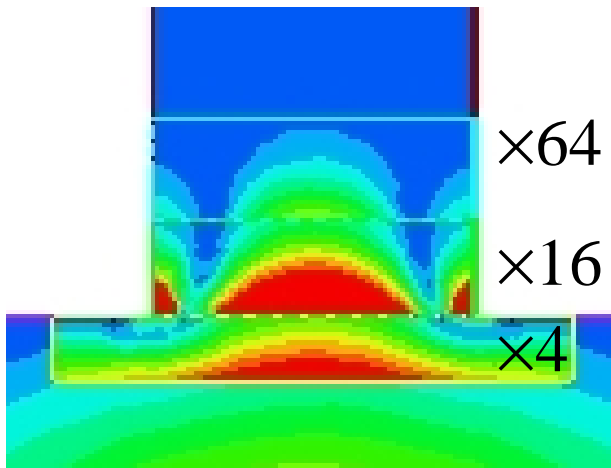


Figure 3. Magnified view of the cut-off waveguide sections from Figure 1.

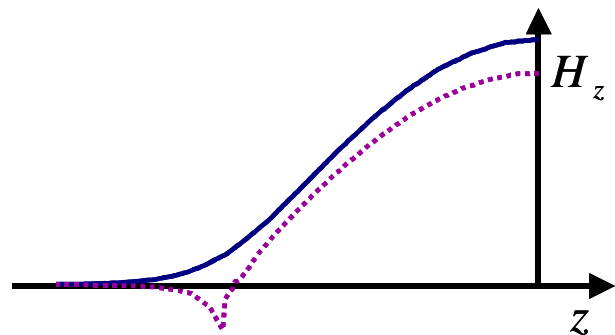


Figure 4. Longitudinal microwave magnetic field as a function of position in the cavity for atoms with no transverse velocity and entering on the symmetry axis of the cavity (solid) and near the edge of the cavity aperture (dashed). Atoms near the edge see a node in the field due to the reversal of the field near the below cut-off waveguide section.

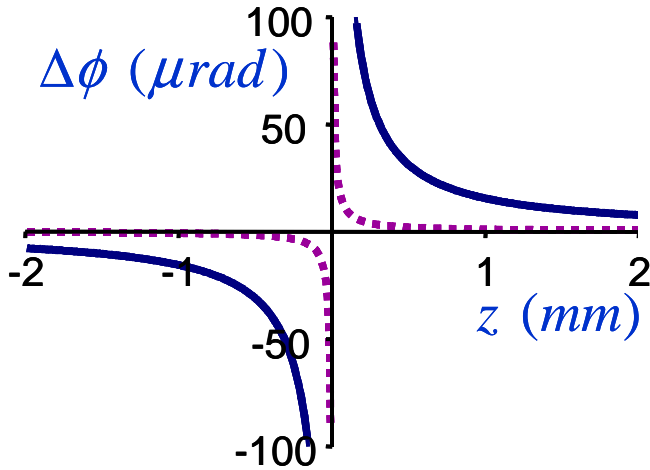


Figure 5. Phase of longitudinal microwave field as a function of distance from node for a TE_{013} cavity (solid) and a TE_{011} cavity (dashed). juggling fountain clock.

inhomogeneities in the cavity produce larger effects than what we calculate for azimuthal symmetry.

Whatever the size of this distributed cavity phase shift error, it is not difficult to eliminate. One cavity design that eliminates this potential error is shown in Figure 6. There, a larger diameter section of cut-off waveguide is used. The field decays in this large diameter section, where the nodes are not sampled by the atomic trajectories, to a sufficiently small level. Then the smaller diameter waveguide section, setting the cavity aperture, follows to insure a sufficiently small microwave leakage.

Currently we are calculating the atomic responses to model the potential distributed cavity phase shifts from a cavity like that in Figure 2. We will also calculate the power dependence, which may be especially interesting for high powers that are not $n\pi/2$ pulses. For a $n\pi/2$ pulse, the sensitivity function[10] has no slope when the atoms pass through the upper portion of the cavity. By integrating the definition of the sensitivity function by parts, it is easy to see that distributed cavity phase shifts are sensitive to the slope of the sensitivity function and therefore we always expect relatively large effects from the bottom region of nodes and large effects from the top only when the impulse for the atoms is different than $n\pi/2$ (or when the power is very high which gives a high frequency oscillation to the sensitivity function and therefore an often steep slope).

5. MICROWAVE PHOTON RECOILS

The principal problem in measuring a loss of contrast due to the microwave photon recoils is inhomogeneities in the microwave field H_z in the cavity. We measure the inhomogeneities in H_z by measuring contrast as a function of power for a single (Rabi) pulse. The Rabi excitation is much shorter than the Ramsey interrogation time so that any momentum spread due to the recoils would cause much less spreading and therefore a negligible loss of contrast.

In Figure 7, we show the measured Rabi contrast for the upward and downward traversals through our rectangular TE_{102} cavity.[1] The upward and downward contrast are different due to the expansion of the ball of atoms launched from our MOT. While the contrast is below that for a cavity

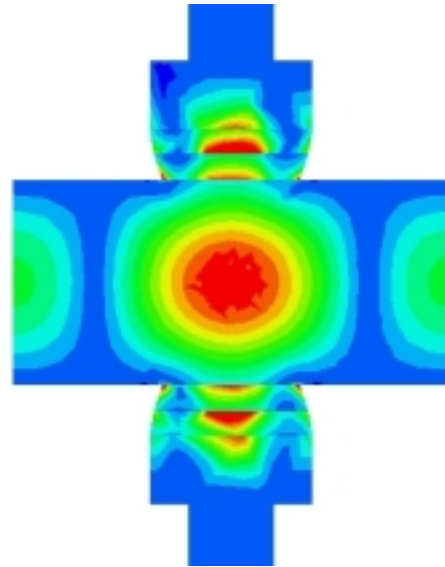


Figure 6. Contours of the magnitude of H_z in a cylindrical TE_{011} cavity with cutoff waveguide sections of different diameter. The larger diameter waveguide sections have nodal lines outside of the region through which atoms pass. In the smaller diameter section, H_z , while it has nodes, can be sufficiently small.

with no holes (which has much higher contrast than the actual cavity because of the field reversal as in Figure 4), we seem to have more contrast than expected from a finite element analysis of our cavity. We do not know the origin of this discrepancy. Nonetheless, by measuring the Rabi contrast, we effectively measure the microwave field inhomogeneities seen by the atoms. We choose to fit a single parameter model which cuts atoms beyond a given radius from the center of the cavity apertures. The contrast for this model is shown as the solid and dashed line in Figure 7.

In Figure 8 we show the measured Ramsey fringe contrast for excitations up to $2 \cdot 19\pi/2$ pulses. The solid line shows the expected contrast from the fitted model to the Rabi contrast in Figure 7. We see no significant loss of contrast beyond that expected from our measurement of our microwave field inhomogeneities. For comparison, the contrast was expected to decrease to of order 50% for $2 \cdot 11\pi/2$ pulses.[6] We have varied the interrogation time (to as short as 0.25s) and increased the temperature of the atoms to 6.7 K and do not see any loss of contrast beyond that expected for the microwave field inhomogeneities.

6. CONCLUSIONS

To achieve the potential accuracy of laser-cooled microgravity clocks with reasonable integration times, atoms must be multiply launched (juggled). The short-term stability is proportional to the launch rate and this in turn implies that high accuracy and stability favor long interrogation regions. Laser-cooled microgravity clocks can achieve short-term stabilities approaching $\sigma_y(\tau) = 3 \times 10^{-15} \tau^{-1/2}$. At this stability, the largest error in a Cs microgravity clock is the cold collision frequency shift. By using ^{87}Rb , the collision shift is 50 times smaller allowing an accuracy of 10^{-17} . We describe the design of our Rb microgravity clock which uses a double-MOT and 2 cavities. This simplifies the trapping and shutter design while maintaining a high throughput of cold atoms, minimizes the local oscillator requirements, eliminates errors due to vibrations, and provides failure and accuracy redundancy.

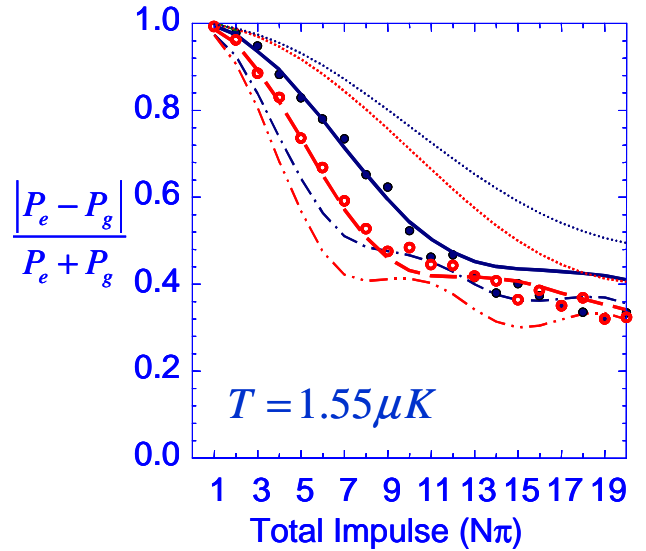


Figure 7. Rabi pulse contrast as a function of impulse on the upward (filled circles) and downward (open circles) traversals through the fountain clock cavity. The dotted (small dashed) lines are a model using the analytic expression for H_z in a rectangular TE_{102} cavity with no apertures for the atoms for the upward(downward) cavity traversal. The dashed-dotted (dashed-double-dotted) lines are calculated using a finite element model of the cavity that includes the cavity apertures. The solid(dashed) lines are from a single parameter fit to the measurements that cuts the cavity apertures.

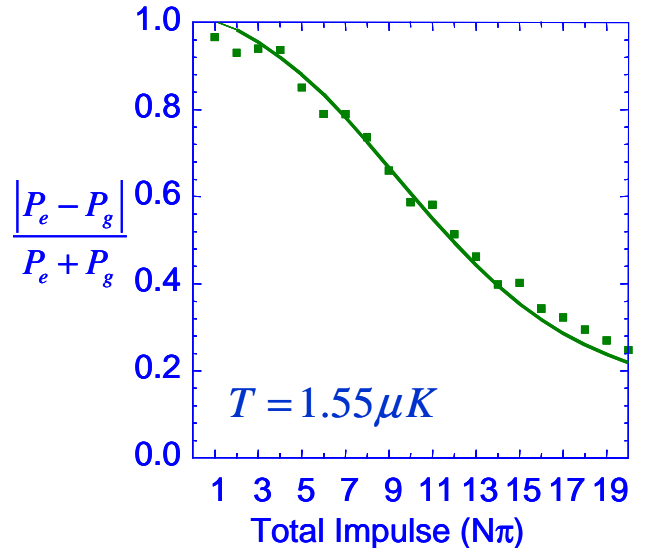


Figure 8. Ramsey fringe contrast (squares) as a function of impulse. The solid line shows the expected loss of contrast due to the inhomogeneities fitted in Figure 6.

The common TE_{011} cylindrical cavities that are used with cutoff waveguide sections have nodes in the field regions sampled by the atoms. These may produce significant phase shifts, especially near the wall of the cutoff waveguide apertures, and may interact with other errors to produce a tilt sensitivity.

We have also measured the Ramsey fringe contrast as a function of power and find no loss of contrast beyond that expected from our measurements and modeling of our microwave field inhomogeneities. This clearly shows the need for more theoretical work to understand the effect of microwave photon recoils on the contrast and to assess the potentially important frequency shift.

7. ACKNOWLEDGEMENTS

We acknowledge financial support from the NASA Microgravity program and Penn State University.

8. REFERENCES

- [1] C. Fertig and K. Gibble, *Phys. Rev. Lett.* **85**, 1622 (2000).
- [2] K. Gibble and S. Chu, *Phys. Rev. Lett.* **70**, 1771 (1993).
- [3] G. Vecchi and A. De Marchi, *IEEE Trans. Instr. Meas.* **42**, 434 (1993).
- [4] P. Lemonde, G. Santarelli, Ph. Laurent, F. Pereira, A. Clairon, and Ch. Salomon, *Proceeding of the Freq. Contr. Symp.*, p. 110, (1998)
- [5] J.L. Hall, Ch. J. Bordé, and K. Uehara, *Phys. Rev. Lett.* **37**, 1339 (1976).
- [6] Wolf, Bize, Clairon, Landragin, Laurent, Lemonde, & Borde, *Proceeding of the Freq. Contr. Symp.*, p. 37, (2001).
- [7] See P. D. Featonby, G. S. Summy, C. L. Webb, R. M. Godun, M. K. Oberthaler, A. C. Wilson, C. J. Foot, and K. Burnett, *Phys. Rev. Lett.* **81**, 495 (1998).
- [8] K. Gibble, S. Chang, and R. Legere, *Phys. Rev. Lett.* **75**, 2666 (1995).
- [9] R. Legere and K. Gibble, *Phys. Rev. Lett.* **81**, 5780 (1998).
- [10] G. Dick, *Proc. Of Precise Time and Time Interval*, p. 133, (1987).

Atom-atom collisions in a very dense Bose-Einstein condensate

Juha Javanainen
University of Connecticut
Storrs, CT 06269-3046

In a dense enough Bose-Einstein condensate, the binary collision approximation underlying the usual description of atom-atom interactions must break down. We propose a new paradigm for the theory of atom-atom interactions in a very dense, quantum degenerate gas: resonance between atomic and molecular condensates. We demonstrate how this way of thinking reproduces the usual collision theory in the limit of a dilute condensate, and report on progress toward finding experiments in which the new approach differs from the standard picture.

All-Optical Trapping and Cooling of a Two-Component Fermi Gas

**Students: Michael Gehm Stephen Granade
Staci Hemmer**

Post Doc: Ken O'Hara

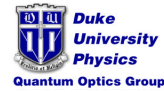
John Thomas, Duke University Department of Physics

Sponsored by: ARO, NSF, NASA, DOE

Outline

- Introduction: [Why Study Fermi Gases?](#)
 - Basic Physics: [Dilute, Degenerate Fermi Gases](#)
 - Single-State Fermi Gas: [Hyperfine Coherence Lifetime](#)
 - Two-State Fermi Gas: [Super-High Temperature Superconductivity](#)
- Ultrastable Optical Traps: [CO₂ Laser Trap](#)
- Evaporative Cooling in Optical Traps: [Degenerate ⁶Li Mixtures](#)
- Recent Progress: [Interactions at B=100-1000 Gauss](#)
- Summary and Future Plans

Why Study Dilute, Degenerate Fermi Gases?

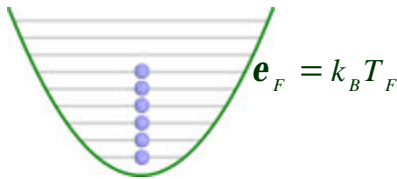


- Fermions are the Building Blocks of Matter
 - Electrons, Protons, Neutrons, Quarks
 - Cold Trapped Fermi Gases Can Mimic Electrons in Metals, Quarks in Nuclear Matter
- Dilute Fermi Gases Provide Fundamental Tests of Theory
 - Tests of Effective Field Theory, Many Body Theory
 - Well Understood Interactions
 - Variable Temperature, Density, Interaction Strength, Spin Composition...
- Enabling Technology
 - Single-Spin Fermi Gas is Free of Interactions
Precision Measurements, Atomic Clocks, Quantum Information Storage...
- Analogs of Superconductivity in Spin-Up Spin-Down Mixtures
 - Super-High T_C Superconductivity: $T_C \sim 0.5 T_F$

Degenerate Fermi Gases

Harmonic Potential:

$$\mathbf{e} = (n_x + n_y + n_z)h\mathbf{n}$$



Zero Temperature

$$N \approx n_x^{\max} n_y^{\max} n_z^{\max}$$

- Fermi Temperature:

$$k_B T_F = h\mathbf{n} (6N)^{1/3}$$

- Phase Space Density (Classical Regime)

$$\mathbf{r} \equiv N \left(\frac{h\mathbf{n}}{k_B T} \right)^3 = \frac{1}{6} \left(\frac{T_F}{T} \right)^3$$

- Optical Trap:

$$\mathbf{n} = (n_x n_y n_z)^{1/3} = 2.4 \text{ kHz}$$

$$N = 2 \times 10^5$$

$$T_F = 12 \text{ } \mu\text{K}$$

At low temperatures, atoms in optical and magnetic traps sit in an approximately harmonic potential, where the quantized energy levels are given by the sum of the x, y, and z oscillator quantum numbers multiplied by the level spacing.

At zero temperature, single state fermionic atoms fill the levels up to a highest occupied state which is denoted by the Fermi energy. The number of atoms N is equal to the number of accessible states, which is given by the product of the maximum x,y and z quantum numbers. Hence, the x,y, and z quantum numbers are each $N^{(1/3)}$. Thus, the Fermi energy is of order $N^{(1/3)}$ times the energy level spacing. The phase space density is approximately the number of atoms divided by the number of accessible states. At a nonzero temperature, the x,y, and z quantum numbers are each just the thermal energy divided by the energy level spacing. Hence, the phase space density scales inversely as the temperature cubed. Degeneracy is attained when the phase space density is of order unity, at a temperature of half the Fermi temperature.

For our optical trap, Fermi temperatures of the order of 10 microkelvin are readily attained.

$$L \cong Rp = Rh / \lambda_{dB} = l\hbar$$

$$R / \lambda_{dB} \ll 1$$



$$l\hbar = 0$$



$\mathbf{y}(r_1 - r_2)$ S-Wave Only

- Bosons

$$\Psi(1,2) = \mathbf{y}(r_1 - r_2) \uparrow_1 \uparrow_2$$

One spin state

- Fermions

$$\Psi(1,2) = \mathbf{y}(r_1 - r_2) \frac{1}{\sqrt{2}} (\uparrow_1 \downarrow_2 - \downarrow_1 \uparrow_2)$$

Need two spin states

At low temperatures, the de Broglie wavelength is large compared to the range R of the collision potential. For example, 6-Li at microkelvin temperatures has a de Broglie wavelength of 10,000 angstroms, while the range is of order a few tens of angstroms. In this case, the relative angular momentum of two colliding atoms is nearly zero, and S-wave scattering is the only allowed channel.

The spatial wavefunction is therefore even under the interchange of the particle labels. Since the overall wavefunction for Fermions must be odd, the corresponding spin wavefunction must be odd for particles to collide.

This necessitates simultaneous trapping of at least two spin states, in contrast to bosons which interact in a spin-polarized gas.

Hyperfine Coherence in a Trapped Fermi Gas

- Pure State –No S-Wave Collisions*

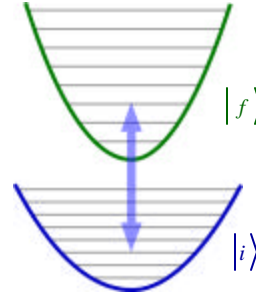
$$|j\rangle = \cos(\mathbf{q}/2)|i\rangle + \sin(\mathbf{q}/2)|f\rangle e^{i\mathbf{j}}$$

- Elimination of Cold-Collision Frequency Shifts
- Suppression of Inelastic Collisions
- Long Coherence Lifetimes in a Dense Vapor
- Quantum Information Storage

- Spread in $n \Rightarrow$ Dephasing

$$\mathbf{j}(t) = 2\mathbf{p} n \Delta n_{vib} t$$

$$T_{COH} \cong \frac{1}{2\mathbf{p} \Delta n_{rms}} = \frac{n_0}{\mathbf{p} n_{HF} n_{vib} \Delta n_{rms}}$$



$$\Delta n_{vib} = \frac{n_{HF}}{2n_0} n_{vib}$$

For ${}^6\text{Li}$	$T = 5 \mu\text{K}$	$T = 0 \mu\text{K}$
T_{COH}	2 sec	145 sec

* Gibble and Verhaar, PRA 52, 3370 (1995)

In a single component Fermi gas, there is no S-wave scattering. Hence, spin polarized fermions are well suited for precision measurements. By using a radiofrequency source to prepare a superposition of two ground hyperfine states, all atoms in the gas are in identical superposition states and cannot collide.

This eliminates cold collision frequency shifts and inelastic scattering, enabling long lifetimes. The lifetime is determined by the dephasing time of the coherence, which is determined by the vibrational energy spread. Since atoms in the upper and lower hyperfine states oscillate at slightly different frequencies, atoms in different vibrational states have slightly different transition frequencies, causing dephasing. At low temperatures, the dephasing rate is determined by the Fermi energy and the minimum trap depth needed to support atoms against the Earth's gravitational field. For ${}^6\text{Li}$, coherence lifetimes of a hundred seconds or more are achievable.

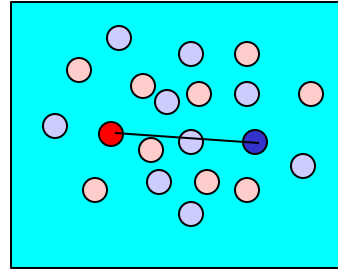
Superfluidity-Cooper Pairing

• Transition Temperature: $T_c = 0.61 T_F e^{-\frac{p}{2 k_F |a|}}$

• Negative Scattering length: a

• Density Important: $k_F \propto n^{1/3}$

• Pair Size: $D_X \sim \frac{1}{k_F} e^{-\frac{p}{2 k_F |a|}}$

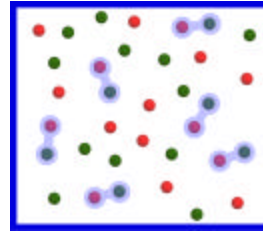
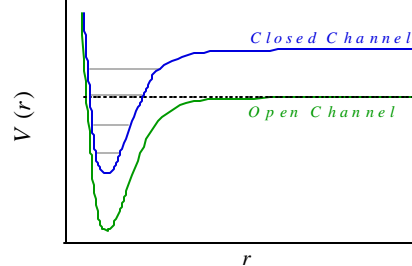


○ = Spin Up ○ = Spin Down

In two-state mixtures of ^6Li , there are attractive interactions which can cause Cooper pairing, potentially enabling study of gas phase analogs of superconductivity. For weak pairing, the transition is exponentially suppressed with respect to the Fermi temperature. The exponent depends on the scattering length, which must be negative and the density, which determines the Fermi wavevector. Typical transition temperatures for weak pairing in atomic gases may be in the range of 0.1 microkelvin. The pairing length scale is large compared to the interparticle spacing.

Resonance Superfluidity*

- Atom-Molecule Coupling via Feshbach Resonance



- Cooper-Paired Gas Coherent with Condensate of Bosonic Molecules
- Study Crossover from BCS Theory to BEC of Composite Bosons
- On Resonance $T_C @ 0.5 T_F$: **Super-High T_C Superconductivity!**

* M. Holland, *et al.* Phys. Rev. Lett. **87**, 120406 (2001)

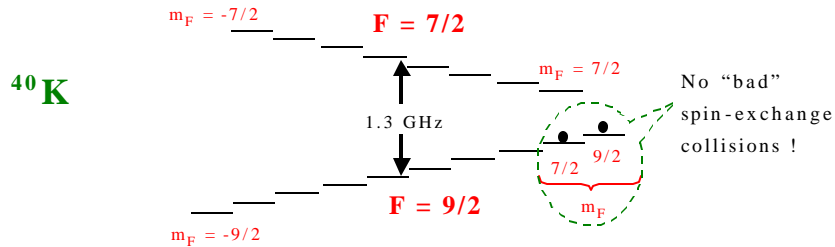
E. Timmermans, *et al.* Phys. Lett. A **285**, 228 (2001)

Recently, two theoretical groups have predicted a super strong pairing interaction which results from a Feshbach resonance. In such a resonance, atoms collide in an energetically open channel, which is coupled by hyperfine interactions to a closed channel. In 6-Li , the open channel interacts via a triplet potential, while the closed channel involves atoms in the singlet potential.

The triplet potential is magnetically tunable and can be shifted with respect to the singlet potential using a magnetic field. When the field is such that the energy of the incoming particles in the triplet potential is degenerate with a molecular bound state in the singlet potential, a large molecular amplitude arises, mediating a very strong pairing interaction. This leads to superfluid transition temperatures of half the Fermi energy, much larger than ordinary high temperature superconductors where the transition occurs at a few percent of the Fermi temperature.

Evaporative Cooling of Fermions

Degenerate Fermi gas in Magnetically Trapped ^{40}K (Deborah Jin, JILA 1999):



- Scattering Length in Magnetically Trapped Mixture is $+157 a_0$

Sympathetic cooling of ^6Li in a magnetic trap

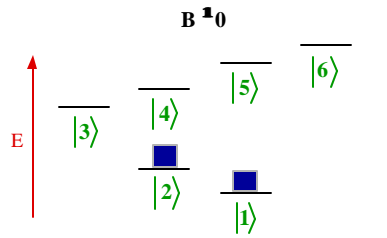
- Randy Hulet (Rice), Christophe Salomon (Paris), Wolfgang Ketterle (MIT)
- Use Bosons as a "Refrigerator" to Cool Fermions
- Degenerate Single Component Fermi Gas (2001,2002)

To explore pairing interactions in a Fermi gas, it is necessary to cool the atoms to degeneracy. Degeneracy was first achieved by the JILA group, using evaporative cooling of a two state mixture of 40-K in a magnetic trap.

Recently, three groups have cooled a single component of 6-Li to degeneracy by using a boson as a refrigerator. However, the states of interest for superfluidity are repelled from a magnetic trap, necessitating transfer to an all-optical trap and subsequent state preparation.

Mixture of ${}^6\text{Li}$ Atoms in States $|1\rangle$ & $|2\rangle$

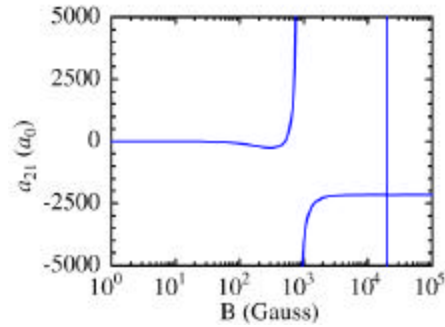
$|2\rangle - |1\rangle$ Mixture



- Spin-Exchange Collisions Forbidden
- Dipole-Dipole Collisions Forbidden

$|2\rangle - |1\rangle$ Scattering Length a_{21}^*

$$S_{el} = 4p a_{21}^2$$



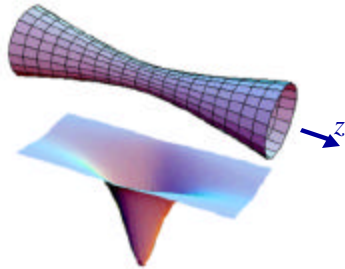
Interactions Easily Turned On/Off

*M. Houbiers, *et al.*, Phys. Rev. A **57**, 1497 (1998)

A mixture of the two lowest hyperfine states of ${}^6\text{Li}$ is well suited for studies of Fermi superfluidity, as these states are stable against two-body inelastic processes and correspond to net (nuclear plus electron) spin of $\frac{1}{2}$ up and $-\frac{1}{2}$ down. Further, they are predicted to exhibit a Feshbach resonance near 800 G, enabling study of super strong pairing. The scattering length is zero at zero magnetic field, enabling interactions to be turned on and off at will by simply applying or not applying a uniform magnetic field. However, at the magnetic fields of interest, both states are repelled from magnetic traps, necessitating the use of an all-optical trap which can confine any spin state.

Optical Dipole Force Trap

Focused Gaussian Laser Beam



Confining Potential

$$U = -U_0 \frac{1}{1+(z/z_0)^2} e^{-2r^2/w_0^2}$$

Magnetic-State-Independent Potential

- Trapping of Multiple Spin States
- Evaporative Cooling of Fermions
- Interacting Fermi Gas
- Trapping of Lowest Energy Spin-States:
Mixtures Suitable for Superfluid Transition

In our experiments, we employ a single focused laser beam as an all-optical trap. Atoms are polarized by the beam and are attracted to the high intensity region near the focal point. The trap potential takes the same form as the laser intensity distribution and is about a millimeter long by 0.1 millimeter wide.

Since the interaction is essentially electrostatic, the trapping potential is nearly independent of the atomic hyperfine states.

Optical Heating

- Larmor Power Formula

$$P = \frac{2}{3} \frac{\overline{\ddot{\mathbf{d}}^2}}{c^3}$$

$$\mathbf{d} = \mathbf{a}_g \mathbf{E} \Rightarrow \ddot{\mathbf{d}} = -\omega^2 \mathbf{a}_g \mathbf{E}$$

$$R_s = \frac{P}{\hbar \omega} = \frac{8p}{3} \frac{\mathbf{a}_g^2 \omega^3}{\hbar c^4} I$$

- For CO₂ Laser Trap*

$$P = 65 \text{ W} \quad \omega_0 = 47 \text{ } \mu\text{m}$$

$$U_0 = 0.7 \text{ mK}$$

$$I \cong 2 \text{ MW/cm}^2$$



$$\frac{1}{R_s} \cong 1800 \text{ sec}$$

Negligible Optical Heating!

*T. Takekoshi, J.R. Yeh, R. J. Knize, Opt. Comm. **114**, 421 (1995).

In such an optical trap, it is necessary to avoid optical scattering which heats the atoms. This is accomplished by using a large detuning and a low laser frequency. The Larmor formula determines the scattered power which scales as the fourth power of the laser frequency, the same reason the sky is blue. The scattering rate is then proportional to the cube of the laser frequency. As pointed out by Randy Knize in 1995, by using a CO₂ laser, the scattering rate is highly suppressed as a consequence of the long 10 micron wavelength. In our trap, the intensity at the focus is 2MW per square centimeter, but the scattering rate is only two photons per hour! Hence, optical heating is negligible.

Prog. Quant. Electr. 1997, Vol. 21, No. 1, pp. 1-79
© 1997 Gordon & Breach Ltd.
Printed in Great Britain. All rights reserved.
0893-3100/97 \$10.00

LASER COOLING AND TRAPPING OF NEUTRAL ATOMS

C. S. ADAMS
Department of Physics, Durham University, Durham DH1 1TA, UK

E. BUIS
Department of Physics and Applied Physics, Strathclyde University,
Glasgow G4 0NG, UK

Abstract: The ability to cool, manipulate, and trap atoms using laser light has allowed a new, rapidly expanding field to emerge. Current research focuses on improving existing cooling techniques, and the development of cold atoms as a source for applications ranging from atomic clocks to studies of quantum degeneracy. This review explains the basic mechanisms used in laser cooling and trapping, and illustrates the development of the field by describing a selection of key experiments. Copyright © 1997 Gordon & Breach Ltd. All rights reserved.

14 C. S. ADAMS & E. BUIS

the excited state hyperfine structure is the same for all the ground-state magnetic sub-levels. Therefore, if the detuning is larger than the excited state hyperfine splitting, all the ground-state magnetic sub-levels move together. This degeneracy of the magnetic sub-levels in a linearly polarized far-off-resonance optical dipole trap allows atoms in an arbitrary spin state to be trapped. Furthermore, if the detuning is larger than the fine-structure splitting, then, as far as the light is concerned, the atom looks like a 2-level system, and the trap depth is given by Eq. (187) with the saturation intensity equal to its 2-level value $I_{\text{sat}} = \pi h c / 4 \sigma \lambda^3$.

A significant problem in optical dipole traps is the heating due to spontaneous scattering. For detunings larger than a few linewidths the spontaneous scattering rate is

$$R_s = \frac{2\Omega^2 \Gamma}{4\Delta^2} \quad (191)$$

For small detunings the relative heating severely limits the lifetime of the trap. A solution to this problem is apparent by comparing equations (187) and (191). Whereas the trap depth is proportional to $1/\Delta^2$, the scattering rate is proportional to $1/\Delta$, so by increasing both the intensity and the detuning one can maintain the trap depth and reduce the relative heating. In the limit of far detuning, one expects the light to create an almost conservative potential, such that in practice the lifetime of the trap is only limited by the background pressure. Figure 17 shows the lifetime of a far-off-resonance trap for different pressures. As expected the lifetime varies linearly with the pressure, except at very low pressures ($\sim 10^{-11}$ Torr) where it tends to saturate at a few seconds due to other possible heating mechanisms (e.g. laser fluctuations).

Fig. 17. Lifetime of a far-off-resonance trap (measured in Torr) as a function of background pressure (measured in Torr) for the different laser powers.

A dipole trap is a single focused Gaussian laser beam focused at the center of the atomic cloud. To establish the feasibility of optical trapping, we estimate the maximum force exerted by a 100 mW laser beam focused into the vacuum D-hole. The trap depth is equivalent to

“In the limit of far detuning, one expects the light to create an almost *conservative potential*, such that in practice the lifetime of the trap is only limited by the background pressure... As expected the lifetime varies linearly with the pressure, except at very low pressures ($\sim 10^{-11}$ Torr) where it tends to *saturate at a few seconds*.”

Prog. Quant. Electr. 21,1-79 (1997).

13

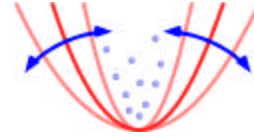
Unfortunately, in 1997, when our group first set out to develop an all-optical trap for fermions, the best optical traps had a very limited lifetime. In a high vacuum, instead of obtaining a background gas limited lifetime of several hundred seconds, lifetimes saturated at a few seconds due to unknown sources of heating.

Non-Optical Heating Sources

- Laser intensity noise

$$\langle \dot{E} \rangle = \Gamma \langle E \rangle \quad \Gamma = p^2 n^2 S_I(2n)$$

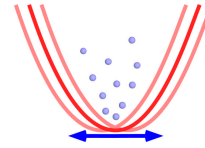
$$\text{Ar}^+ \text{ Laser} : \Gamma^{-1} \cong 10 \text{ sec}$$



- Laser pointing noise

$$\langle \dot{E} \rangle = \dot{Q} \quad \dot{Q} = 4p^4 M n^4 S_x(n)$$

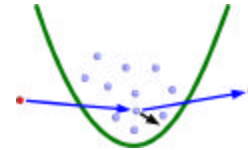
$$\text{Ar}^+ \text{ Laser} : \dot{Q} \leq 20 \text{ nK / sec}$$



- Diffractive background gas collisions

$$\langle \dot{E} \rangle = \dot{Q} \quad \dot{Q} = 0.37 g_c U_0^2 / e_d$$

$$\text{Cs Vapor Cell Trap} : \dot{Q} = 3.4 \text{ nK / sec}$$



Phys. Rev. A **56**, R1095 (1997)

Phys. Rev. A **60** R29 (1999)

By investigating non-optical sources of heating, we discovered that laser intensity fluctuations might play an important role in limiting the trap lifetime. We developed the first theory of noise induced heating to estimate the heating rates.

When the intensity fluctuates, the trap spring constant fluctuates, causing parametric heating. This causes an exponential increase in the energy with a rate constant proportional to the square of the trap oscillation frequency and the laser noise power spectrum at the second harmonic. Laser pointing noise also heats the atoms. Finally, we also showed that a vacuum at finite pressure has a fundamental insulation limit determined by quantum diffractive collisions of thermal background gas atoms with the trapped atoms. This source of heating is readily made small by using ultrahigh vacuum and the noise induced heating is suppressed by using a very stable trapping laser.

Ultrastable CO₂ Laser Trap

- Stable Commercial Laser



- Typical Trap Parameters

$$P = 65 \text{ W}$$

$$w_0 = 47 \text{ mm} \quad z_0 = 0.7 \text{ mm}$$

$$U_0 = 0.7 \text{ mK}$$

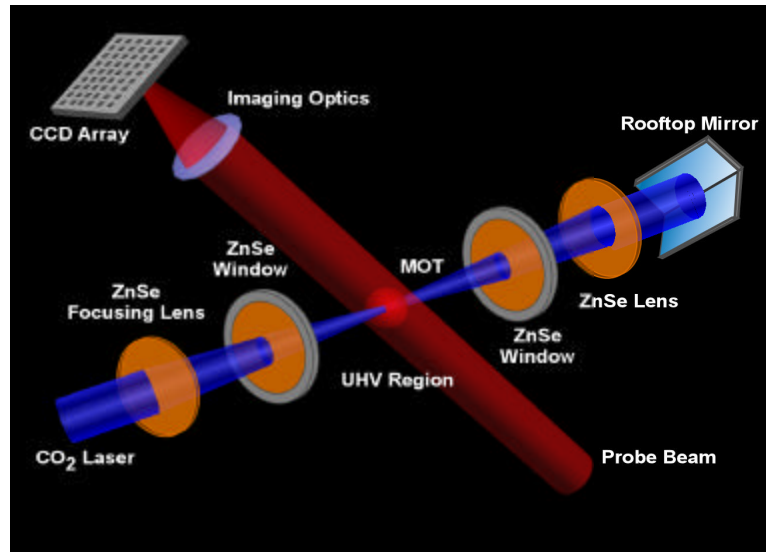
$$n_r \cong 6.6 \text{ kHz} \quad n_z \cong 340 \text{ Hz}$$

- Negligible Optical Heating
 - Scattering Time @ 1/2 hour
 - Recoil Heating @ 18 pK/s
- Extremely Low Noise
 - Intensity Noise Heating
$$\Gamma^{-1} \geq 5 \times 10^4 \text{ sec}$$
 - Position Noise Heating
$$\dot{Q} \leq 50 \text{ nK/s}$$
- Ultra-High Vacuum
 - Pressure: $< 10^{-11}$ Torr
 - Heating: < 5 nK/sec

Currently, we use a commercial ultrastable CO₂ laser producing 140 W.

The laser is focused into the trap region yielding an intensity of 2 MW/cm² and a recoil heating rate of only 18 pK/sec. The intensity noise heating time constant as determined from the laser noise power spectrum is many tens of thousands of seconds. The position noise is actually not measurable with our detection baseline noise. We observe heating rates less than 5 nK/sec over 200 seconds and a trap lifetime of 400 seconds.

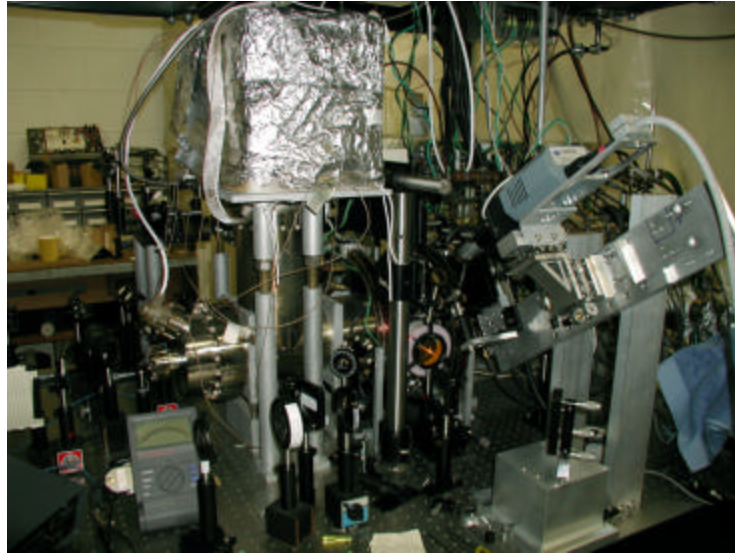
Experimental Setup



The experiment employs ZnSe windows and lenses to focus the CO₂ laser beam into the trap region. The laser trap is loaded from a standard 6-Li MOT and then all optical beams are extinguished leaving only the infrared CO₂ laser trap. The CO₂ laser beam is recollimated and retroreflected with a rooftop mirror, increasing the trap laser intensity during the loading phase. This increases the loaded number of atoms by a factor of 3 to about 3.5 million.

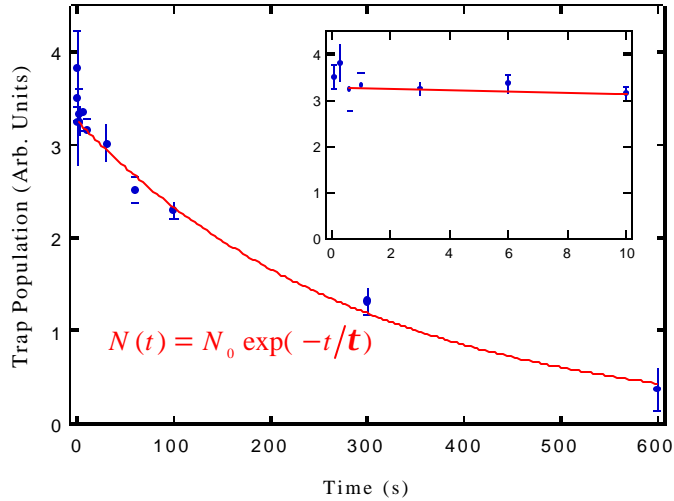
The backgoing beam is slowly blocked during free evaporation, producing a sample of atoms in a single beam trap. Then the trap is slowly lowered to achieve forced evaporation to degeneracy. Finally, the trap is recompressed to full depth. The atoms are then released from the trap and a picture of the cloud is obtained by time-of-flight absorption imaging.

Experimental Apparatus



The essential features of the trap region include a CCD camera, top right, and a large ion pump with a sublimation pumping region. The orange ZnSe entrance window is observable on the right.

Trap Lifetime



$\tau \cong 300$ sec

Optical Trap with a
Lifetime Consistent
with 10^{-11} Torr

O'Hara et al., Phys. Rev. Lett. **82**, 4204 (1999)

Using our original custom built stable CO2 laser, we achieved trap 1/e lifetimes of 300 seconds, surpassing previous traps by nearly two orders of magnitude.

This was the first all-optical trap to achieve a lifetime comparable to the background gas limit at 10^{-11} Torr.

Enhanced Loading of CO₂ Laser Trap

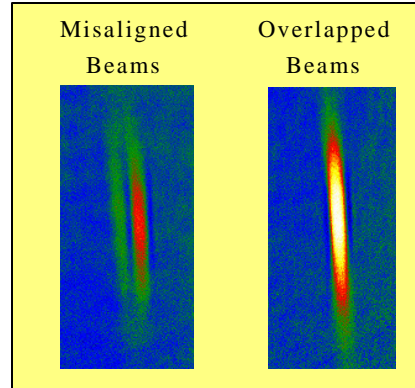
- Optical trap in thermal and diffusive equilibrium with MOT:

$$W_{eq}(\mathbf{x}, \mathbf{p}) = \frac{n_{MOT}}{(2\pi m k_B T)^{3/2}} \exp\left[-\frac{H(\mathbf{x}, \mathbf{p})}{k_B T}\right]$$

$$n(\mathbf{x} = 0) = n_{MOT} \exp\left[\frac{U_0}{k_B T}\right]$$

- Loading dynamics:
Fokker-Planck Equation
- Neglects Density Dependent Loss

Phys. Rev. A **63**, 043403 (2001)

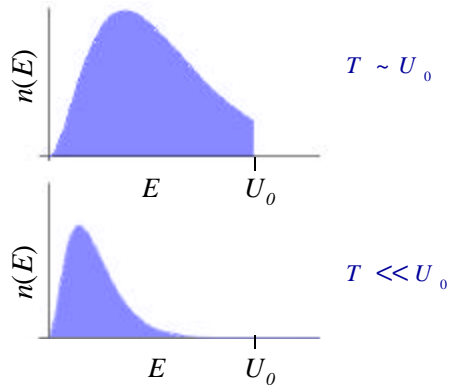


- Factor of 3 increase in trap number
- Routinely load 3.5×10^6 atoms

During the loading phase, the retroreflected and forward CO₂ laser beams are overlapped. When they are misaligned, as shown on the left, the number of atoms in the weaker backgoing trap is only about 50 % of that contained in the forward trap. Overlapping the beams (right) increases the total number by a factor of 3 compared to the forward trap alone, suggesting that the Boltzmann factor plays an important role in the loading phase.

Evaporation in an Optical Trap

- Evaporation from a Well of Fixed Depth:



- Evaporation Rate $\propto \exp(-U_0 / T)$

Evaporation Stagnates for $T \cong \frac{U_0}{10}$

Once our stable optical trap was developed, we chose evaporation as the second cooling method as it has been successfully applied to achieve Bose-Einstein condensation. In a trap of fixed depth, hot atoms leave the trap. The remaining atoms rethermalize by collisions to lower temperature. However, as the thermal energy becomes small compared to the trap depth U_0 , the number of atoms with enough energy to leave the trap is suppressed by a Boltzmann factor, and the evaporation stagnates.

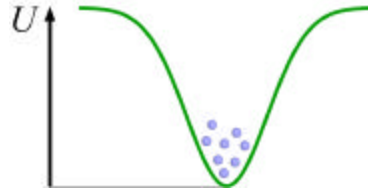
Forced Evaporation: Scaling Laws

Adiabatic Decrease of CO₂ Laser Power

– Energy Loss Rate:

$$\dot{E} = (U + k_B T) \dot{N} + \frac{\dot{U} E}{U} \frac{1}{2}$$

↑ Evaporation Work Done by Potential



– Energy in Harmonic Oscillator Limit

$$E = 3Nk_B T \Rightarrow \dot{E} = 3\dot{N}k_B T + 3Nk_B \dot{T}$$

– Assume Stagnation is Maintained:

$$\frac{U}{kT} = \mathbf{h} = \text{constant} \approx 10$$



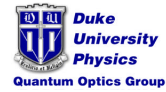
$$\frac{N_f}{N_i} = \left(\frac{U_f}{U_i} \right)^{\frac{3}{16}}$$

To cool further, it is necessary to force evaporation by lowering the trap laser intensity. The question is whether to lower by a factor 10 or 10,000 and how fast. To answer this question, we developed a simple scaling law theory of trap lowering based on the energy loss rate. The energy leaving the trap arises from two sources. The first is evaporation. The evaporation power is the number of atoms per second leaving the trap multiplied by the energy taken away per atom.

This energy is the order of the trap depth U plus some thermal energy.

In addition, the atoms do work on the trap potential as it is lowered. This latter term assures that the phase space density does not change as the trap is lowered without evaporation. The important point is that the phase space density is not lost as the trap is lowered, and increases by evaporation exactly as in a magnetic trap using a radiofrequency knife method. Assuming the atoms behave as classical harmonic oscillators, and assuming that the ratio of the trap depth to thermal energy is a large constant (as is typical in optical traps), these equations are readily solved.

Evaporative Cooling: Scaling Laws



Phase Space Density w.r.t. Well Depth:	$\frac{r_f}{r_i} = \left(\frac{U_i}{U_f}\right)^{1.3}$	$h \cong 10$
Phase Space Density w.r.t. Atom Number:	$\frac{r_f}{r_i} = \left(\frac{N_i}{N_f}\right)^{6.8}$	$r_i = 2.5 \times 10^{-3}$
Collision Rate w.r.t. Well Depth:	$\frac{g_f}{g_i} = \left(\frac{U_f}{U_i}\right)^{0.7}$	$\frac{U_i}{U_f} = 100$
		\Downarrow
		$r_f = 1$

O'Hara et al, Phys. Rev. A **64** 051403 (2001)

The results of the scaling laws show that the phase space density increases as the inverse power of the trap depth to the 1.3 power. Decreasing the trap depth by a factor of 100 increases the phase space density by a factor of 400. Since our initial phase space density is 8×10^{-3} , degeneracy is readily obtained. The results also show that little number loss is needed in the ideal case.

Scaling Laws vs. Boltzmann Equation

S-Wave Boltzmann Eqn.

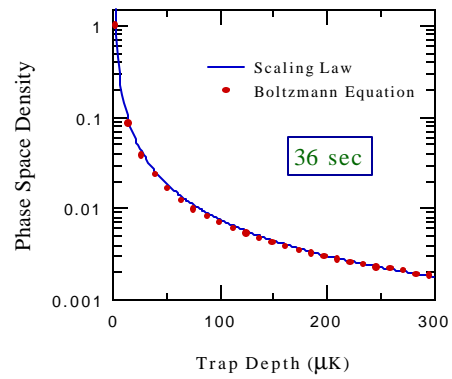
- Includes Time-Dependent Potential,
- Gaussian Potential,
- Background Gas Collisions,
- Fermi Statistics (Pauli Blocking)

To Maintain $U = \hbar k_B T$:

$$U(t) = U_i \left(\frac{1}{1 + t/\mathbf{t}} \right)^{1.45}$$

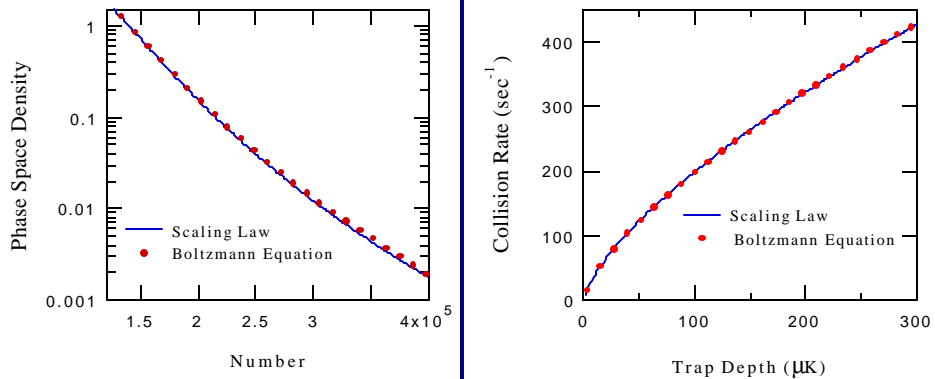
$$\mathbf{t} = 1.2 \text{ sec}$$

Scaling Law vs. Boltzmann Eqn:



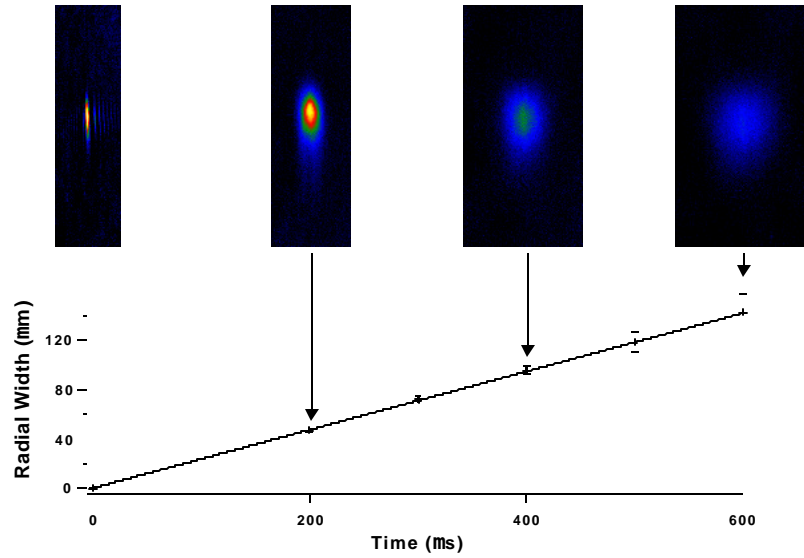
Comparing the scaling law results to an S-wave Boltzmann equation model, including Fermi statistics and the gaussian laser beam trap potential, shows excellent agreement. To maintain a constant ratio of trap depth to thermal energy, the trap is lowered in a special way.

Scaling Laws vs. Boltzmann Equation



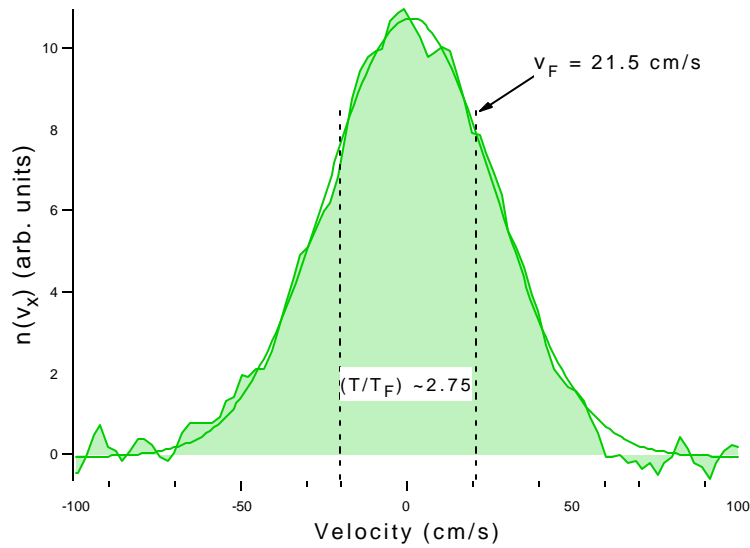
The Boltzmann model calculations take several hours on a fast computer, while the scaling law results are analytic and take just a few seconds to plot. Hence, the scaling law should be used when the s-wave Boltzmann equation is valid. Of course, if sufficient ergodicity does not hold, both the Boltzmann and scaling law results can be invalid.

Time-of-Flight Temperature Measurement



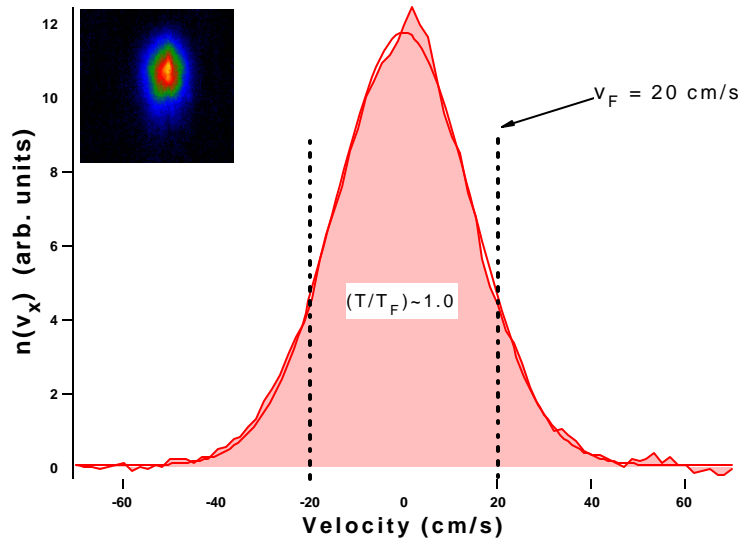
Releasing the atoms from the trap, by turning off the trap laser in a microsecond, enables time of flight absorption imaging to determine the velocity distribution and temperature. The linear relation between the cloud radius and the time of flight shows that the imaging method is working correctly.

1-D Velocity Distribution at $t=0$ sec



Initially, 1.2 million atoms at a temperature of 50 microkelvin are contained in the trap after free evaporation at full trap depth. The Fermi temperature is about 16 microkelvin and the gas is at a temperature of 50 microkelvin, in the classical regime.

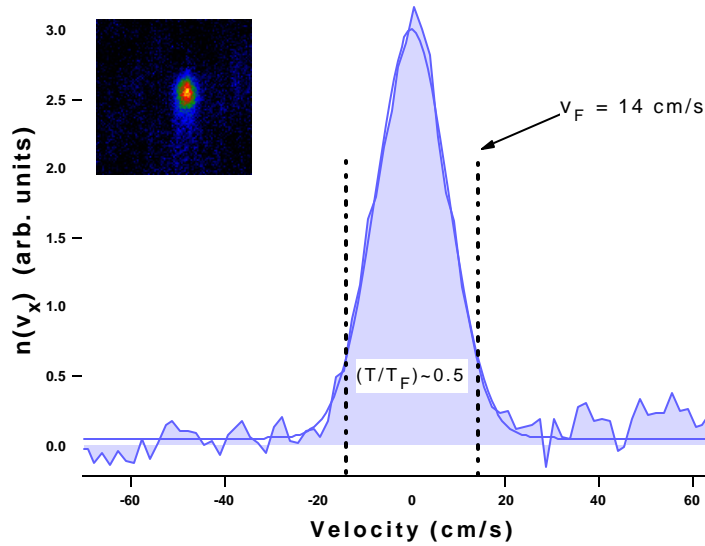
1-D Velocity Distribution at $t=10$ sec



Lowering the trap for 10 seconds by a factor of about 20 greatly increases the phase space density. The trap is recompressed to full trap depth and the cloud is released to determine the velocity distribution. The number of atoms is reduced to 800,000, the Fermi temperature changes to 15 μ K and the gas is at a temperature of 15 μ K, nearing degeneracy.

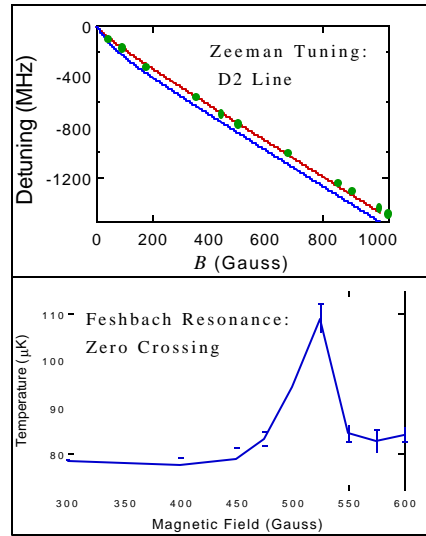
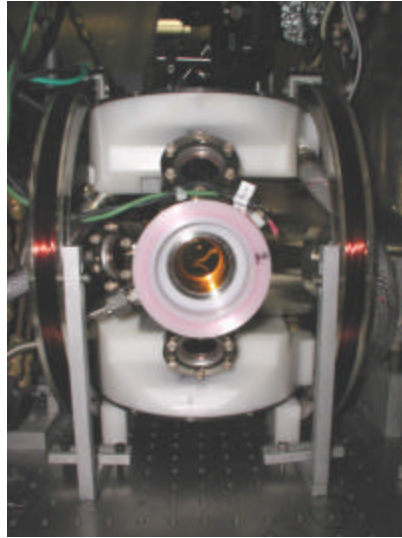
Degeneracy is attained after 40 seconds of evaporation. With 300,000 atoms remaining, the ratio of the temperature to the Fermi temperature is 0.55.

1-D Velocity Distribution at $t=60$ sec



Lowering the trap for a total of 60 seconds, and recompressing to full trap depth leaves 100,000 atoms in the trap. The Fermi temperature is 8 microkelvin, the atom temperature, determined using a Thomas-Fermi model, is 4 microkelvin, and the gas is degenerate.

High-Field Magnet Experiments



Following the publication of our paper on achieving all-optical production of a degenerate Fermi gas, we installed a new high field magnet system (white coils, top and bottom). This permits fields up to 1100 gauss in the trap region. Zeeman tuning curves are in good agreement with theory.

The location of the Feshbach resonance is important for superfluidity studies. Since the scattering length is negative at moderate B-fields and increases rapidly to a positive value just before the Feshbach resonance, the scattering length and hence the evaporation rate must pass through zero at some magnetic field. The predicted value is between 500 and 600 gauss. By loading the trap and performing free evaporation at fixed trap depth for various magnetic fields, we find the zero crossing is near 520 gauss in our initial measurements.

Summary

- Many Applications of Trapped Fermi Gases
 - Long Coherence Lifetimes in Single Component Mixtures
 - Super-High Temperature Superconductor in Two State Mixtures
- Two-State ${}^6\text{Li}$ Mixtures Suitable for Superfluid Transition
 - Stable mixtures with large attractive interaction
 - Require optical trap
- Stable CO_2 Laser Trap
 - Identified and minimized non-optical sources of heating
 - Confinement of stable two-state ${}^6\text{Li}$ mixtures
 - Demonstrated lifetime consistent with pressure $< 10^{-11}$ Torr
- Evaporation in Optical Traps
 - Scaling laws for adiabatic lowering
 - Forced evaporative cooling of ${}^6\text{Li}$ to degeneracy
 - Study of Resonant Interactions

Future Plans

- **Degeneracy**
 - Forced Evaporation to $T \ll T_F$
 - Collective Oscillations and Damping (Spin-Dipole Mode)
- **Feshbach Resonance**
 - Phase Separation
 - Mechanical Stability
 - Three-Body Recombination
- **Superfluidity**
 - Collective Oscillations and Damping
 - Molecular Condensate
 - Crossover from BCS to BEC
- **Coherence Lifetime at Low Temperature**
 - Fermionic Superposition States

Magnetism in a lattice of spinor Bose condensates

K. Gross, C. P. Search, H. Pu, W. Zhang, and P. Meystre
University of Arizona
Tucson, AZ 85721

Condensates of ^{87}Rb confined at each site of an optical lattice behave like mesoscopic spin magnets that can interact with each other through both magnetic and light-induced dipolar interactions. We show that for a blue-detuned lattice, such an array of spin magnets, can undergo a ferromagnetic or an antiferromagnetic phase transition, depending on the dimensionality of the confining lattice. We discuss the ground state spin configuration and related magnetic properties of these systems.

Towards Testing Fundamental Physics with Ultracold Bosons and Fermions

Kai Dieckmann

Wolfgang Ketterle

Dave Pritchard

Massachusetts Institute of Technology
The Center for Ultracold Atoms at MIT and Harvard



\$\$\$: NASA, NSF, ARO, ONR, DLPF

2002 NASA/JPL Workshop on Fundamental Physics in Space

10 May, 2002

Part 1

Contrast Interferometry Using Bose-Einstein Condensates to Measure h/m and α

S. Gupta, K. Dieckmann, Z. Hadzibabic, and D.E. Pritchard,

cond-mat/0202452, 25 Feb 2002

Route to a high precision measurement of the fine structure constant α

(B. Taylor, 1994)

Atomic physics:

0.008 ppb: hydrogen spectroscopy, (Udem et al., 1997; Schwob et al., 1999)

QED corrections not needed for current precision goal!

$$\alpha^2 = \left(\frac{e^2}{\hbar c} \right)^2 = \frac{2R_\infty}{c} \frac{h}{m_e} = \frac{2R_\infty}{c} \frac{m_p}{m_e} \frac{m}{m_p} \frac{h}{m}$$

Na: 0.17 ppb: penning trap mass spectr.

(Bradley et al., 1999)

Cs: 0.12 ppb: frequency comb

(Udem et al., 1999)

$$\omega_{\text{rec}} = \frac{1}{2} \frac{\hbar}{m} k^2$$

Atom Interferometry

Cs: (Young et al., 1997): 56 ppb

(Hensley, PhD Thesis, 2001): 6 ppb

2 ppb: penning trap mass spectroscopy

(Farnham et al., 1995)

Application for Bose-Einstein condensates

Why using BEC?

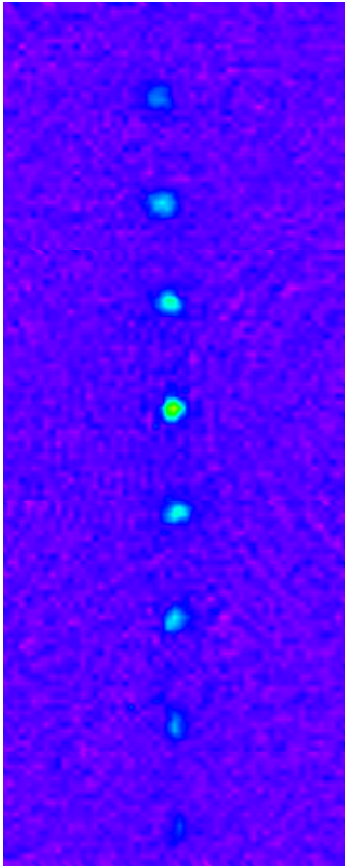
- sub recoil momentum distribution:

Kapitza-Dirac & Bragg scattering with single internal state



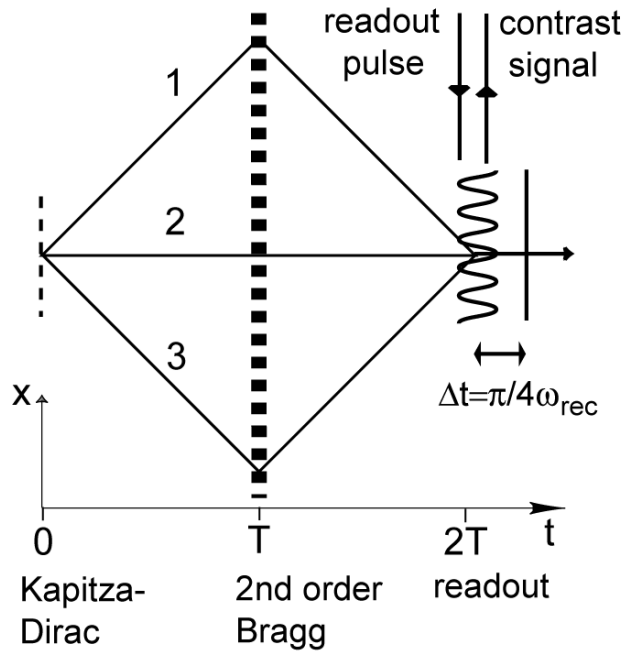
reduced systematics, e.g. AC-Stark effect

- bright source \Rightarrow good S/N



Kapitza-Dirac scattering

Demonstrating a new contrast interferometer with BEC



Advantages:

- no sensitivity to mirror vibrations, ac stark shift, rotation, magnetic field gradients
- quadratic enhancement with additional momenta
- single shot acquisition of interference pattern

The phase of the matter wave grating is encoded in oscillating contrast.

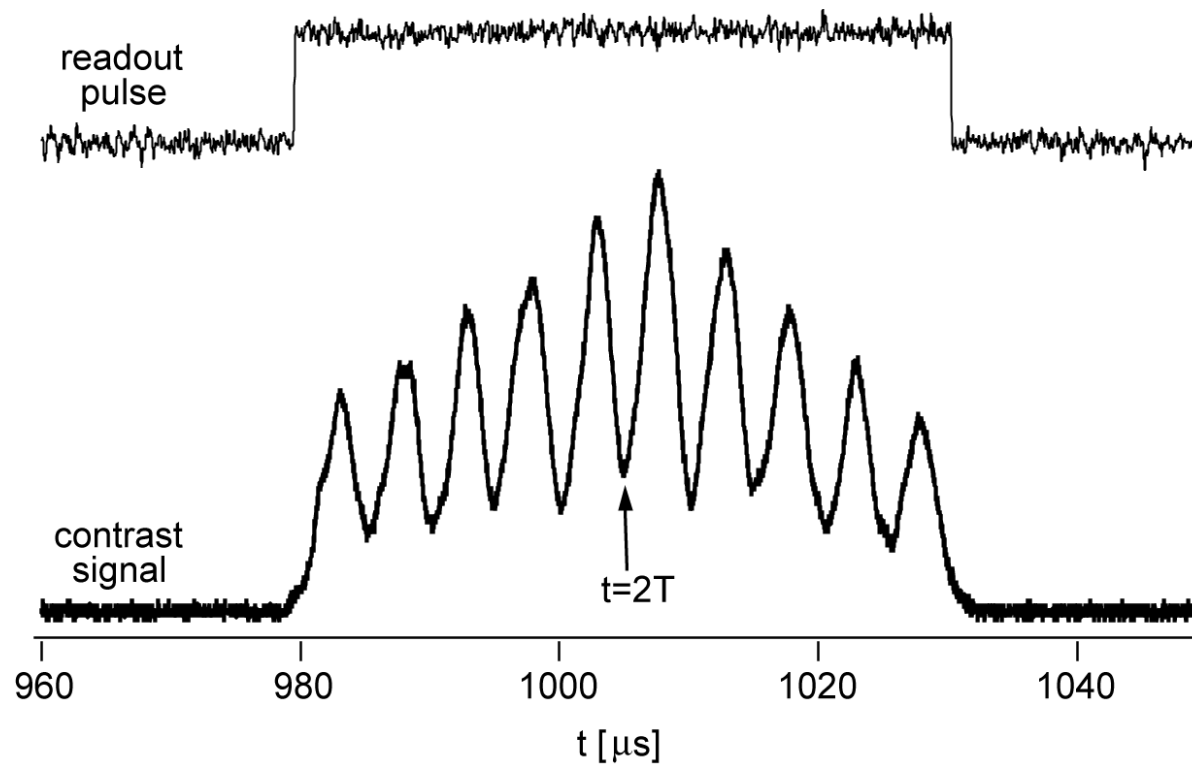
$$S(T, t) = C(T, t) \sin^2 \left(\frac{\Phi_1(t) + \Phi_3(t)}{2} - \Phi_2(t) \right) = C(T, t) \sin^2 (8\omega_{rec} T + 4\omega_{rec} \Delta t)$$

The phase of the contrast signal for various T gives ω_{rec} .

The contrast interferometer signal

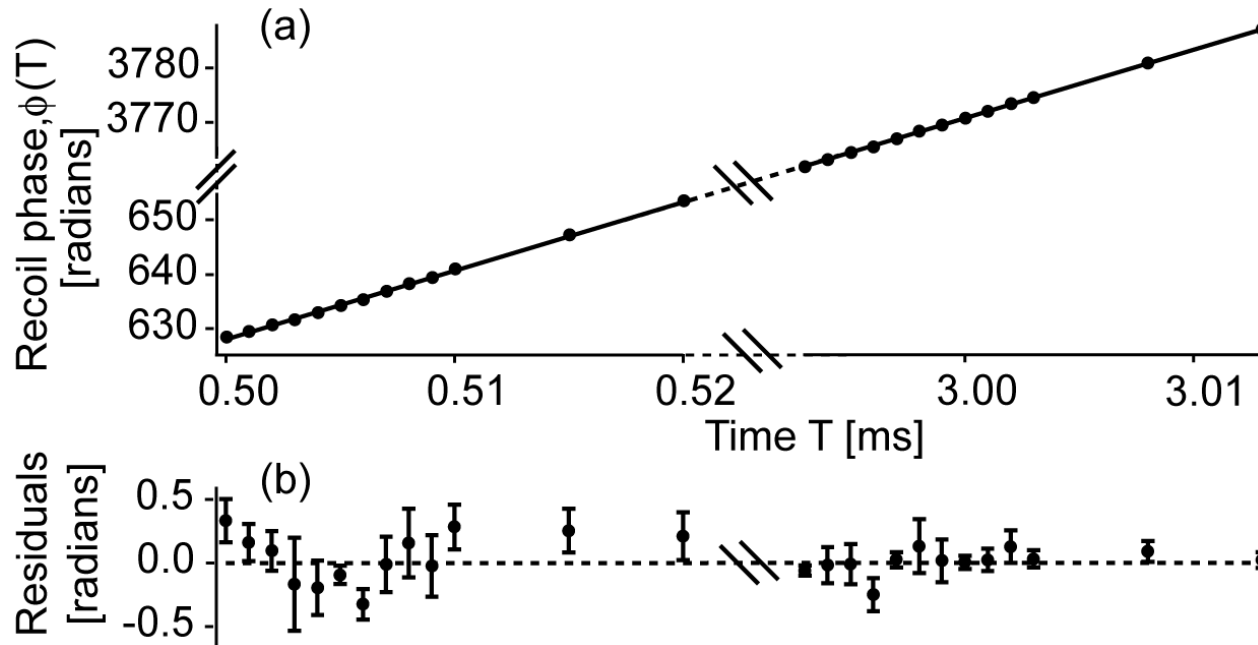
Demonstration of the principle was realized in BEC1 machine (sodium).

Single shot:



fit of central fringes: 10 mrad uncertainty

Determination of the recoil frequency



$$\omega_{\text{rec,Na}} = 2\pi \times 24.9973 \text{ kHz} (1 \pm 1.5 \times 10^{-5})$$

- precision: shot to shot fluctuations of 200 mrad
- accuracy: deviations on the 100 ppm level

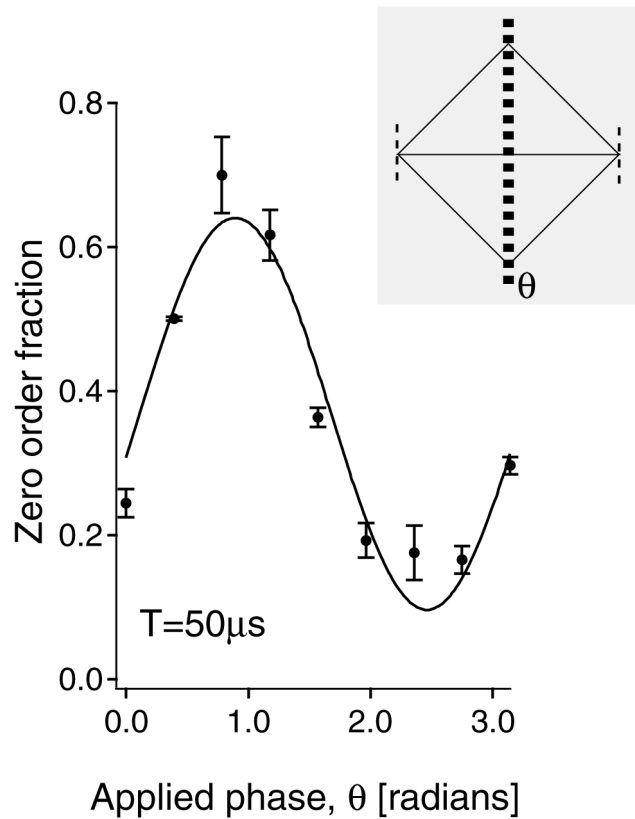


systematics:

- spurious gratings
- mean field energy

Contrast interferometry is insensitive to mirror vibrations

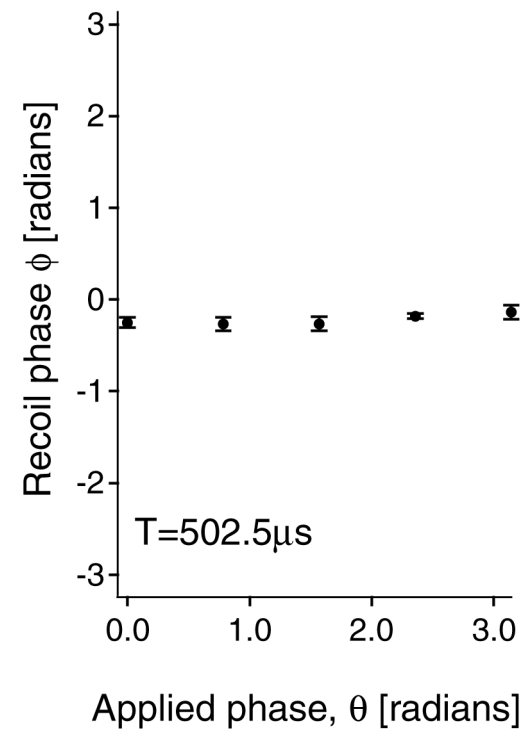
phase sensitive interferometer with variation of the light phase



no visibility at $T=3\text{ms}$

Contrast interferometer with variation of the light phase

$$S(T, t) = C(T, t) \sin^2 \left(\frac{\Phi_1(t) + \Phi_3(t)}{2} - \Phi_2(t) \right)$$



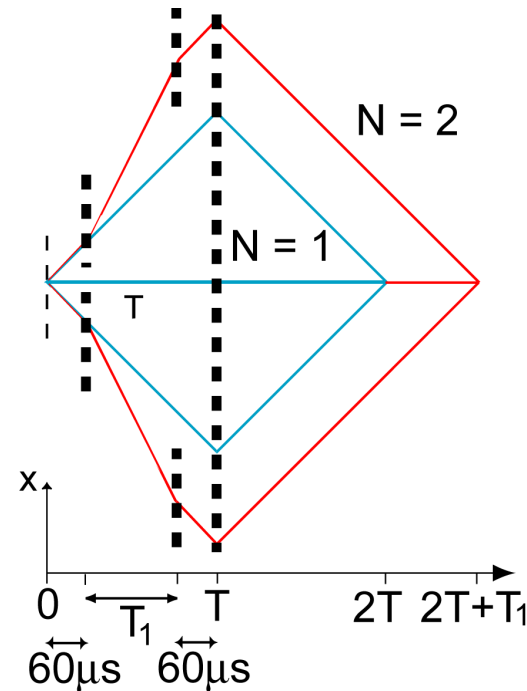
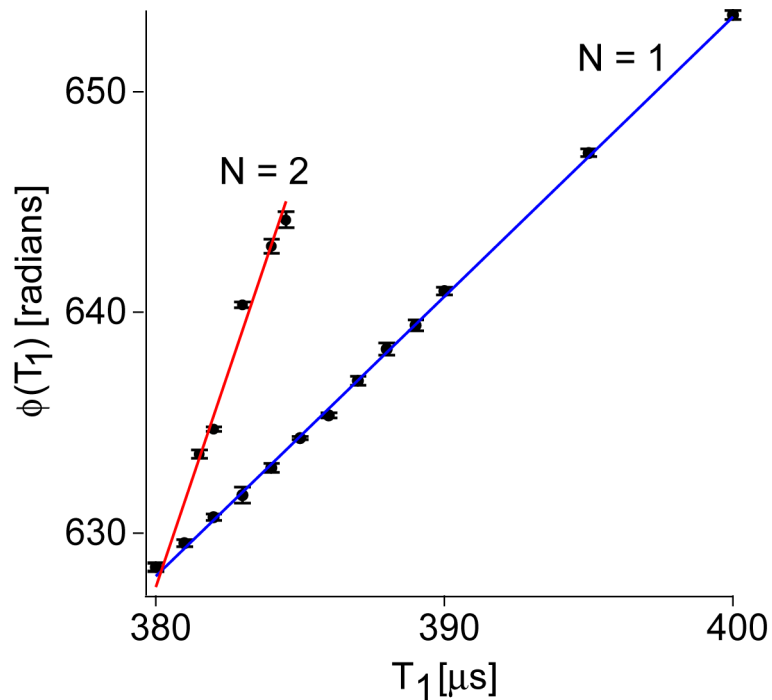
Enhancing the sensitivity

sensitivity $\sim k^2 \sim E$

So far: $|\pm 2\hbar k\rangle$ during time T , $N=1$

Now: $|\pm 4\hbar k\rangle$ during time T_1 , $N=2$

Deceleration necessary, as readout is only sensitive to $|\pm 2\hbar k\rangle$ states.



ratio of the slopes:

$$\frac{\partial \Phi}{\partial T_1} = 2 \times 2^2 \omega_{\text{rec}} = 8 \omega_{\text{rec}}$$

$$\frac{\partial \Phi}{\partial T_1} = 4^2 \omega_{\text{rec}} + (1+1) \times 2^2 \omega_{\text{rec}} = 24 \omega_{\text{rec}}$$

experiment: 3.06

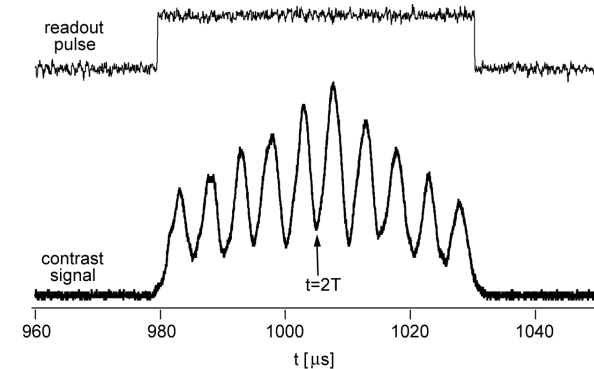
precision in timing is needed

Conclusions & Outlook

Part 1

- BEC is a useful source for atom interferometry
- new contrast interferometer scheme demonstrated
- basic advantages demonstrated:

insensitivity to vibrations
quadratic sensitivity to transferred momentum
single shot signal acquisition



Precision \propto measurement in a future setup ?

- precision: promising for scaling in a fountain setup

$$T=100\text{ms}, N=20 \rightarrow 1\text{ppb}$$

- accuracy: study of systematics

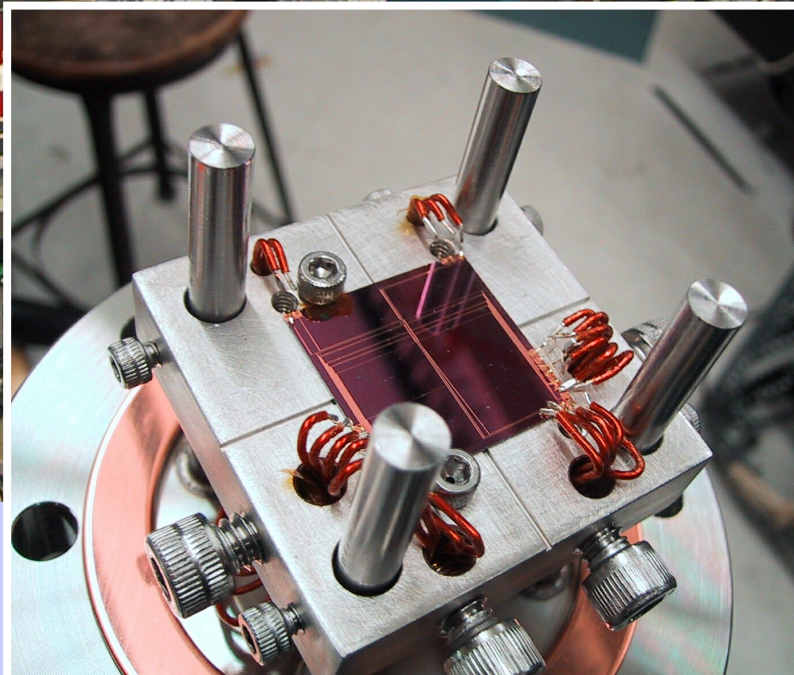
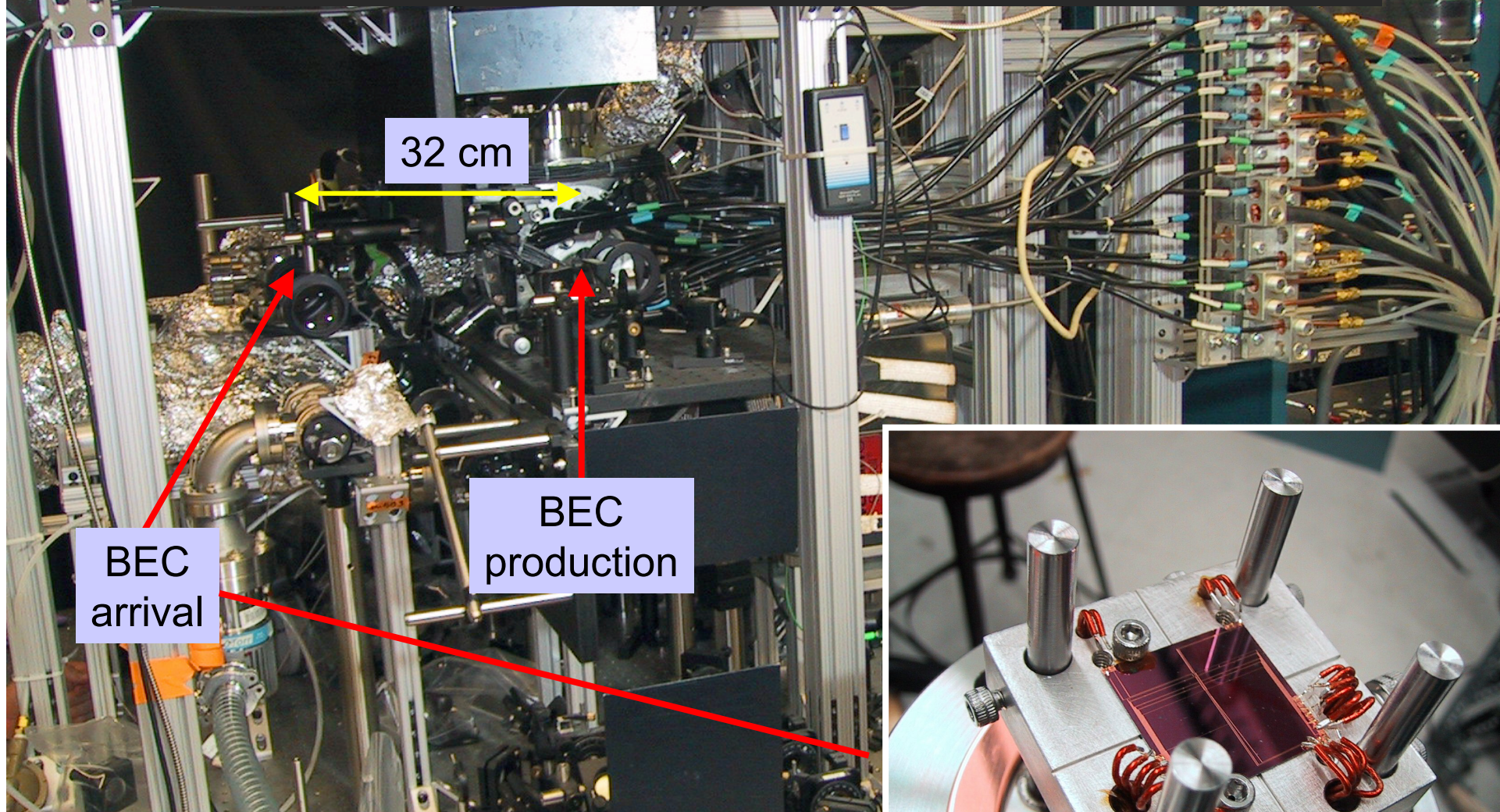
mean field effects
spurious gratings

Part 2

Propagation of Bose-Einstein condensates in a magnetic waveguide

A.E. Leanhardt, A.P. Chikkatur, D. Kielpinski, Y. Shin, T.L. Gustavson,
W. Ketterle, D.E. Pritchard

Loading sodium BECs into atom chips with optical tweezers

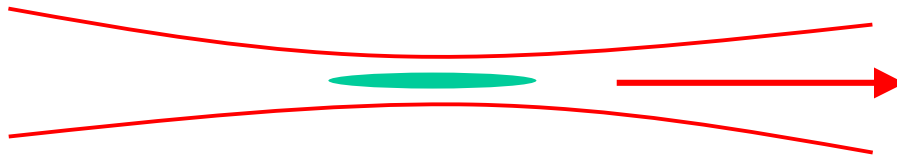


T.L.Gustavson, A.P.Chikkatur, A.E.Leanhardt, A.Görlitz, S.Gupta, D.E.Pritchard, W. Ketterle, Phys. Rev. Lett. **88**, 020401 (2002).

Loading a waveguide with a BEC

Loading:

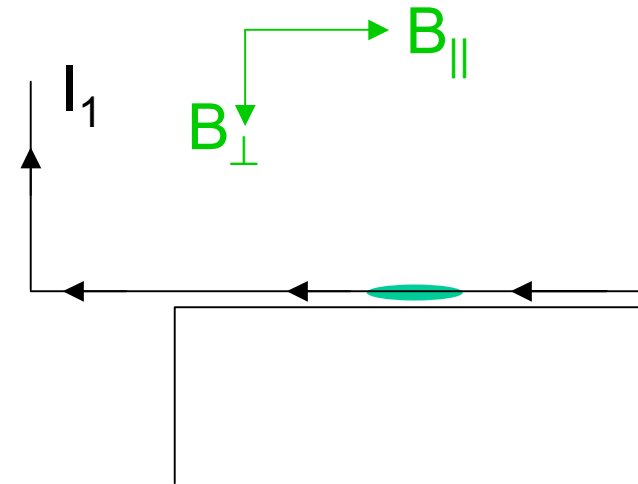
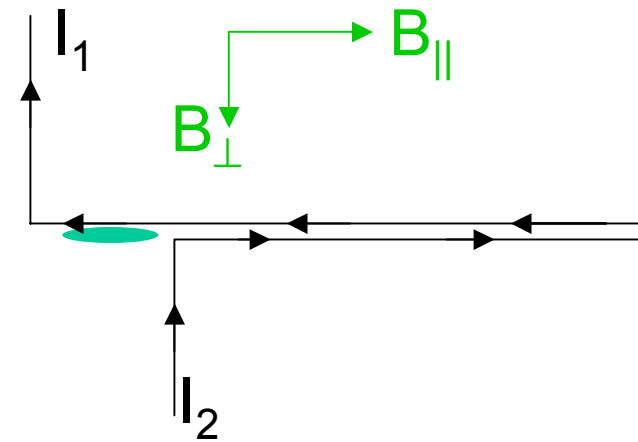
optical dipole trap:



Waveguide:

Turning off I_2 allows the BEC to propagate down the single-wire waveguide

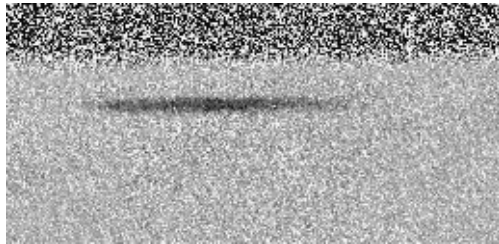
Z-wire trap: $\sim 2 \times 10^6$ Na BEC



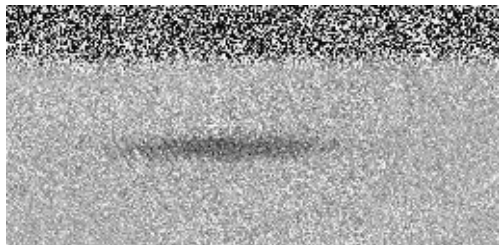
Excitationless “single mode” propagation

$$\omega_{\text{radial}} \sim 2\pi \times 600 \text{ Hz}, r_{\text{surface}} \sim 200 \mu\text{m}, N \sim 10^6$$

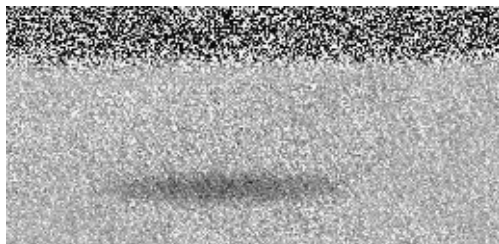
just after release from Z-wire trap



5 ms TOF

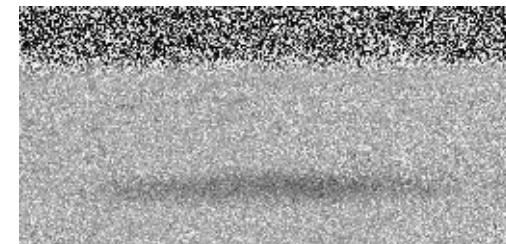
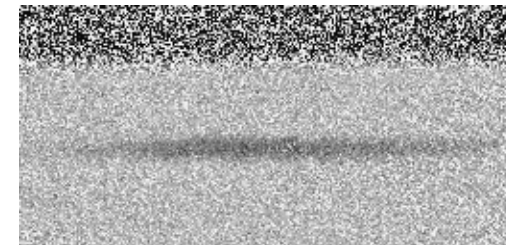
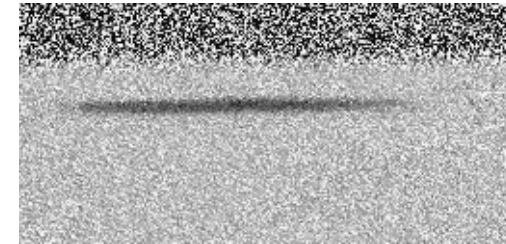


8 ms TOF



← 2 mm →

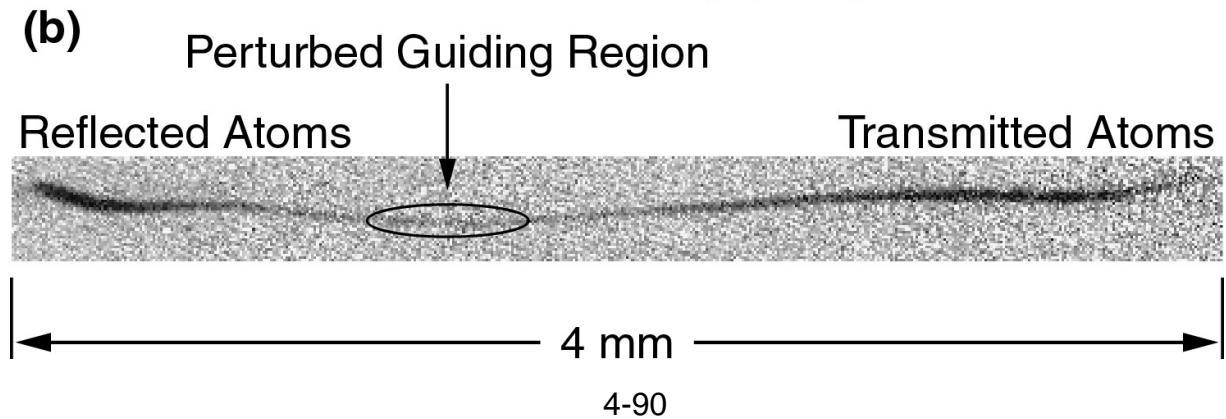
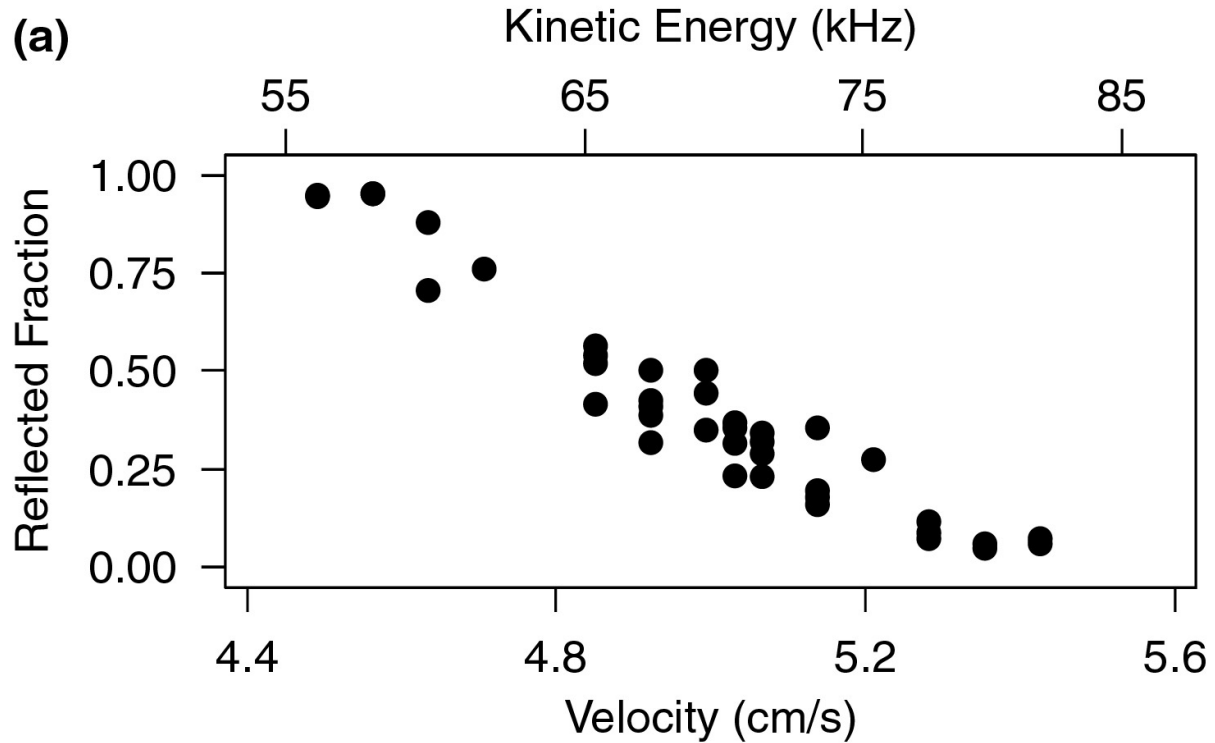
after 100 ms and 4 mm
(speed ~ 4 cm/s)



← 2 mm →

Reflection of BEC from waveguide perturbation

Perturbation (displacement of the wire) $\begin{cases} \text{reflection} \\ \text{excitation} \end{cases}$



Part 3

Two-species Mixture of Quantum Degenerate Bose and Fermi Gases

Z. Hadzibaic C. A. Stan, K. Dieckmann, S. Gupta, M. W. Zwierlein, A. Görlitz,
and W. Ketterle,

PRL, 88, (2002), #160401

Mixed Fermionic and Bosonic System

No s-wave collisions in single-component fermionic cloud \Rightarrow use mixtures

Fermion-Fermion:

- two Zeeman states of ^{40}K (Jin, Boulder, 1999)
- two ZM states of ^6Li (Thomas, Duke, 2001)

Fermion-Boson:

- ^6Li - ^7Li (upper HFS) (Hulet, Rice, 2001; Salomon, Paris, 2001)
- ^6Li - ^7Li (lower HFS) (Salomon, Paris, 2001)
- ^{40}K - ^{87}Rb , (Inguscio, Florence, preprint 2002)

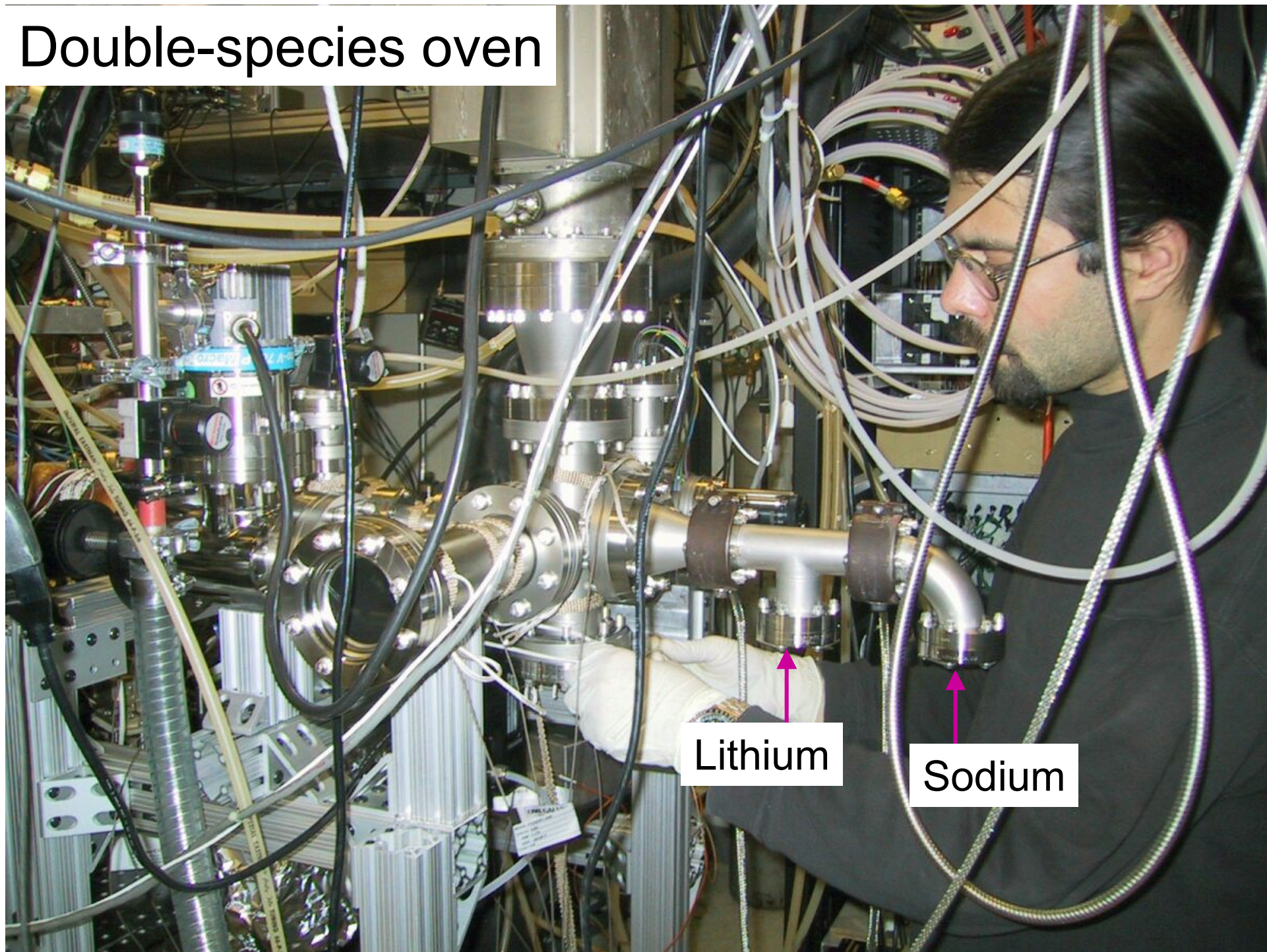
^6Li ^{23}Na

sympathetic cooling with large and stable reservoir

Interacting degenerate Fermions:

- phase separation (Li-Na mixture), (K.Molmer, PRL 80 (1998) 1804)
- suppression of 3 body decay, Feshbach resonance, (M. Houbiers, PRA 57 (1998) R1497)
- resonance super fluidity, Stoof, et al., PRL, 76 (1996) 10, Combescot, PRL, 83 (1999) 3766, Holland, et al., PRL, 87 (2001), 120406-1, ...
- long range interaction in quasi 2D traps, (Petrov)

Double-species oven



Lithium

Sodium

Sympathetic cooling of ${}^6\text{Li}$ by ${}^{23}\text{Na}$ in a magnetic trap

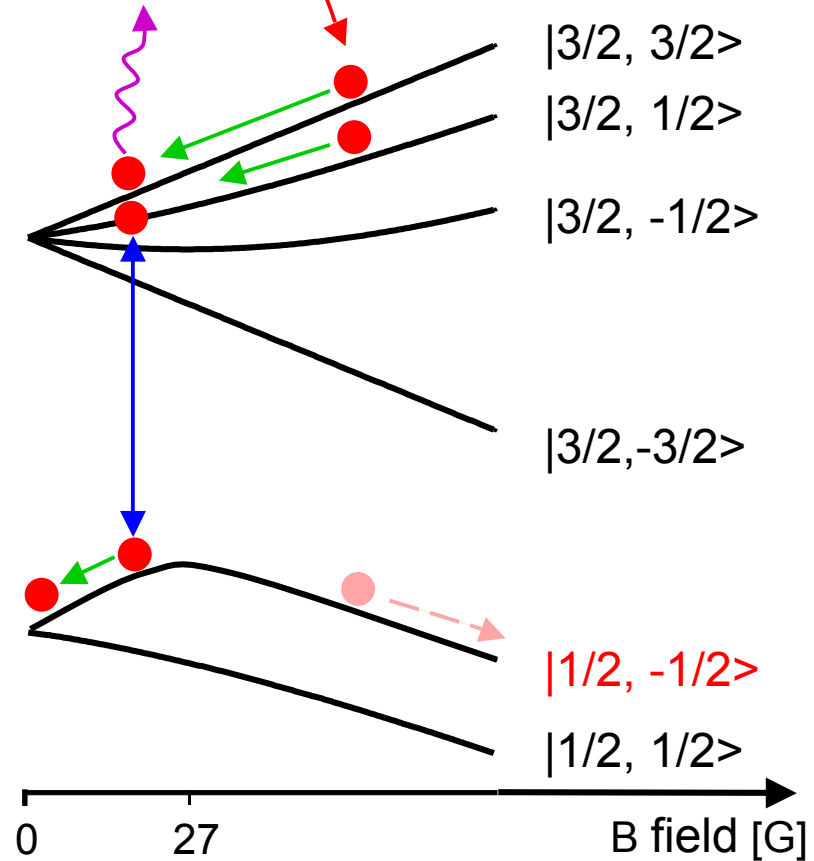
loading & optical pumping:
Li: $N = 5 \times 10^6$, $T = 700 \mu\text{K}$

rapid 5 s forced evaporative cooling
of ${}^{23}\text{Na}$: $|1, -1\rangle$ on hf transition: $50 \mu\text{K}$

hyperfine transfer @ 228 MHz

removal of $|3/2\rangle$ left-overs
by light pulse

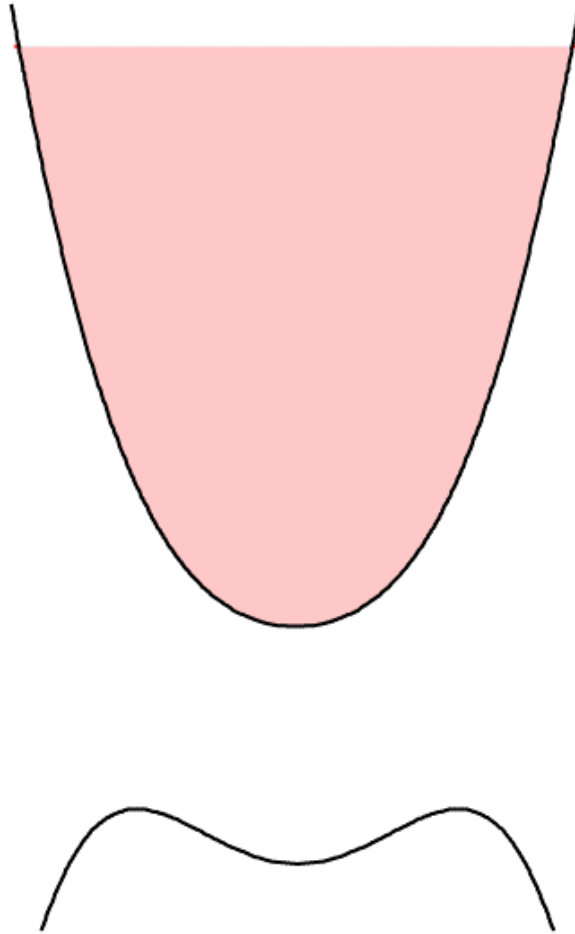
final 10 s evaporation of ${}^{23}\text{Na}$: $< 1 \mu\text{K}$



trap depth for $|1/2, -1/2\rangle$: $27 \text{ G} \cong 330 \mu\text{K}$

Sympathetic cooling of ${}^6\text{Li}$ by ${}^{23}\text{Na}$ in a magnetic trap

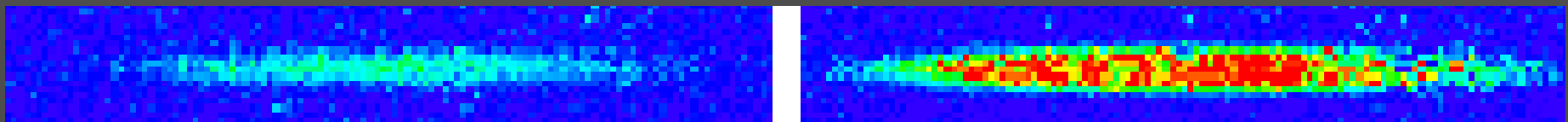
MOT & optical pumping, Li: $N = 5 \times 10^6$, $T = 700 \mu\text{K}$



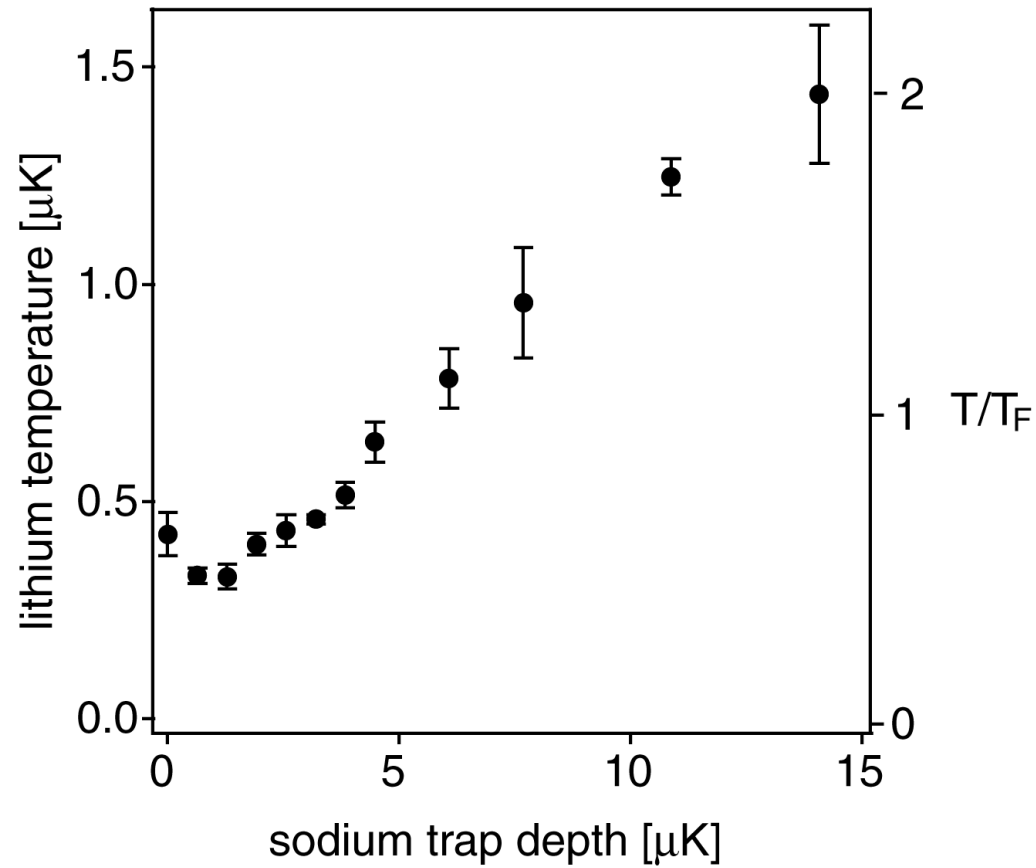
Final stage of sympathetic cooling

Lithium

Sodium



Fermi degeneracy



lithium:

$$N_{\text{Li}} = 1.5 \times 10^5$$

$$T_{\text{Li}} = 330 \text{ nK}$$

$$T_F = 660 \text{ nK}$$

sodium:

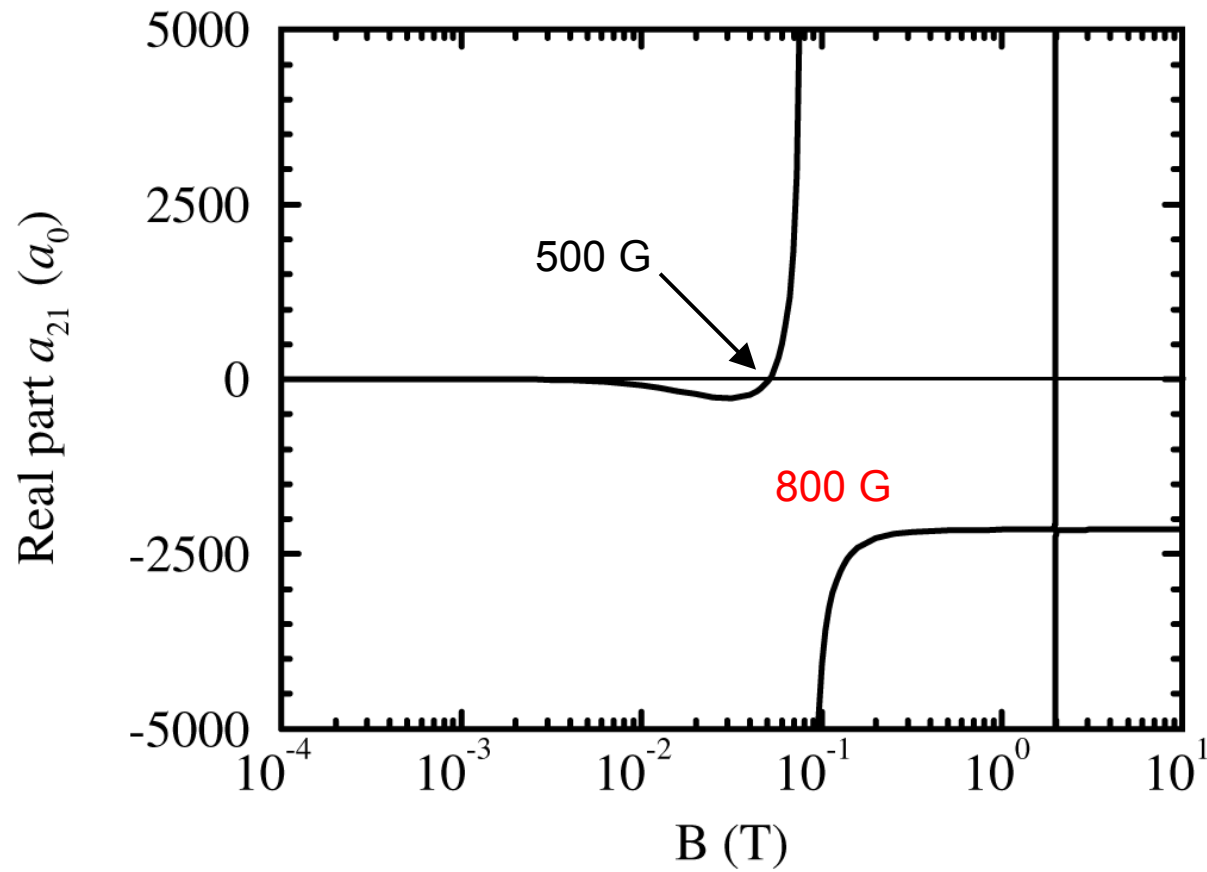
$$N_{\text{Na}} = 2 \times 10^6$$

$$T < 170 \text{ nK}$$

Predicted ${}^6\text{Li}$ Feshbach resonance

Houbiers, et al., PRA 57 (1998) R1497

spin mixture: $|1\rangle, |2\rangle$

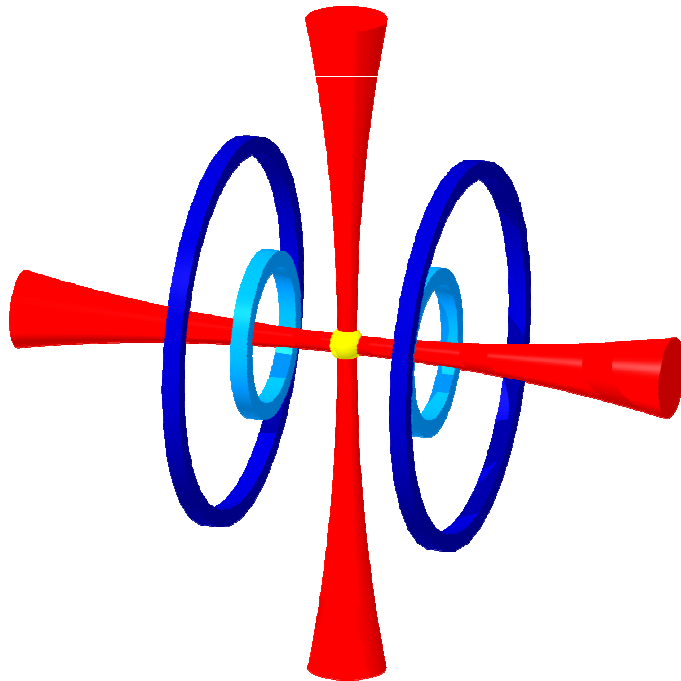


Resonance
superfluidity:

$$\frac{T_C}{T_F} \sim C \exp\left(-\frac{\pi}{2k_F|a|}\right)$$

Optical trapping

0.6 W @ 1064nm



single horizontal beam:

$f = (9, 9, 0.14)$ kHz

$E_{\text{trap}} = 114 \mu\text{K}$

25 s lifetime

magnetic well: $E_{\text{trap}} = 40 \mu\text{K}$

crossed optical dipole trap

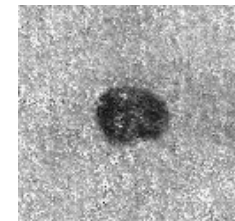
$f = (200, 280, 200)$ Hz

$E_{\text{trap}} \approx 3 \mu\text{K}$

evaporation



Li in ODT



Na in ODT



Time scales

Collisional times:

- single beam optical dipole trap (9 kHz):
- crossed optical dipole trap (200 Hz):

$$a = -2000 a_0$$

$$800 \text{ kHz}$$

$$10 \text{ kHz}$$

$$a = -200 a_0$$

$$8 \text{ kHz}$$

$$100 \text{ Hz}$$



entering the hydrodynamic regime: $\omega\tau_{el} \ll 1$



time resolved observation of elastic scattering very difficult



observe inelastic decay

Na Feshbach resonance:

Stenger et al., PRL 82 (1999) 2422

$$\tau_{\text{decay}} \leq 1 \mu\text{s}$$

Pairing time required:

Stoof et al., PRA 59 (1999) 1556

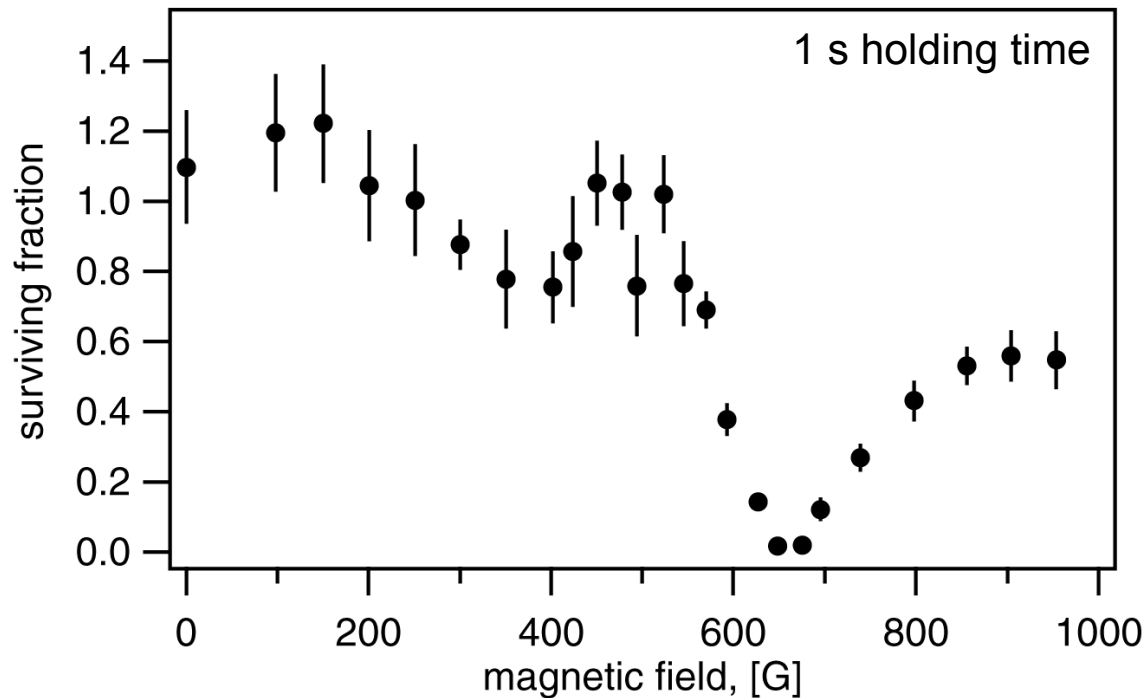
$$\tau_{\text{pairing}} = \frac{h}{k_B T_F} \left(\frac{T_F}{T_C} \right)^2 \leq 10^{-3} \text{ s}$$

suppression 3-body decay due to fermionic symmetry

$$\uparrow + \uparrow + \downarrow = \text{forbidden for s-wave}$$

Observation of resonant behavior of inelastic decay

suppression 3-body decay due to fermionic symmetry



assume 3-body decay:

$$L_{Li-6}(\text{high } a) \leq 10^{-31} \text{ cm}^6 \text{ s}^{-1}$$

$$L_{Rb-87}(\text{low } a) = 2 \cdot 10^{-29} \text{ cm}^6 \text{ s}^{-1}$$

$$L_{Na}(\text{low } a) = 10^{-30} \text{ cm}^6 \text{ s}^{-1}$$

Observed decay is slowest expected time scale!

Conclusions & Outlook

- collisional properties of the mixture are favorable
- Fermi degeneracy: $T = 330\text{nK} = 0.5 T_F$, $N=1.5 \times 10^5$
- optical trapping of spin mixture with long lifetimes
- resonance type of behavior observed in decay
- timescale of decay is long

future investigation:

- understanding of inelastic decay, temperature dependence
- find elastic properties: frequency shifts, phase separation

The Team

- **Graduate students**

Ananth Chikkatur

Deep Gupta

Zoran Hadzibabic

Jamil Abo-Shaeer

Aaron Leanhardt

Claudiu Stan

Kaiwen Xu

Micah Boyd

Erik Streed

Jit Kee Jin

Yong-II Shin

Gretchen Campbell

- **Undergraduates**

Edem Tsikata

Pavel Gorelik

Christian Schunck

- **Postdocs**

Johnny Vogels

Yoshio Torii

Kai Dieckmann

Dominik Schneble

David Kieplinski

- **Prof. D. E. Pritchard**



New Measurement of Cesium Polarizability Using Laser-Cooled Atoms

Single Laser-Cooled Ion Trapping at the University of Washington

Warren Nagourney
University of Washington
Seattle, WA 98195

It is generally accepted that single, laser-cooled ions have some very favorable qualities which greatly aid in ultra-high resolution spectroscopy: They are free from transit-time shifts, Doppler shifts (to all orders), collision shifts and (with appropriate choice of species) are free from magnetic and electric field shifts. As a result, they are excellent candidates for an optical frequency/time standard, where the very high clock frequency together with this freedom from shifts makes an optical standard with an inaccuracy of one part in 10^{18} a reasonable near-term goal. These experiments are facilitated by the use of the "shelving" technique to extract the maximum amount of information from this very small sample of one ion. It is also possible to use "shelving" with single laser-cooled ions to perform extraordinarily precise radio-frequency spectroscopic measurements. This presentation will describe experiments of both types. In particular, optical spectroscopy using single indium ions will be discussed with data presented on moderate-resolution "clock" transition resonances, which should very soon be narrowed by at least a factor of 1000. In addition, the technique of "spin-sensitive-shelving" will be described and recent 15-Hz wide radio-frequency transitions in single barium ions using this method will be presented. Finally, future light-shift and electric-quadrupole-shift measurements in single barium ions will be discussed.

High-Order Inertial Force Phase Shifts for Microgravity Optical Clocks and Inertial Sensors

Kai Bongs

Romain Launay

Mark Kasevich (PI)

Yale University, Dept. of Physics

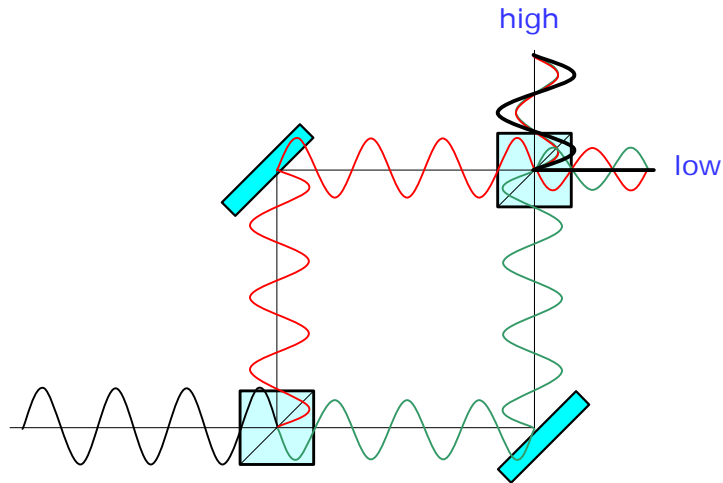
May 2002

Outline

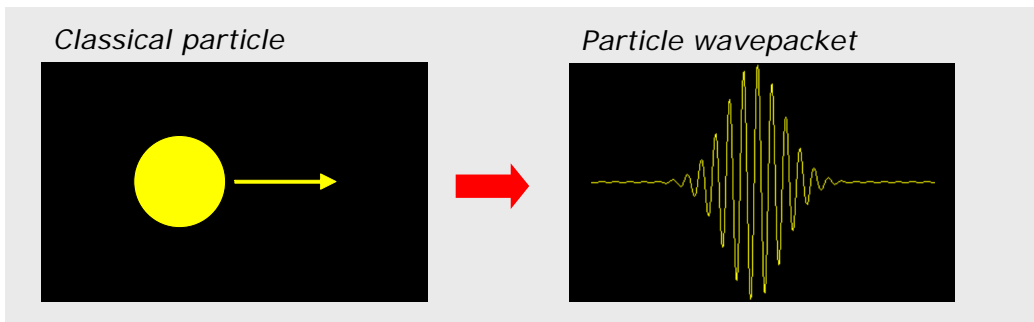
- Introduction to atom interferometry
- Calculation considerations
- Phase contributions in different setups

Interference

- Example: Mach-Zehnder Interferometer



de Broglie Wave Interference



$\lambda = h/p = h/mv$ de Broglie wavelength

h = Planck's constant

m = mass

v = particle velocity

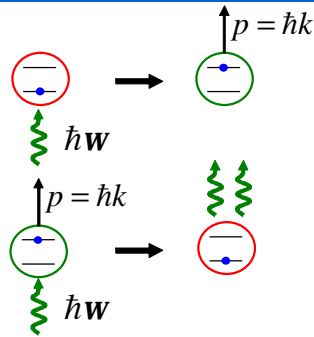
For Cs atoms at $v \sim 1\text{m/s}$:

$$\lambda \sim 10^{-9} \text{ m}$$

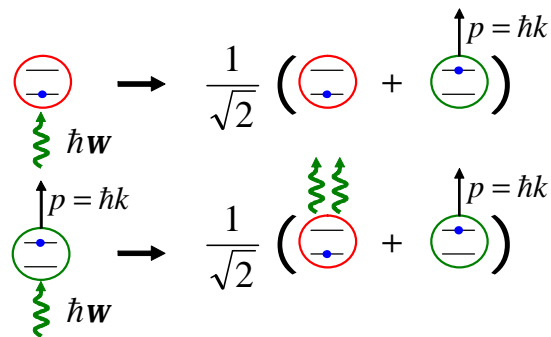
Short-wavelength interferometers are more sensitive to small changes in particle propagation path lengths (induced, for example by external forces)

Light Pulse Mirrors/Beamsplitters

p- pulse -> mirror



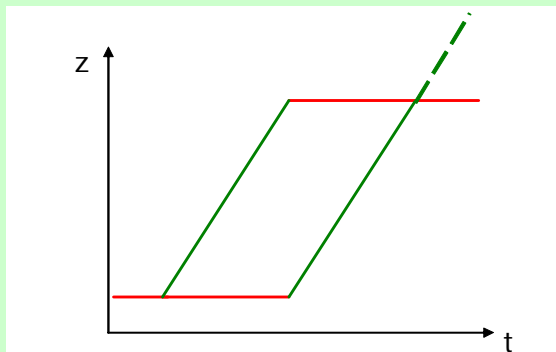
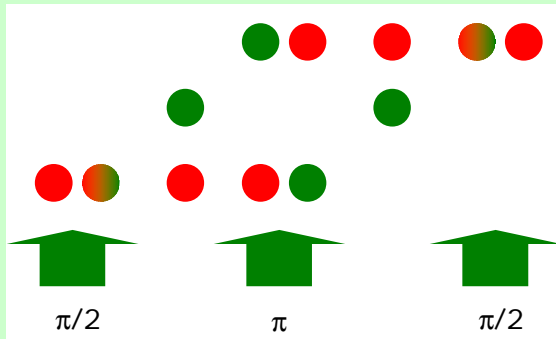
p/2- pulse -> beamsplitter



Light Pulse Atom Interferometer

Phase depends on:

- Rotation
- Acceleration
-> force / gravity sensor
- Frequency detuning -> clock
- Photon recoil
-> h/m measurement
- Background gas
-> collision parameters
- Magnetic / electric field
- Laser phase (e.g. mirror vibrations)
- ...

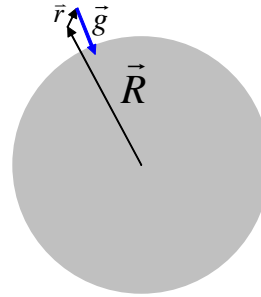


The Gravity Field

- Potential energy Taylor expansion:

$$\begin{aligned}
 U &= -\frac{Gm_a M}{|\vec{R} + \vec{r}|} \\
 &= C - m_a \vec{g} \cdot \vec{r} - \frac{m_a}{2} \vec{r} \cdot \vec{T} \cdot \vec{r} + O(r^3)
 \end{aligned}$$

↑
↑
gravity vector
gravity gradient Tensor



The Gravity Gradient Tensor

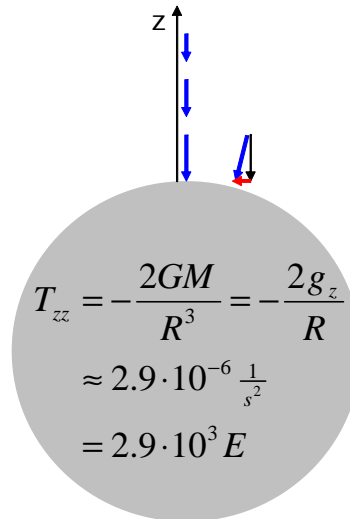
Definition:

$$T_{ij} = \frac{\partial g_i}{\partial j} = \frac{\partial^2 U}{\partial i \partial j}$$

Properties:

$$T_{ij} = T_{ji}$$

$$\text{trace}(\vec{T}) = T_{xx} + T_{yy} + T_{zz} = 0$$



→ 5 independent components

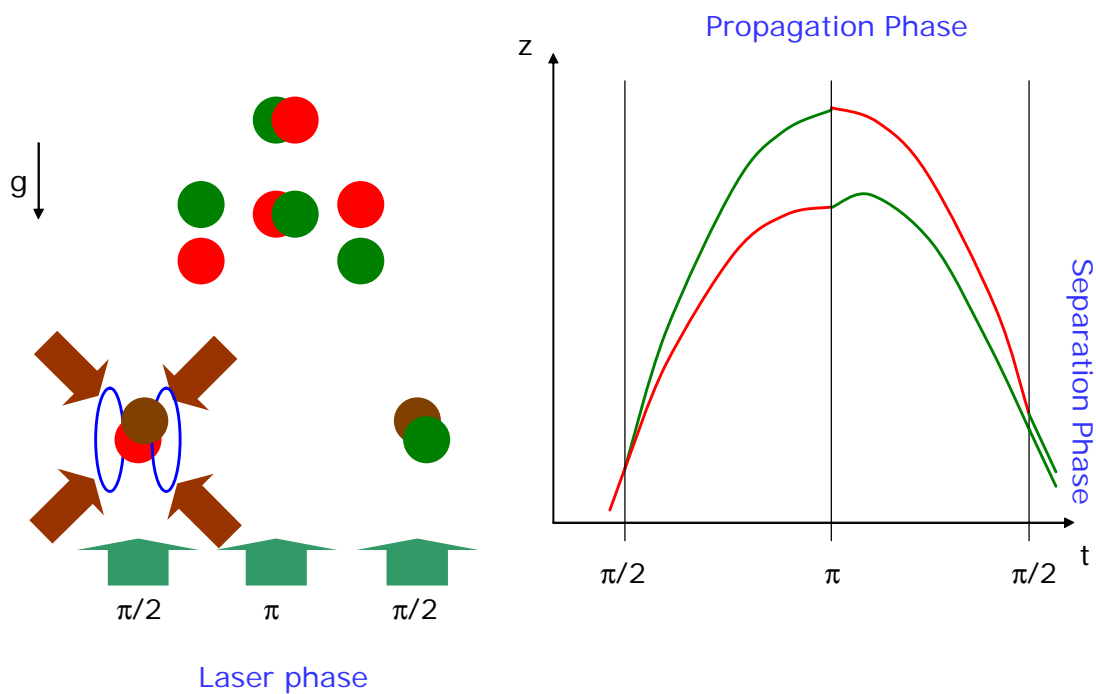
Phase Calculations

- Full quantum mechanic approach, including inertial forces and relativistic effects exists

C. J. Bordé, C. R. Acad. Sci. Paris, t. 2, Série IV, 509 (2001)

- Implement approximations:
 - Easy inversion of phase expressions
 - Coverage of a variety of platforms while avoiding higher order inertial force errors
 - Concentrate on inertial force effects

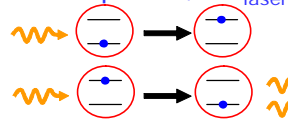
Atom Interferometric Accelerometer



Phase Contributions

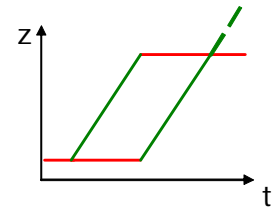
$$\Delta\Phi_{\text{total}} = \Delta\Phi_{\text{laser}} + \Delta\Phi_{\text{prop}} + \Delta\Phi_{\text{sep}}$$

– imprinted laser phase, $\Delta\Phi_{\text{laser}}$

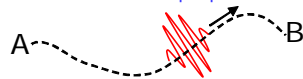


$$\Delta\Phi_{\text{laser}} = \vec{k} \cdot \vec{r}$$

$$\Delta\Phi_{\text{laser}} = -\vec{k} \cdot \vec{r}$$

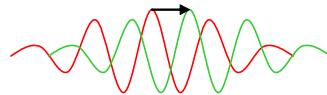


– propagation phase, $\Delta\Phi_{\text{prop}}$



$$\Delta\Phi_{\text{prop}}(AB) = \frac{1}{\hbar} S_{cl,AB} = \frac{1}{\hbar} \int_{t(A)}^{t(B)} L[\vec{r}(t), \vec{v}(t)] dt$$

– separation phase, $\Delta\Phi_{\text{sep}}$

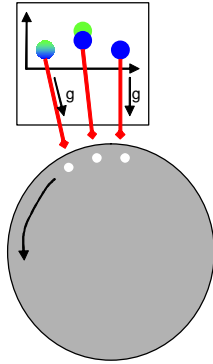


$$\Delta\Phi_{\text{sep}} = \frac{m\vec{v} \cdot \Delta\vec{r}_{\text{sep}}}{\hbar}$$

P. Storey and C. Cohen-Tannoudji, Journal de Physique II, T.4, 1999 (1994)
 E. J. Heller, J. Chem. Phys. **62**, 1544 (1975)

Choice of Frame

Freely falling frame

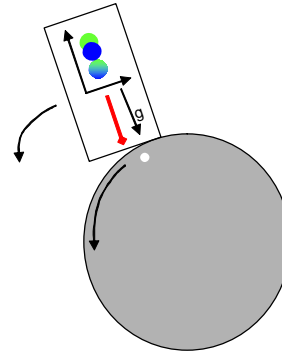


- no analytic classical trajectory if gravity rotates
- higher order errors if one assumes

$$\vec{g}(\vec{r}) = \vec{g}(0) + \vec{r} \cdot \tilde{T}_{gg}$$

- gravity anomalies hard to include

Laboratory frame



- analytic solution of sufficient accuracy, if gravity gradient is treated as perturbation
- platforms moving with constant acceleration included in our treatment
- easy physical insight in phase contributions

Equations of Motion

Neglect gravity gradients in order to get analytic expressions

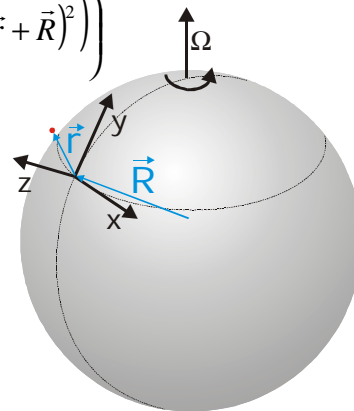
Lagrangian:

$$L(\vec{r}, \vec{v}) = m \left(\frac{v^2}{2} + \vec{g} \cdot \vec{r} + \vec{\Omega} \cdot ((\vec{r} + \vec{R}) \times \vec{v}) + \frac{1}{2} (\vec{\Omega} \times (\vec{r} + \vec{R}))^2 \right)$$

Euler Lagrange equation:

$$\frac{\partial L}{\partial \vec{r}} = \frac{d}{dt} \frac{\partial L}{\partial \vec{v}}$$

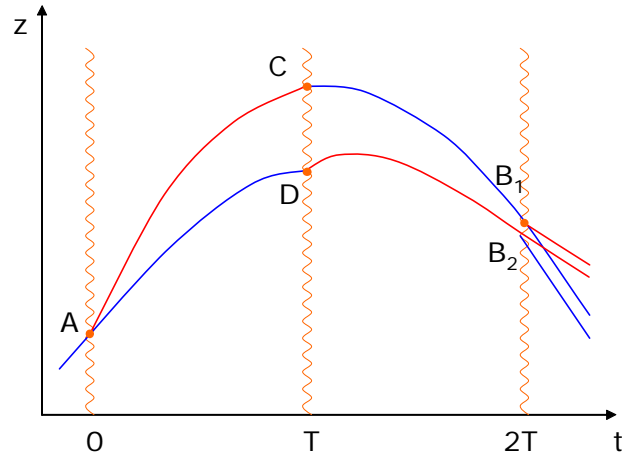
-> classical trajectories



Phase Calculations – Laser Phase

Laser phase (output state 2):

$$\Delta\Phi_{laser} = \vec{k} \cdot (\vec{r}_A - \vec{r}_C - \vec{r}_D + \vec{r}_{B_1})$$



Phase Calculations – Propagation Phase

Propagation phase:

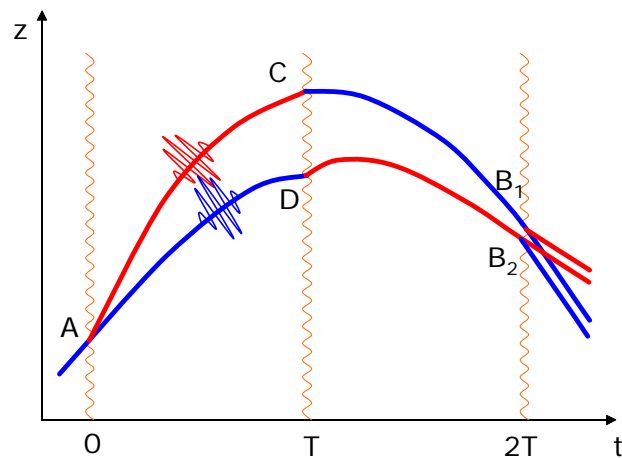
$$\Delta\Phi_{prop} = \frac{1}{\hbar} (S_{cl,ACB_1} - S_{cl,ADB_2})$$

with

$$S_{cl,path} = \int L[\vec{r}(t), \vec{v}(t)] dt$$

and the full Lagrangian:

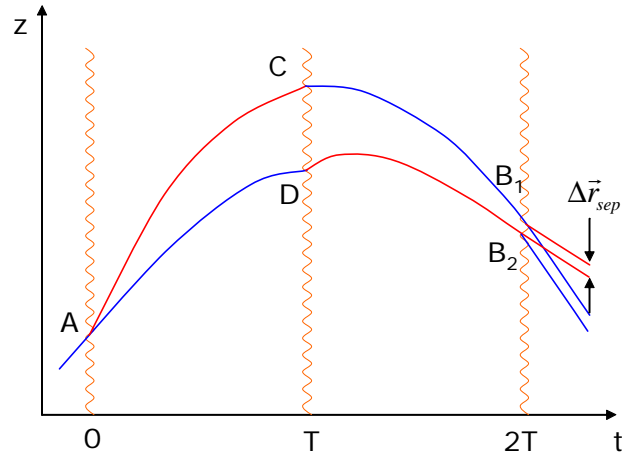
$$L(\vec{r}, \vec{v}) = m \left(\frac{v^2}{2} + \vec{g} \cdot \vec{r} + \frac{1}{2} \vec{r} \cdot \tilde{T}_{gg} \cdot \vec{r} + \vec{\Omega} \cdot ((\vec{r} + \vec{R}) \times \vec{v}) + \frac{1}{2} (\vec{\Omega} \times (\vec{r} + \vec{R}))^2 \right)$$



Phase Calculations – Separation Phase

Separation phase:

$$\Delta\Phi_{sep} = \frac{m\vec{v} \cdot \Delta\vec{r}_{sep}}{\hbar}$$



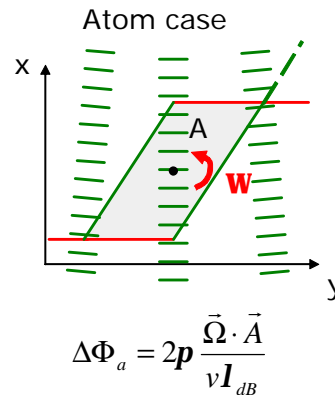
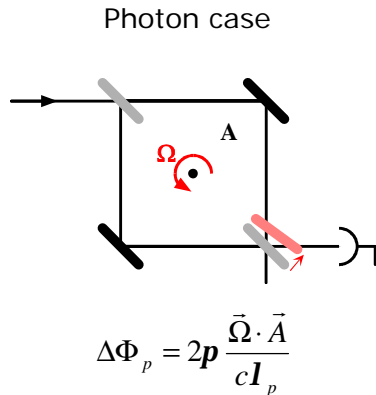
Accelerometer Phase Terms

Term	phase	rel. phase
$k_z T^2 g_z$	$-2.32 \cdot 10^7$	1.0
$k_z T^2 \omega_y^2 R$	$4.44 \cdot 10^4$	$1.9 \cdot 10^{-3}$
$k_z T^3 v_z T_{zz}$	$1.08 \cdot 10^1$	$4.7 \cdot 10^{-7}$
$\frac{7}{12} k_z T^4 g_z T_{zz}$	-6.32	$2.7 \cdot 10^{-7}$
→ $-3k_z T^3 v_z \omega_y^2$	$-3.11 \cdot 10^{-2}$	$1.3 \cdot 10^{-9}$
→ $-\frac{7}{4} k_z T^4 g_z \omega_y^2$	$1.81 \cdot 10^{-2}$	$7.8 \cdot 10^{-10}$
$\frac{7}{12} k_z T^4 T_{zz} \omega_y^2 R$	$1.21 \cdot 10^{-2}$	$5.2 \cdot 10^{-10}$
$\frac{\hbar}{2m} k_z^2 T^3 T_{zz}$	$9.71 \cdot 10^{-3}$	$4.2 \cdot 10^{-10}$
$-\frac{7}{4} k_z T^4 \omega_y^4 R$	$3.47 \cdot 10^{-5}$	$1.5 \cdot 10^{-12}$
$-\frac{3\hbar}{2m} k_z^2 T^3 \omega_y^2$	$2.79 \cdot 10^{-5}$	$1.2 \cdot 10^{-12}$
$-\frac{7}{4} k_z T^4 \omega_y^2 \omega_z^2 R$	$2.62 \cdot 10^{-5}$	$1.1 \cdot 10^{-12}$

Values for Cs atoms, T=0.4s, launch velocity for a symmetric fountain and vertical laser beams

Rotation Sensor

Rotations induce path length differences by shifting the positions of beam splitting optics



Rotation Sensor Phase Terms

Term	phase	rel. phase
$2k_x T^2 \omega_z v_y$	4.69	1.0
$\rightarrow -2k_x T^3 \omega_y g_z$	$6.28 \cdot 10^{-4}$	$1.3 \cdot 10^{-4}$
$-2k_x T^3 \omega_y^3 R$	$-1.20 \cdot 10^{-6}$	$2.6 \cdot 10^{-7}$
$-2k_x T^3 \omega_y \omega_z^2 R$	$-9.09 \cdot 10^{-7}$	$1.9 \cdot 10^{-7}$
$\frac{\hbar}{2m} k_x^2 T^3 T_{xx}$	$3.11 \cdot 10^{-9}$	$6.6 \cdot 10^{-10}$

\rightarrow coupling of gravity becomes important due to earth rotation

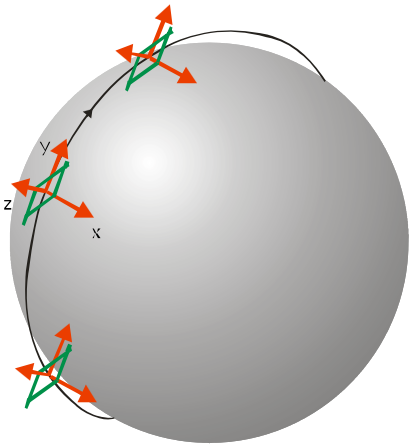
Values for Cs atoms, $T=1/290$ s, $v_y=290$ m/s, lasers in east west direction

Rotation Sensor in Space

High precision rotation sensing
to confirm general relativity

Lense-Thirring: approx. $7 \cdot 10^{-15}$ rad/s

Assume:
Laser in x direction to avoid
rotating gravity gradient tensor
 $T=1$ s
 $v_y=1$ m/s



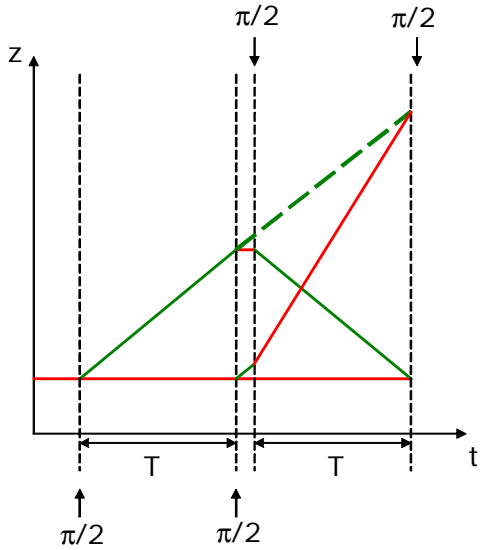
Term	phase	rel. phase
$\frac{\hbar}{2m} k_x^2 T^3 T_{xx}$	$7.59 \cdot 10^{-2}$	1.0
$-2k_x T^2 \omega_z v_y$	$-2.07 \cdot 10^{-7}$	$2.7 \cdot 10^{-6}$

Optical Clock

Scheme:

Prospects to reach time
definition to 1 part in 10^{18}
using narrow optical
transitions

$\omega_{\text{optical}} \sim 10^{15}$ 1/s
1 mrad readout
-> $T \sim 1$ s



Optical Clock Phase Terms

Term	phase	rel. phase
$k_z T^2 g_z$	$-2.32 \cdot 10^7$	1.0
$k_z T^2 \omega_y^2 R$	$4.44 \cdot 10^4$	$1.9 \cdot 10^{-3}$
$-k_z^2 T \frac{\hbar}{m}$	$-4.16 \cdot 10^4$	$1.8 \cdot 10^{-3}$
$k_z T^3 v_z T_{zz}$	$1.08 \cdot 10^1$	$4.7 \cdot 10^{-7}$
$\frac{7}{12} k_z T^4 g_z T_{zz}$	-6.32	$2.7 \cdot 10^{-7}$
$-3 k_z T^3 v_z \omega_y^2$	$-3.11 \cdot 10^{-2}$	$1.3 \cdot 10^{-9}$
$-\frac{7}{4} g_z k_z T^4 \omega_y^2$	$1.81 \cdot 10^{-2}$	$7.8 \cdot 10^{-10}$
$\frac{7}{12} k_z T^4 R T_{zz} \omega_y^2$	$1.21 \cdot 10^{-2}$	$5.2 \cdot 10^{-10}$
$\rightarrow \frac{\hbar}{3m} k_z^2 T^3 T_{zz}$	$6.48 \cdot 10^{-3}$	$2.7 \cdot 10^{-10}$

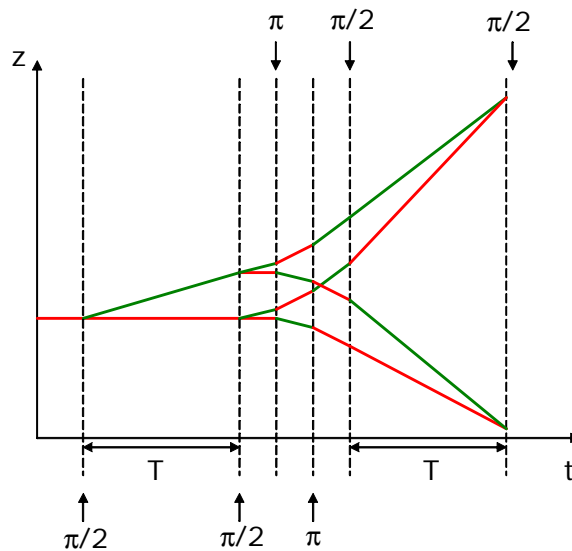
Values for Cs mass, T=0.4s, launch velocity for a symmetric fountain and vertical laser beams

Recoil Measurement

Scheme:

Enlarge recoil shift with additional pulse sequence

Difference measurement is immune to most error sources



D.S. Weiss, B.C. Young and S. Chu, App.Phys. B-Lasers and Optics **59** (3): 217-256 (1994)

Recoil Measurement Phase Terms

Term	phase	rel. phase
$\frac{2N\hbar}{m} k_z^2 T$	$8.39 \cdot 10^5$	1.0
$\frac{N\hbar}{3m} k_z^2 T^3 T_{zz}$	$6.89 \cdot 10^{-3}$	$8.2 \cdot 10^{-9}$
$\frac{N^2\hbar}{2m} k_z^2 T^2 T_{rec} T_{zz}$	$8.22 \cdot 10^{-4}$	$9.8 \cdot 10^{-10}$
$\frac{(2N^3+N)\hbar}{6m} k_z^2 T T_{rec}^2 T_{zz}$	$4.36 \cdot 10^{-5}$	$5.2 \cdot 10^{-11}$

Values for Cs atoms, $T=0.13s$, 30 π -pulses separated by $T_{rec}=1/3000s$ and vertical laser beams (similar to the experiment of Chu)

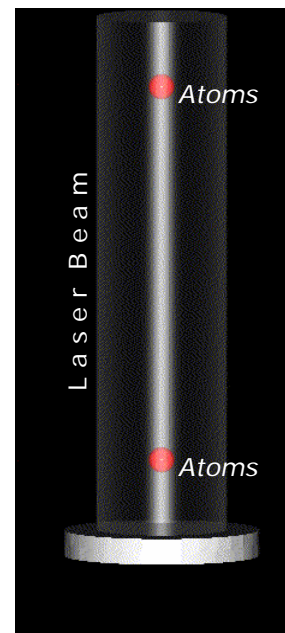
Gradiometer Phase Terms

Gradient measurements: Distinguish gravity induced accelerations from those due to platform motion.

- Simultaneously measure \mathbf{g} at two locations with atom interferometer accelerometers
- Difference acceleration signal contains gradient information

Term	phase	rel. phase
$k_z T^2 T_{zz} dz$	$4.32 \cdot 10^{-1}$	1.0
$k_z T^2 \omega_y^2 dz$	$4.13 \cdot 10^{-4}$	$9.6 \cdot 10^{-4}$

- Differential measurement eliminates most terms
- easy interpretation
- alignment is critical



Conclusions and Outlook

- Atom interferometric measurements in space show prospects for highest precision
- High order inertial corrections will become important for these instruments
- High precision full tensor gravity gradient data can be collected with accelerometer arrays

PARCS: A LASER-COOLED ATOMIC CLOCK IN SPACE*

D.B. SULLIVAN

*National Institute of Standards and Technology (NIST), 325 Broadway
Boulder, CO 80305-3328, USA
E-mail: donald.sullivan@boulder.nist.gov*

PARCS Challenges

D.B. Sullivan

*National Institute of Standards and Technology (NIST), 325 Broadway
Boulder, CO 80305-3328, USA
E-mail: donald.sullivan@boulder.nist.gov*

After presenting a very brief outline of this flight program, this paper discusses some of the key challenges that must be met for successful flight. These include the comparison of the frequency of the PARCS cesium clock with Earth-bound cesium clocks using the GPS carrier-phase method, the implementation of the phase modulation scheme needed to minimize the impact of space-station vibrations on the cesium clock, the evaluation of the cesium spin-exchange frequency shift, the design of shutters for the cesium beam, and the acquisition of tracking and acceleration data essential to measurement of the relativistic frequency shift and transfer of the realization of the second to Earth. Among advances reported in this paper are the development of the new concept of phase modulation and detailed analysis of the limitations of the carrier-phase frequency comparison system. Preliminary designs for several key components of the flight package are also presented.

PARCS successfully completed its Science Concept Review in January 1999 and its Requirements Design Review in December 2000, and is now moving toward its Preliminary Design Review. This paper starts with a short summary of the PARCS program, and this is followed by the set of viewgraphs presented at the meeting.

1. Introduction

A more accurate and stable clock in space can achieve several purposes including: tests of gravitational theory, study of GPS satellite clocks, study of neutral atoms in microgravity, and a more accurate realization of the second, which can then be made available worldwide. PARCS¹ and two other atom-clock programs, Atomic Clock Ensemble in Space (ACES)² and Rubidium Atomic Clock Experiment (RACE)³, are also scheduled for flight on the International Space Station (ISS).

Several relativistic effects on clocks will be measured in this experiment. Significant measurements include the relativistic frequency shift, which can be determined within an uncertainty about 35 times better than was done previously, and local position invariance, which can be tested at an uncertainty about 120 times better than the best current experiments on earth. Should this experiment fly concurrently with SUMO (Superconducting Microwave Oscillator)⁴, which is also scheduled to fly on the ISS, local position invariance could be tested about three orders of magnitude better than current experiments, and a Kennedy-Thorndike test could be done nearly five orders of magnitude better than the most accurate experiments done on earth. Finally, the realization of the second in space can be achieved at an uncertainty of 5×10^{-17} (1 μ s), a factor of 20 better than that presently achieved on earth.

PARCS completed its NASA Science Concept Review in January 1999 and its Requirements Design Review in December of 2000. Preliminary designs of many components are nearing completion and a number of prototype components have been developed and tested. PARCS is currently scheduled to fly in 2005.

2. System Design

The desired location for the experiment (see Fig. 1) is on a forward section of the External Facility (EF) of the Japanese Experimental Module (JEM). This location provides reasonable zenith and nadir views, which are important for time transfer (frequency comparisons). Furthermore, the available power (3 kW), closed-fluid cooling (2 kW), and available space (1.8 _ 1.0 _ 0.8 m) are well suited to the experimental requirements.

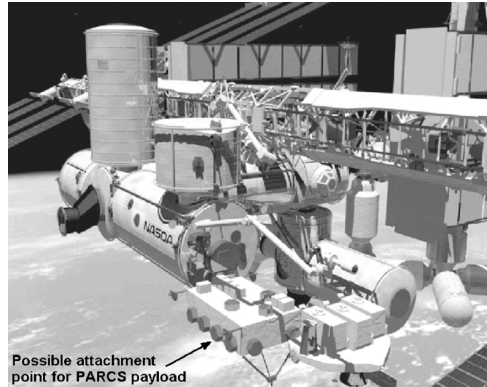


Figure 1. Projected location of PARCS on the ISS.

Figure 2 shows a block diagram of the main space and earth components. The local oscillator is a space-qualified hydrogen maser produced for the Russian Space Station Mir (but never flown) by the Harvard-Smithsonian Center for Astrophysics.⁵ The output of the maser is fed to the low-phase-noise microwave synthesizer,⁶ which, under control of the computer, produces synthesized frequency offsets steered to the appropriate resonances in the cesium spectrum. The synthesizer also delivers a cesium-based reference signal to the GPS receiver for common-view comparisons with atomic clocks on earth. The GPS common-view method is described below. Clock control signals, as well as clock and GPS-receiver data, are sent through the relatively low-data-rate communication link shown near the top right of the figure.

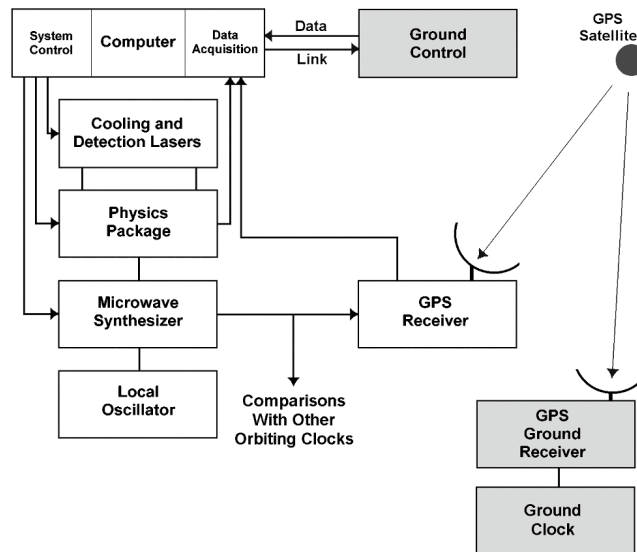


Figure 2. Block diagram of the PARCS experiment showing the major ISS and ground-station components. The ground components are shaded.

Frequency (and to some extent, time) is transferred using reception of the GPS carrier phase in the common-view method. Receivers at the ground station and on the ISS receive the same signal from one individual GPS satellite. The data acquired at each location are the differences between readings from the reference clock at that location and from the GPS clock, with an added signal-transit delay. In differencing the data sets acquired at the two points, the GPS clock drops out, leaving the difference between the two clock readings, plus the differential transit delay. This differential delay has some common-mode components. Using ionospheric-delay data obtained from dual-frequency GPS measurements and tropospheric delay estimates, the difference term can be evaluated quite well. Dramatic improvement over single observations is then obtained by taking and averaging additional clock differences using all available GPS satellites within common view of the two observing stations. The best result for measurements of this type (for two earth stations) has been an RMS time noise of 30 ps.

Figure 3 shows the limitations imposed by time transfer, spacecraft tracking, clock stability, and inaccuracy of the ground clock. For the time-transfer-system limits alone, the two curves would continue downward, but measurements are ultimately limited by uncertainties in the position of the ISS.

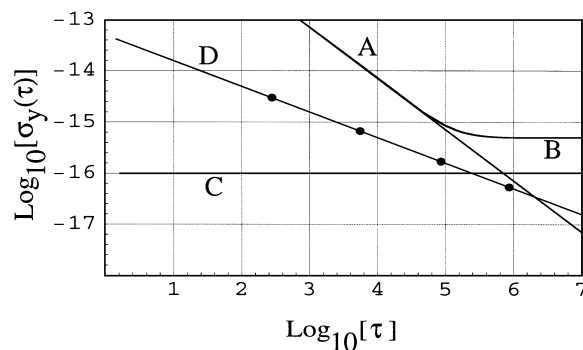


Figure 3. Allan variance of the stability limits for the full-level objectives and science requirements. Curve A is the time-transfer limit. Curve C represents the fractional frequency shift from spacecraft position tracking (using GPS) at an uncertainty of 1 m. The clock stability is curve D. Curve B is the composite experimental stability obtained from an integration-by-parts method. This includes contributions from tracking, space-clock stability, and ground clock inaccuracy. The long-term limit is determined by the inaccuracy of the ground clock (uncertainty projected to be 5×10^{-16} by 2005). The averaging times for 1 pass of the ISS, one orbit of the ISS, 1 day and 10 days are shown from left to right by the solid dots on curve D.

Figure 4 shows a schematic diagram of the proposed clock. The core of the clock, the physics package, is made up of (1) the atom-preparation region, where atoms are laser cooled, trapped and launched; (2) a TE₀₁₁ microwave cavity, where state preparation is completed by moving atoms from the $F=4$ ground state to the $F=3$ ground state; (3) a microwave cavity where atoms are subjected to microwave radiation near the cesium frequency of 9 192 631 770 Hz; and (4) a detection region where laser fluorescence is used to determine whether the microwaves have induced a transition.

The requirements for the laser-cooled clock are selected to achieve a reasonable match with the local oscillator (a hydrogen maser) and the GPS time-transfer system. The hydrogen maser achieves a stability (beyond ~ 50 seconds) of $\sigma_y(\tau) = 5 \times 10^{-14} \tau^{-1/2}$, and this is the stability around which PARCS has been designed. As seen in Figure 4, this stability lies below the limit set by the time-transfer system, thus assuring that the laser-cooled-cesium clock does not degrade the overall stability transferred from the ISS to earth. The system

requirements for the clock physics package, the local oscillator, electronic systems, time-transfer systems, and environmental requirements are described below.

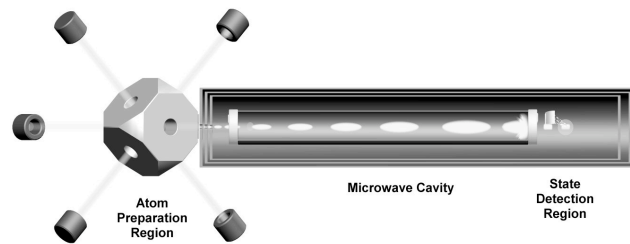


Figure 4. Diagram of the PARCS laser-cooled space clock. Atoms in the source (atom-preparation) region are cooled and trapped and then launched. The state-detection lasers are not shown. State detection involves not only detection of the atoms that have changed states, but also measurement of the number of atoms arriving in each measurement cycle so as to normalize detection to the number of atoms launched and thus remove shot-to-shot fluctuations. Shutters (not shown) at ends of the cavity are closed during laser interactions with atoms to prevent scattering of laser light into the cavity. Three concentric magnetic shields are shown surrounding the microwave cavity and state-detection region.

The atoms are cooled and trapped using conventional optical-molasses techniques. Traditional atomic clocks use frequency-modulation methods to find the center of the atomic resonance. A large number of atom balls are launched and detected before the frequency is moved from one side of the line to the other. This minimizes the stability limit imposed by the dead time (the Dick effect). To achieve the desired stability, we estimate that we must launch ~ 2 balls per second at a velocity of 15 cm/s with a transverse temperature of 2 μ K and a total of 1×10^6 atoms (in the $m=0$ state) in each ball. For a cavity length of 75 cm, this gives a Ramsey time of 5 s. The cycle time (the time spent on each side of the line) is projected to be 15 s. These parameters are within the state of the art, and a trap system was constructed to verify that we could achieve them.

Two different approaches to locating the center of the resonance line have been studied, and while the conventional approach of frequency modulation remains an option, the very low velocity of the atoms in this clock provides opportunity for a new approach that both reduces the sensitivity of the clock to acceleration noise and increases the duty cycle (that is, reduces the Dick effect). The now favored method involves independent phase modulation of the two Ramsey regions (a concept first described at a conference in Italy⁶ and discussed in more detail in the proceedings of the 2001 IEEE Frequency Control Symposium⁷). In this approach, the two cavity ends are operated at a phase difference of 90° to produce a discriminator-like response rather than a true resonance. When the phase of the far-end cavity (closest to detection region) is then inverted by 180° , a second, flipped discriminator curve is produced. The intersection of the two curves is the center of the resonance. The servo-control system used to stay on resonance operates in the same way as the system used for frequency modulation. That is, the amplitudes of signals derived from the two discriminator curves (180° phase difference) are driven by the servo system to be equal, and this is then the true location of the resonance center. The fact that the system runs on resonance rather than on the sides of the resonance, makes it first-order insensitive to vibrations. This method of interrogation was tested on the NIST cesium-fountain clock, and, at an uncertainty level on the order of 1×10^{-15} , the location of the center of the resonance was identical to that found using the conventional method.

This process does not eliminate the need for measuring end-to-end cavity phase shift. That is done by varying launch velocity and extrapolating the response to zero velocity. To first order, the frequency shift caused by an end-to-end phase asymmetry is a linear function

of the launch velocity. The larger question in this modulation scheme is the short-term control of the relative phases (modulo 90°) at the two cavity ends. One possible approach is to independently monitor the power reflected from each of the end cavities, and since this provides a measure of the phase in each cavity, to control short-term variations in phase with a fast servo-control system. Phase-noise measurements made using a test TE_{011} cavity and a reflection detector show that it is straightforward to achieve the phase sensitivity needed to achieve this short-term control.

Figure 5 shows a simple outline of the key parts of the physics package along with their dimensions.

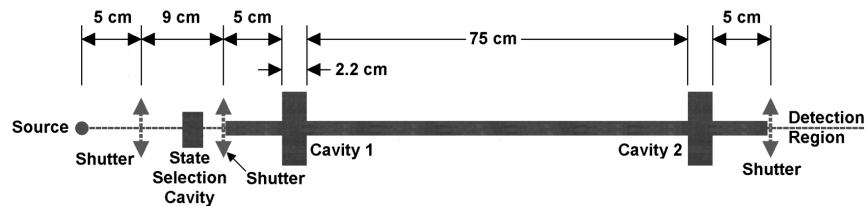


Figure 5. Dimensions for the PARCS laser-cooled clock.

One of the larger systematic frequency shifts to be evaluated and corrected is the spin-exchange frequency shift. This shift is large (0.5 to 1×10^{15} for typical earth-bound clocks). Fortunately, this shift scales down dramatically with increasing Ramsey time and is projected to be nearly two orders of magnitude smaller for the chosen PARCS parameters. The spin-exchange and other systematic shifts will have to be carefully measured and corrected to achieve the desired long-term stability, but there appear to be no major issues associated with correcting these shifts.

It has long been recognized that the spin-exchange shift in rubidium is much smaller than that in cesium, and therefore it might be a good candidate for advanced atomic clocks. While this is true, the spin-exchange shift is not a limiting consideration for PARCS. There are several advantages to staying with cesium, including the facts that (1) the cavity can be smaller because the resonance frequency is higher, (2) the SI definition of the second is based on cesium, and (3) there are many existing cesium primary standards around the world that can be compared directly with the PARCS clock, yielding improved measurement of the relativistic frequency shift.

3. Prototype Development

A number of components have been either designed or fabricated in prototype form. These include the following.

- The shutters, which are critical to operation of the PARCS clock, have been fabricated, and preliminary testing of them has begun. These shutters must produce a minimum of magnetic field and vibration, have an open aperture of > 1 cm, operate at a rate of at least 10 Hz, and should survive $\sim 2 \times 10^8$ actuations.
- Collimators for the trapping and detection lasers, as well as a prototype trapping chamber, have been constructed of titanium, and a prototype for the clock is under development.
- A microwave synthesizer with a performance well beyond that needed for PARCS has been constructed, and measurements of phase stability confirm that it meets the required performance. A second synthesizer, incorporating features that better match it to PARCS and which uses a number of space-qualified components, is nearing completion.⁹
- Preliminary designs for the laser system have been produced using, as much as possible, commercially available components. Some components have already been evaluated for vibration immunity. A laser-welding system will be used to assemble a

number of the components requiring exacting alignment. A jig system for achieving correct alignment before welding has been constructed.

- A design for the microwave cavity was completed, and prototype cavity has been fabricated. Testing of the cavity has just started.

4. Summary

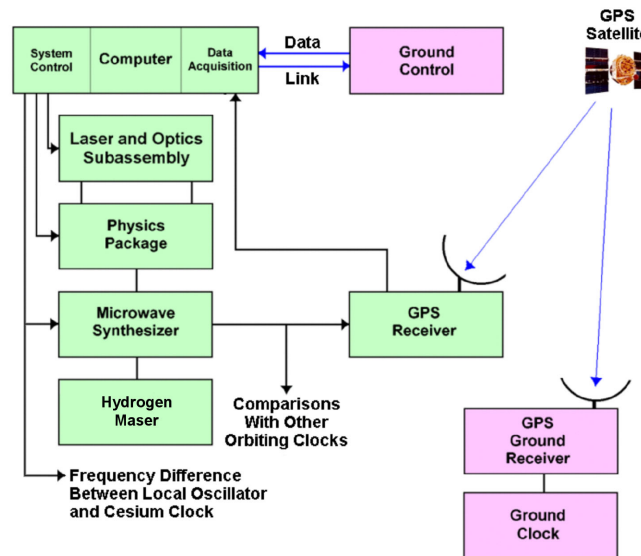
In summary, PARCS development is proceeding on schedule, and all critical issues are being addressed through modeling and prototype construction. It appears that, as long as shutter problems can be solved, the requirements for atom density and systematic frequency shifts should be achievable.

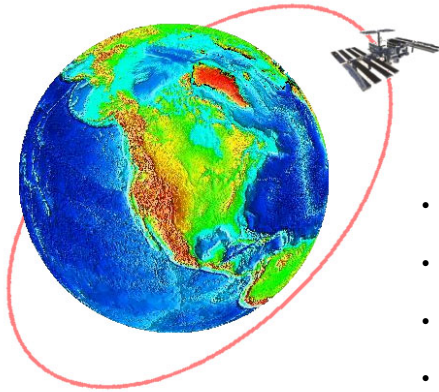
References

- * Contribution of the U.S. Government, not subject to copyright.
1. S.R. Jefferts, T.P. Heavner, L.W. Hollberg, J. Kitching, D.M. Meekhof, T.E. Parker, W. Phillips, S. Rolston, H.G. Robinson, J.H. Shirley, D.B. Sullivan, F.L. Walls, N. Ashby, W.M. Klipstein, L. Maleki, D. Seidel, R. Thompson, S. Wu, L. Young, and A. DeMarchi, "PARCS: a primary atomic reference clock in space," *Proc. 1999 Joint Meeting of the European Frequency And Time Forum and the IEEE Frequency Control Symposium*, IEEE Cat. No. 99CH36313, pp. 141-144 (1999).
 2. S. Feltham, F. Gonzalez, and P. Puech, "ACES: a time and frequency mission for the international space station," *Proc. 1999 Joint Meeting of the European Frequency And Time Forum and the IEEE Frequency Control Symposium*, IEEE Cat. No. 99CH36313, pp. 148-151 (1999). Also see Ch. Salomon in this volume.
 3. C. Fertig, K. Gibble, B. Klipstein, J. Kohel, L. Maleki, D. Seidel, and R. Thompson, "Laser-cooled microgravity clocks," *Proc. 1999 Joint Meeting of the European Frequency And Time Forum and the IEEE Frequency Control Symposium*, IEEE Cat. No. 99CH36313, pp. 145-147 (1999).
 4. J. Lipa, M. Dong, S. Wang, S. Buchman and J. Turneure, "Status of the superconducting microwave oscillator clock experiment," *Proc. 1998 NASA/JPL Microgravity Fundamental Physics Workshop*, June 23-25, 1998, Oxnard, CA, NASA Document D-18442, pp. 309-316 (1999).
 5. E.M. Mattison and R.F.C. Vessot, "Design of a Hydrogen Maser for Space," *Proc. 11th European Frequency And Time Forum*, Neuchâtel, Switzerland, pp. 525-528 (1997).
 6. A. Sen Gupta, D. Popovic, and F.L. Walls, "Cs Frequency Synthesis: A New Approach," *Proc. 1999 Joint Meeting of the European Frequency And Time Forum and the IEEE Frequency Control Symposium*, IEEE Cat. No. 99CH36313, pp. 615-619 (1999).
 7. T.P. Heavner, L.W. Hollberg, S.R. Jefferts, D.M. Meekhof, T.E. Parker, W. Phillips, S. Rolston, H.G. Robinson, J.H. Shirley, D.B. Sullivan, F.L. Walls, N. Ashby, W.M. Klipstein, L. Maleki, D. Seidel, R. Thompson, S. Wu, L. Young, R.F.C. Vessot, E.M. Mattison, and A. DeMarchi, "PARCS – A Primary Atomic Reference Clock in Space," *Proc. 1st Int. Symp on Microgravity Research and Applications in Physical Sciences and Biotechnology*, pp. 739-745, Sorrento, Italy, 10-15 September 2000.
 8. W.M. Klipstein, G.J. Dick, S.R. Jefferts, and F.L. Walls, "Phase Modulation with Independent Cavity-Phase Control in for Laser-Cooled Clocks in Space," *Proc. 2001 IEEE International Frequency Control Symposium*, IEEE Cat. No. 01CH37218, pp. 25-32 (2001).
 9. A. Sen Gupta, J.F. Garcia Nava, C. Nelson, D.A. Howe, and F.L. Walls, "Microwave Synthesizers for Atomic Frequency Standards," 6th Symposium on Frequency Standards and Metrology, September 9-14, 2001, St. Andrews, Scotland.

- **Review of Objectives**

- **Discussion of Key Challenges**
 - **GPS Carrier-Phase Time Transfer**
 - **GPS Tracking Requirements**
 - **Phase Modulation**
 - *Spin-Exchange Frequency Shift*
 - *Shutter Design*





- Relativistic Frequency Shift **x 35**
- Gravitational Frequency Shift **x 12**
- Local Position Invariance Test **x 120**
- Realization of the Second **5×10^{-17}**
- Study of Dynamics of Atoms in Microgravity
- Analysis of GPS Satellite Clocks

- **JPL Designed Receiver**
 - **Successfully Flown**
 - **Cost-Effective Solution**
 - **Adequate Performance**
- **Issue**
 - **Multipath Effects**

JPL: Sien Wu, Larry Young, and Ian Harris

JPL Designed Receiver

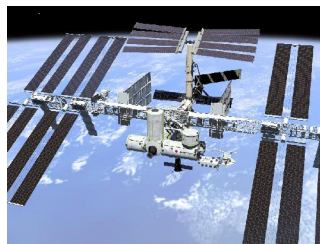
- Tracking Systems and Applications Section
- Global Positioning Satellite (GPS) Systems Group
- Orbiter and Radio Metric Systems Group
- Advanced Radio Metric Instrument Development Group
- Processor Systems Development Group



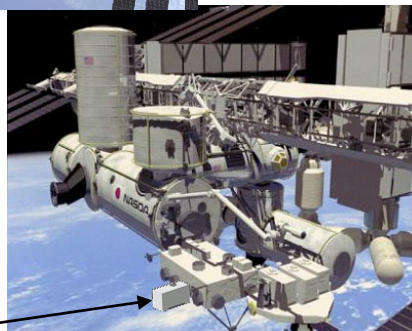
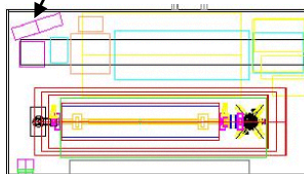
JPL Receiver and Antennas



Successful SRTM (Shuttle Radar Topography Mission) used the new "Blackjack" receiver

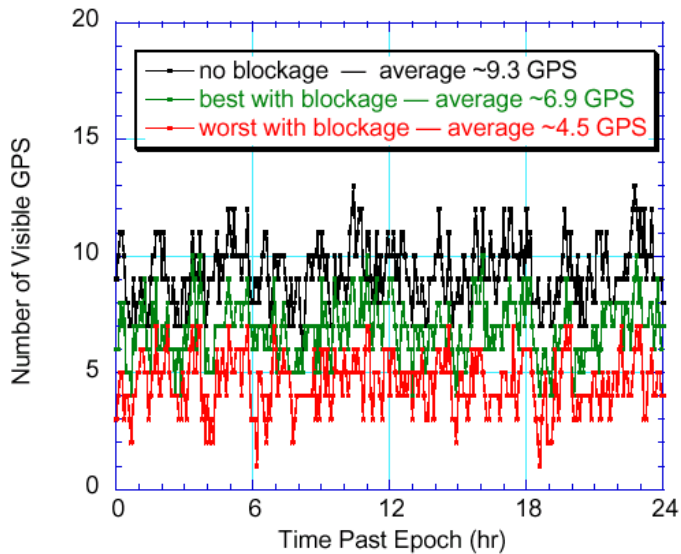
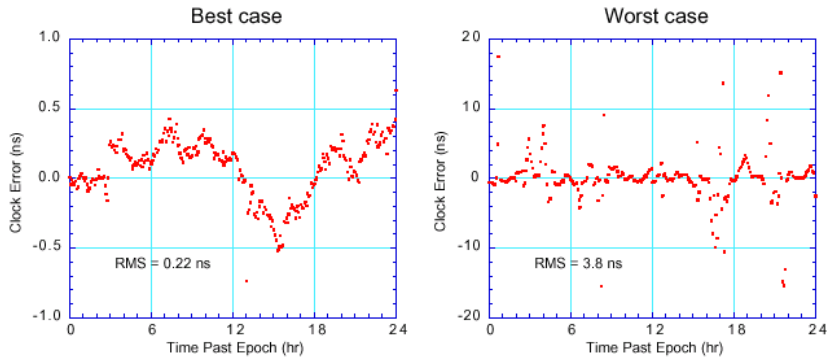


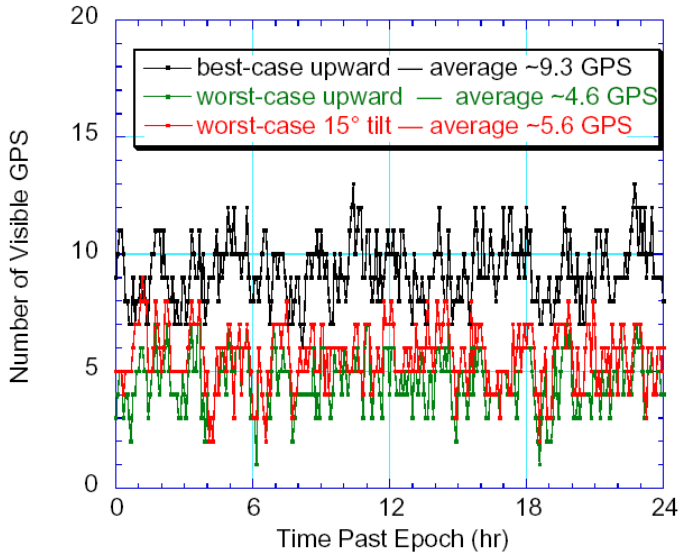
GPS Antenna



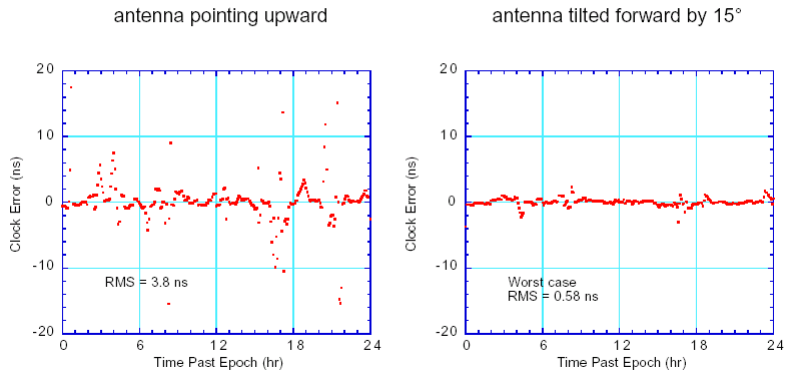
PARCS

- Best case: RMS error ~ 2.5x worse than ideal case
- Worst case: RMS error ~ 40x worse than ideal case



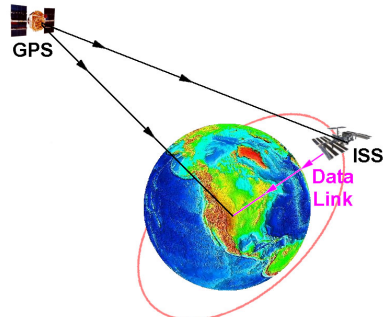


Worst-Case Blockage



Accumulated Phase Observable:

$$\frac{\tau_B - \tau_A}{\tau_A} = \frac{\alpha_G}{\tau_A} \int_{t_1}^{t_2} dt \left[\frac{\Phi_B - \frac{1}{2} \mathbf{r}_B \cdot \nabla \Phi_B - \Phi_A}{c^2} \right] + \frac{\alpha_D}{\tau_A} \int_{t_1}^{t_2} dt \left[\frac{v_A^2}{2c^2} \right] - \frac{\alpha_D}{2c^2 \tau_A} [\mathbf{r}_B \cdot \mathbf{v}_B]_{t_1}^{t_2} - \frac{\alpha_D}{2c^2 \tau_A} \int_{t_1}^{t_2} dt [\mathbf{r}_B \cdot \mathbf{a}_B]_{Non-Grav}$$



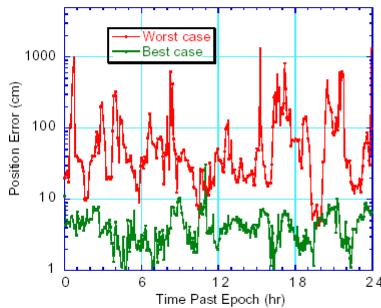
Frequency Shift Measurement

Limitation: Ground Clock uncertainty of 5×10^{-16} .

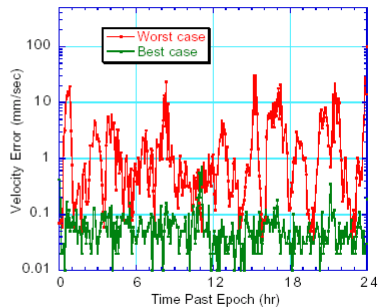
Expected Results: 1.7 ppm

Requirements: position uncertainty of 1 m
velocity uncertainty of 10 m/s
non-gravitational acceleration of $400 \times 10^{-9} g$

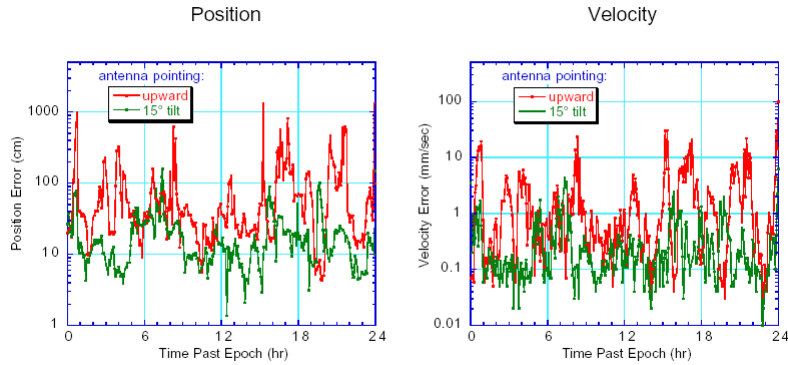
Position



Velocity



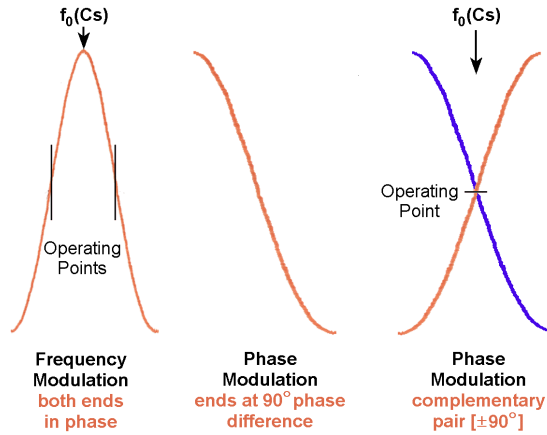
Worst-Case Blockage



- **Terrestrially Proven Concept**
 - Used on Fountain Clocks
 - Reduces Vibration Sensitivity
 - Can Decrease Dead Time
- **Issues**
 - Phase Stability of Feeds
 - Phase Dependence on Power Level

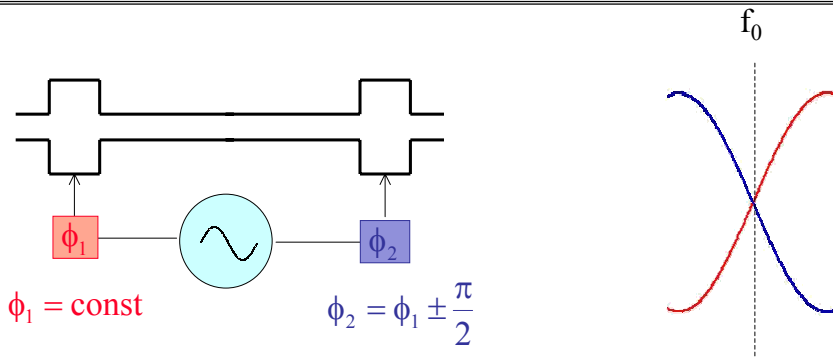
JPL: Bill Klipstein and John Dick

NIST: Steve Jefferts, Tom Heavner, and Fred Walls

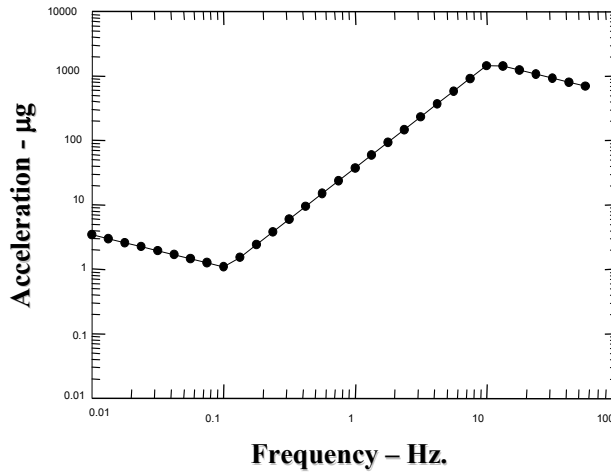


Advantages:

Decreased sensitivity to Acceleration, Reduced Dead Time, and System Is Always On Resonance $f_0(Cs)$



Shorter attack times
(clearing time is for second cavity only)

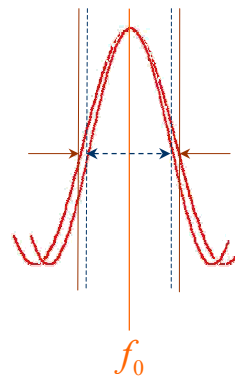


Width of central fringe is $\frac{1}{2T_R}$

Changing T_R results in fringe "breathing"
(Pierre Lemonde, PhD thesis)

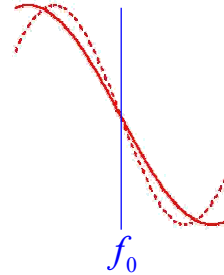
Velocity Dispersion
results in line broadening

Dead time while atoms clear entire cavity



Microwave source is run slightly off of f_0

Change in T_R results in change in slope: no first order apparent frequency noise



OTHER NOISE REMAINS:

Phase delay

(photons not carried along with moving structure)

$$\frac{y_{pd}(f)}{x(f)} = \frac{1}{c^2 t_i}$$

Mechanical compression:

$$\frac{y_{mc}}{\delta x(f)} = \frac{2(\pi f l)^2}{v_s^2 c t_i}$$

Frequency Modulation:

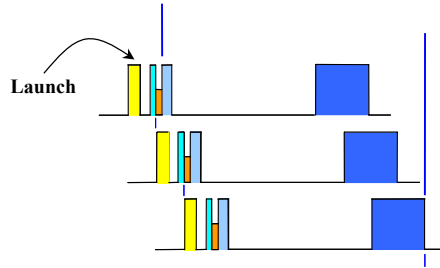
$$\frac{y_{FM}(f)}{\delta x(f)} \approx 10^{-11} \text{ m}^{-1}$$

Accelerations at harmonics of the modulation frequency alias in to DC

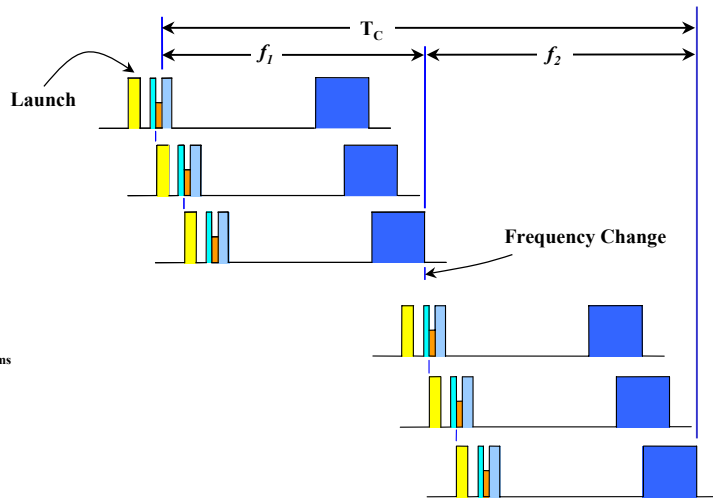
Phase Modulation:

$$\frac{y_{PM}(f)}{\delta x(f)} \approx 10^{-16} \text{ m}^{-1}$$

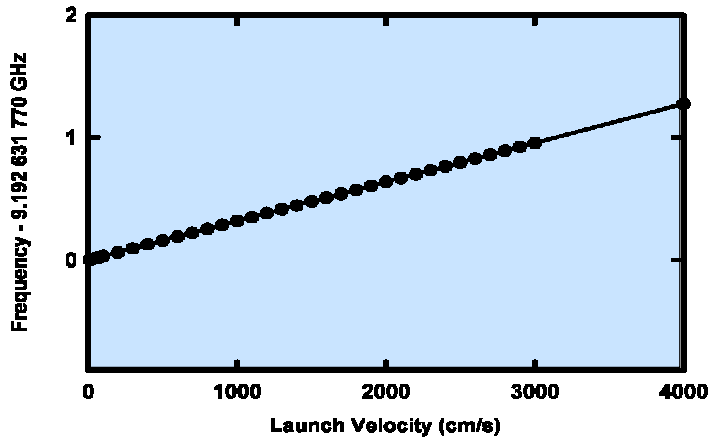
Dramatic reduction in sensitivity to vibrations



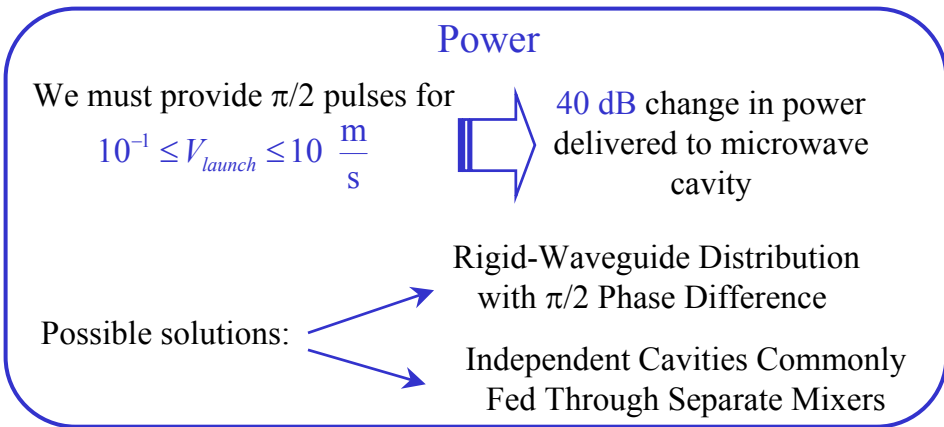
- Collect
- Clear F=4 atoms
- Shutter #1
- Shutter #2
- Shutter #3



- Collect
- Clear F=4 atoms
- Shutter #1
- Shutter #2
- Shutter #3

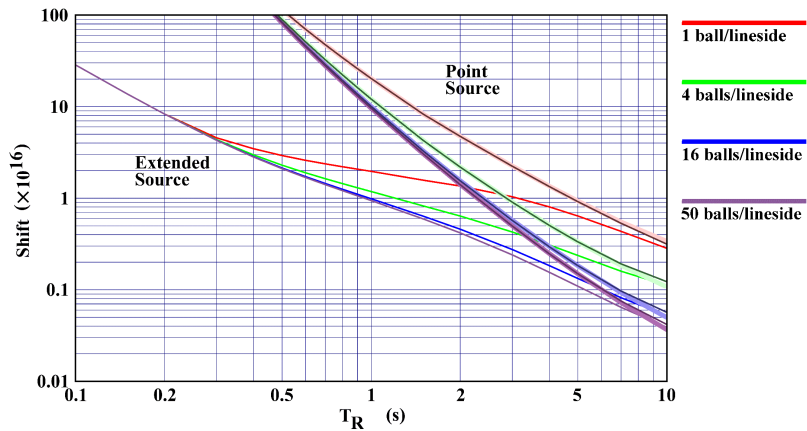


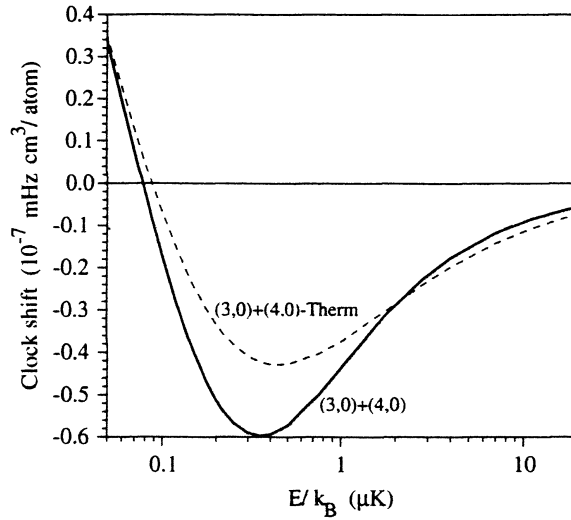
In microgravity the launch velocity is easily tuned



- **Key Systematic Uncertainty**
 - Reduced by Lower Velocity
- **Issues**
 - Proper Modeling
 - Extrapolation to Zero Density

NIST: Steve Jefferts, Tom Heavner,
 Carl Williams, and Vanessa Venturi
 JPL: Bill Klipstein





From: P.J. Leo, P.S. Julienne, F.H. Mies, and C.J. Williams, *Phys. Rev. Lett.*, **86**, 3743 (2001).
(several curves have been removed for clarity)

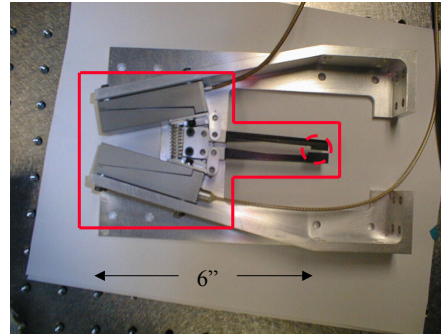
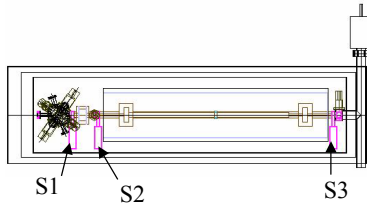
- **Needed to Block Scattered Light**
 - **Allows Multiple Ball Tosses**
- **Issues**
 - **Long-Term Reliability**
 - **Magnetic-Field Generation**
 - **Vibration Generation**

JPL: Bob Bamford, Bob Glaser, and Gerhard Klose

Shutters are used inside the vacuum system to shield the atoms in the clock region from laser light.

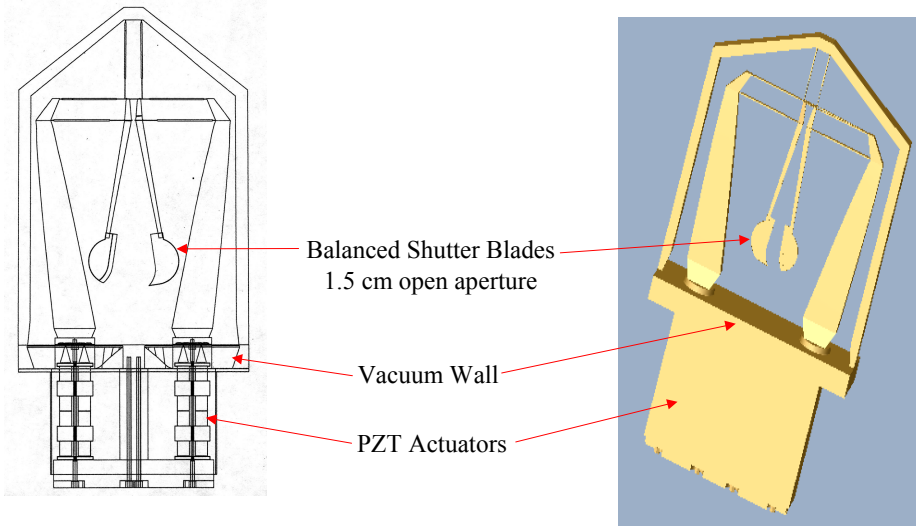
Design Goals include:

- High reliability (1 year operation at 10Hz)
- Fast (< 1 ms time from 100% closed to 90% open)
- Non-magnetic (< 1-2 μG stray field at 1cm)
- Ultra-high vacuum compatible (< 10^{-12} atm)
- Relatively large aperture (> 1 cm)
- Cannot disturb microgravity environment.
- Light tight



First Prototype of Shutter

Uses commercial PZT actuators and non-magnetic materials.



Quantum Phase separation dynamics of BEC mixtures

S. T. Chui

Bartol Research Institute, University of Delaware
Newark, DE 19716

We discuss our recent work on phase separation dynamics in mixtures of Bose-Einstein condensates. We show that the coupled two component one-dimensional Gross-Pitaevskii equations can be solved by the inverse scattering method. This opens the door for the investigation of different excitations for the two by constructing exact extended periodic solutions of this equation. We call these type solutions "solitons", in analogy to solitons that are localized solutions. Our solution suggests that the experimentally observed long-lived metastable intrinsic striation structure is a new kind of excitation of the two component Bose-Einstein condensates. We can find these solutions only in some region of parameter space. We numerically solved the coupled GP equations for different system parameters and found fascinating scenarios of the space time development of the density distributions. Only in some parameter regimes is the periodic fluctuation stable.

High-Density Trapped Atoms in a Holographic Atom Trap

T. G. Walker, R. Newell, J. Sebby, and M. Saffman

Department of Physics, University of Wisconsin-Madison, Madison, Wisconsin 53706

(Dated: July 9, 2002)

We describe experiments to realize trapping of atoms at high densities. We achieve densities in excess of 10^{14} cm^{-3} in a far-off-resonance trap produced by imaging a 8 W YAG laser diffracted from a holographic beam splitter. The atoms are imaged using spatial heterodyne imaging. The small (few μm), high density atoms are ideal for new ideas in quantum processing of neutral atoms using Rydberg states. An example is using dipole blockade to make single photon sources.

Conventional light-force atom traps, in particular the magneto-optical trap (MOT), are limited in density by radiation trapping to typically 10^{11} cm^{-3} [1, 2]. In the experiments described here, we attain in far-off-resonance traps (FORTs) densities that exceed this by typically 3 orders of magnitude. At these densities interesting new collision phenomena can be studied and potentially exploited for quantum manipulation and entanglement of atoms.

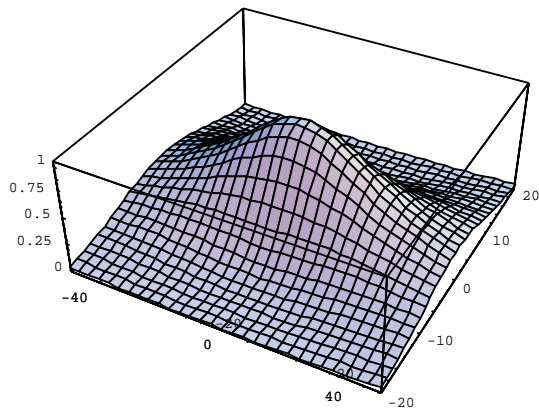


FIG. 1: A typical FORT produced by focussing a laser.

A typical FORT[3] is illustrated here. Using Rb atoms, with a polarizability α of about 100 \AA^3 , and 10 W of YAG power focussed to about $80 \mu\text{m}$, one obtains a trap depth of typically $300 \mu\text{K}$ according to the relation $U(\mathbf{r}) = -2\pi\alpha I(\mathbf{r})/c$.

At a given temperature T , the density depends not only on the trap depth but on its curvature: $n \sim (k/T)^{3/2}$, where $k = |\partial_{\mathbf{r}}^2 U|$. Therefore much higher densities can be obtained by keeping roughly the same trap depth as above but forming an interference pattern (optical lattice) to obtain a rapid spatial variation in the intensity.

In our experiments we achieve a type of optical lattice, called a Holographic Atom Trap (HAT), by interfering the diffracted orders of a holographic phase plate, as shown in Fig. 2. At the intersection of the 5 laser beams an interference pattern is produced. The resulting potential is shown in Fig. 3. Along the propagation

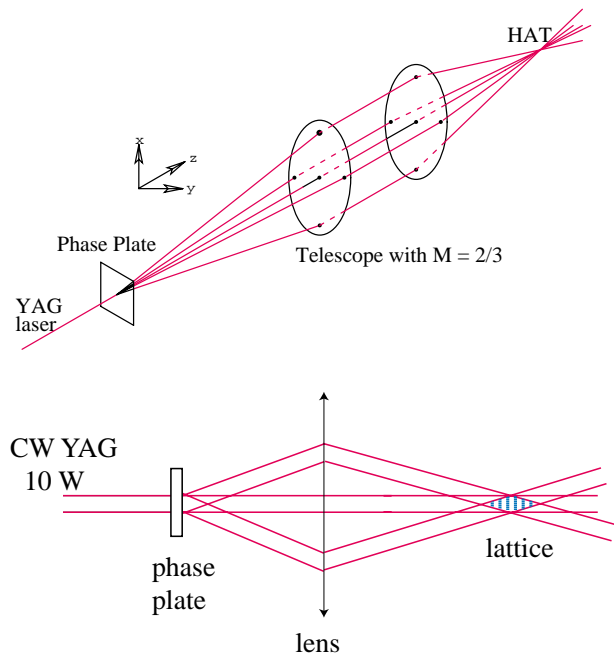


FIG. 2: Two perspectives of the optics used to produce the HAT.

direction of the light the interference arises from the Talbot effect. The lattice sites are $10 \mu\text{m} \times 10 \mu\text{m} \times 100 \mu\text{m}$ in size; with the individual beams focussed to $80 \mu\text{m}$ and a total power of 8 W the trap depth is $500 \mu\text{K}$ and the oscillation frequencies of Rb atoms trapped near the bottom of the lattice sites are 17 kHz, 17 kHz, and 0.7 kHz. Since the lasers are nearly copropagating, the potential is quite stable against vibrations and the YAG laser can be multimode. The relatively large lattice sites allows many atoms (~ 10000) to be trapped in each site.

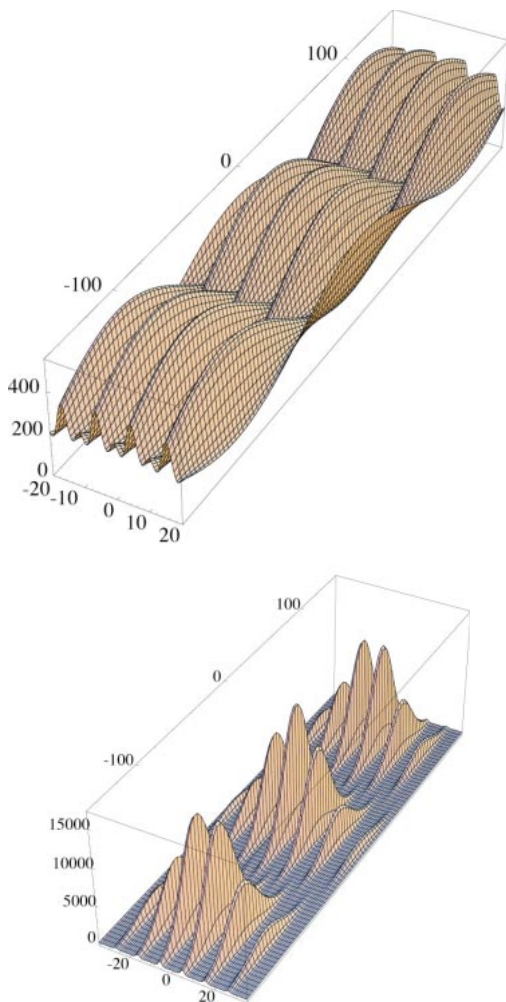


FIG. 3: Trapping potential and density distribution at the center of the HAT.

A calculated density distribution for atoms trapped in the HAT is shown in Fig. 3. A low-resolution image is shown in Fig. 4, making clear the isolation of the atoms in the Talbot fringes. Quantitative analysis of such images, combined with temperature measurements made by time-of-flight methods, gives about 10,000 atoms per lattice site at temperatures of about $50 \mu\text{K}$, densities exceeding $1 \times 10^{14} \text{ cm}^{-3}$, and phase space density of $1/200$.

Key to this success is a proper loading protocol. We

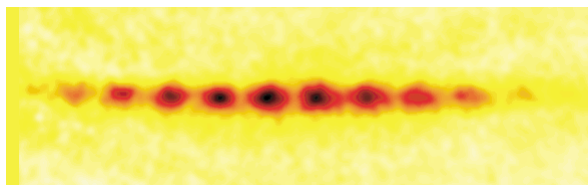


FIG. 4: Low resolution image of the HAT, showing the confinement in the Talbot fringes.

begin with a forced dark spot with 50% of the 10^7 atoms in each of the hyperfine ground states ($F=1,2$) of ^{87}Rb . The dark spot is achieved by imaging an opaque object in the hyperfine repumping beam. We add a “depumping” laser, tuned between the $F=2$ and an $F'=2$ excited level, to purposely force more atoms down to the $F=1$ ground state. We compress the cloud by increasing the MOT magnetic field for 50 msec, then turn on the HAT laser. AC Stark shifts tune the repumping beam out of resonance, and the depumping beam toward resonance, so that atoms in the HAT are extremely dark (~ 0.001 in $F=2$). Over 50 msec the atoms load in to the HAT, after which the lasers are extinguished. The MOT to HAT transfer efficiency is about 15%.

We show in Fig. 5 the temperature vs time for the HAT atoms. As can be seen, the temperature rapidly decreases to a value of about $50 \mu\text{K}$, $1/10$ of the trap depth. This is consistent with evaporation being the mechanism for cooling the atoms in the HAT. The time scale is quite short due to the very high densities. The elastic collision rate is estimated to exceed 3000/s.

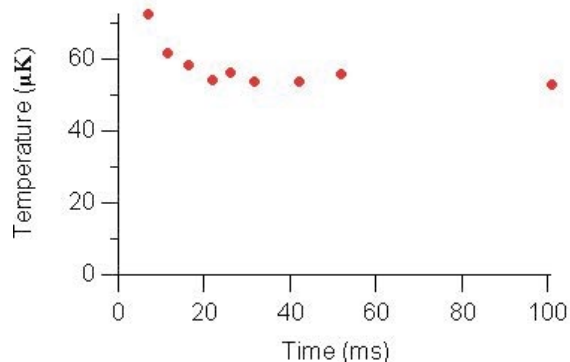


FIG. 5: Evaporative cooling of the atoms after the cooling lasers are switched off.

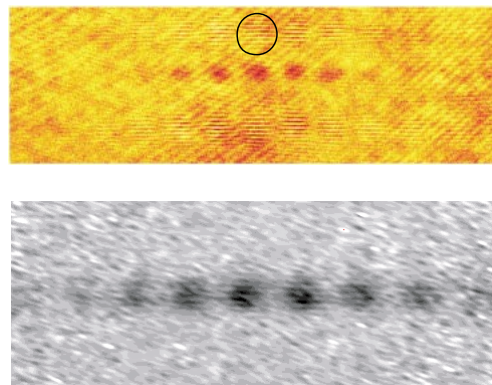


FIG. 6: Top: 1st order Bragg diffraction is shown in the fringes. One is circled. Bottom: Image showing microtraps.

Looking at higher resolution, we have observed Bragg diffraction of the atoms in the microtraps, as shown in

Fig. 6. Alternatively, we can directly image the microtraps. An interesting observation from Fig. 3 is that there should be a relative misalignment of the microtraps in successive Talbot fringes. This is confirmed by the spatial profiles shown in Fig. 7

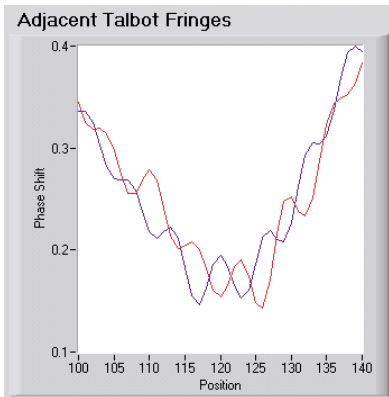


FIG. 7: Spatial profiles of two neighboring Talbot images. The microtrap structure is shifted between the two, as expected.

These high density samples are of potential interest for a variety of experiments. To give an example, we now explain how one might realize a single-photon source by appropriate manipulations of the atoms in a microtrap. The idea is based on the proposal of Lukin *et al.* [4] to achieve entanglement of many atoms using a ‘‘Rydberg blockade’’.

The Rydberg blockade utilizes the strong dipole-dipole coupling of atomic Rydberg states to inhibit quantum transitions in one atom based on the state of another atom. For example, suppose we have a system of N atoms that we try to excite to a Rydberg state r with a narrowband laser. Once a single atom is excited, the dipole-dipole interaction causes the energy of the same Rydberg state for a second atom to shift from its original position. If this shift is greater than the linewidth of the Rydberg state, no other atoms (other than the first) can be excited.

We use this blockade concept to propose a directed single photon source[5]. The energy levels are shown in Fig. 8. In a cloud of N atoms, we use a two-photon transition to drive a single atom to a Rydberg state. Of course, there is no way to know which atom, so the wavefunction for the collection of atoms must be a coherent superposition (massively entangled) of amplitudes for each atom to be excited. We then drive a one-photon transition down to the state e . The wavefunction for the atoms is

$$|\psi\rangle = \frac{1}{\sqrt{N}} \sum_j e^{i(\mathbf{k}_1 + \mathbf{k}_2 - \mathbf{k}_3) \cdot \mathbf{r}_j} |e_j\rangle \quad (1)$$

Note that the amplitude for the j th atom to be excited is multiplied by a phase factor reflective of that atom’s position in the three waves with propagation vectors \mathbf{k}_1 , \mathbf{k}_2 ,

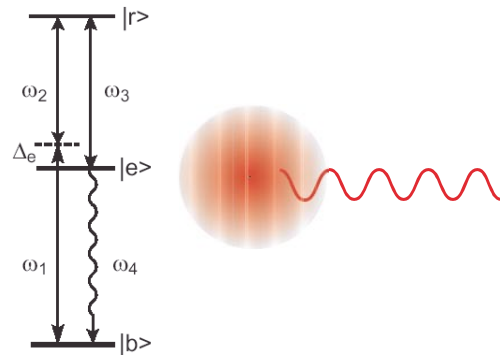


FIG. 8: Energy levels for single-photon emission using the Rydberg blockade. The lasers imprint their phases onto the wavefunction of the atom cloud so that the atoms emitted preferentially in the phase-matched direction.

\mathbf{k}_3 . Thus this wavefunction has spatially varying phase information in it.

We now ask for the amplitude for emission of a photon into direction \mathbf{k} . It is proportional to

$$|\langle b|a^\dagger e^{-i\mathbf{k}\cdot\mathbf{r}}|\psi\rangle|^2 = \left| \frac{1}{\sqrt{N}} \sum_j e^{i(\mathbf{k}_1 + \mathbf{k}_2 - \mathbf{k}_3 - \mathbf{k}) \cdot \mathbf{r}} \right|^2 \quad (2)$$

which has a \sqrt{N} enhancement in the phase matched direction $\mathbf{k} = \mathbf{k}_1 + \mathbf{k}_2 - \mathbf{k}_3$. Note first that we are guaranteed, through the Rydberg blockade, that one and only one photon will be emitted. Second, that photon will be emitted into a diffraction-limit solid angle. The predicted angular distribution is shown in Fig. 9.

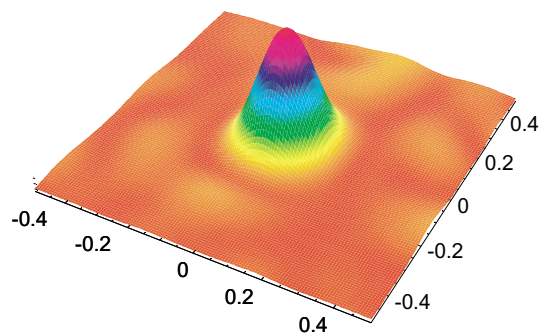


FIG. 9: Expected angular distribution from the single photon source.

In conclusion, the HAT is an excellent source for quickly and easily producing high densities of cold atoms. These high densities should make it possible to study fascinating new physics such as the Rydberg blockade and may lead, among other things, to high efficiency directed sources of single photons.

ACKNOWLEDGEMENTS

The authors are grateful for the support of NASA, the NSF, and the ARO.

-
- [1] T. Walker, D. Sesko, and C. Wieman, Phys. Rev. Lett., **64**, 408 (1990).
- [2] W. Ketterle, K. Davis, M. A. Joffe, A. Martin, and D. E. Pritchard, Phys. Rev. Lett., **70**, 2253 (1993).
- [3] J. D. Miller, R. A. Cline, and D. J. Heinzen, Phys. Rev. A, **47**, R4567 (1993).
- [4] M. D. Lukin, M. Fleischhauer, R. Cote, L. M. Duan, D. Jaksch, J. I. Cirac, and P. Zoller, Phys. Rev. Lett., **87**, 037901 (2001).
- [5] M. Saffman and T. G. Walker, quant-ph/0203080.

Tunable Interactions in Bose and Fermi Gases

K. S. Strecker, A. Truscott, and R. G. Hulet
Department of Physics and Astronomy, Rice University

Abstract

Lithium has two naturally occurring isotopes, ${}^6\text{Li}$ and ${}^7\text{Li}$, with opposite exchange symmetry. In this paper, we describe experiments with ultracold, trapped gases of the lithium isotopes. We have exploited the nonlinear interactions between atoms in a Bose-Einstein condensate of ${}^7\text{Li}$ to form matter wave solitons in a one-dimensional (1D) optical trap. By changing the interactions from repulsive to attractive, the condensate is observed to form a multi-soliton “train” of up to 15 individual solitons, each of which is a Bose-Einstein condensate. The soliton train is set in motion by displacing it from the center of the harmonic trapping potential and releasing it. The solitons are observed to maintain their size and shape for a propagation time of up to 3 s. The train forms with alternating phase between nearest neighbors. This phase structure gives rise to a repulsive interaction between neighboring solitons, whose effect can be seen in their relative motion. The number of solitons produced is observed to increase linearly with the initial velocity of the condensate, which we ascribe to the phase-gradient imposed upon the condensate by its motion. We are also pursuing the possibility of creating Cooper pairs of fermionic ${}^6\text{Li}$ atoms, the atom analog of superconductivity. Our scheme for doing this involves many of the experimental ingredients of the soliton demonstration. Specifically, the formation of Cooper pairs relies on tuning the interactions between ${}^6\text{Li}$ atoms to strongly attractive using a magnetically-tuned Feshbach resonance.

Introduction

Lithium is an attractive atom for investigations of the effects of quantum statistics because its two naturally occurring isotopes, ${}^6\text{Li}$ and ${}^7\text{Li}$, have opposite exchange symmetry. Since ${}^6\text{Li}$ is composed of an odd number of spin- $1/2$ particles (3 electrons, 3 protons, 3 neutrons), it is itself a half-integer composite particle obeying Fermi-Dirac statistics. On the other hand, because of its extra neutron, ${}^7\text{Li}$ is a composite boson. The phenomena exhibited by each isotope, therefore, should be vastly different at ultra-low temperatures, where effects of quantum degeneracy are manifested. For example, we have shown that ${}^7\text{Li}$ undergoes Bose-Einstein condensation (BEC) [1], the paradigm of all quantum statistical phase transitions. Although fermions cannot directly Bose condense, it is well known that fermions can undergo a BEC-like phase transition in which particles form Cooper pairs. This effect is responsible for electronic superconductivity and for superfluidity of ${}^3\text{He}$.

In this paper, we describe two recent experiments with ultracold lithium atoms. These are the observations of Fermi pressure in a gas of fermionic ${}^6\text{Li}$ [2] and the formation and propagation

of matter wave solitons made from Bose-Einstein condensates of ^7Li .

Fermi Pressure in a Gas of Trapped Atoms

The creation of a Fermi superfluid from ultracold trapped atoms, requires that the atoms be cooled significantly below their Fermi temperature T_F [3]. For the same number of atoms of approximately the same mass, $T_F \approx 2T_c$, where T_c is the critical temperature for BEC. However, one of the main methods used to achieve BEC in traps, evaporative cooling, does not directly work for fermions. This is because the Pauli Exclusion Principle does not allow identical fermions to undergo s -wave interactions. P -wave interactions are allowed, but are very weak at the ultralow energies involved. In our experiment, we get around this difficulty by using ^7Li atoms to “sympathetically” cool the ^6Li [2]. A mixture of both isotopes is laser slowed using the Zeeman slower technique and loaded into a magneto-optical trap (MOT). These atoms are then transferred to a pure magnetic trap made from electro-magnetic coils. The ^7Li atoms are directly evaporated as usual, while the ^6Li atoms are cooled by contact with the ^7Li .

Three pairs of images of the trapped atoms are shown in Fig. 1, corresponding to three

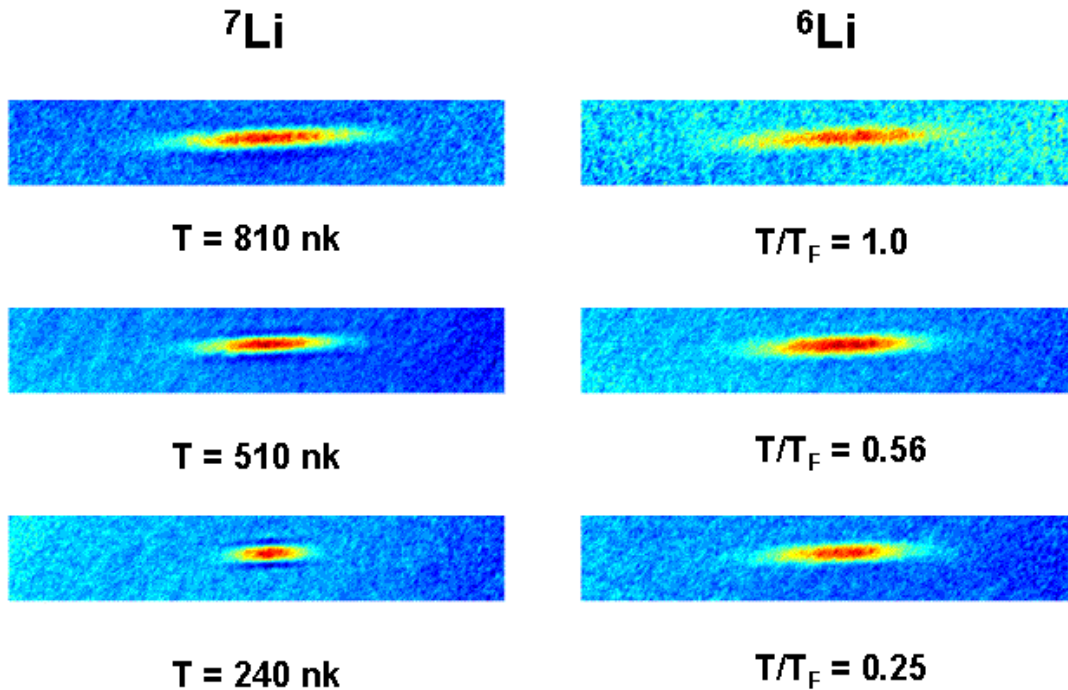


Figure 1. Images of bosons (^7Li) and fermions (^6Li). Both species are spatially overlapping and are well thermalized to each other. Each pair of images corresponds to the single temperature indicated. At the highest temperature, the bosons and fermions clouds have the same width, while at the lowest temperature, the fermion spatial distribution is distinctly larger.

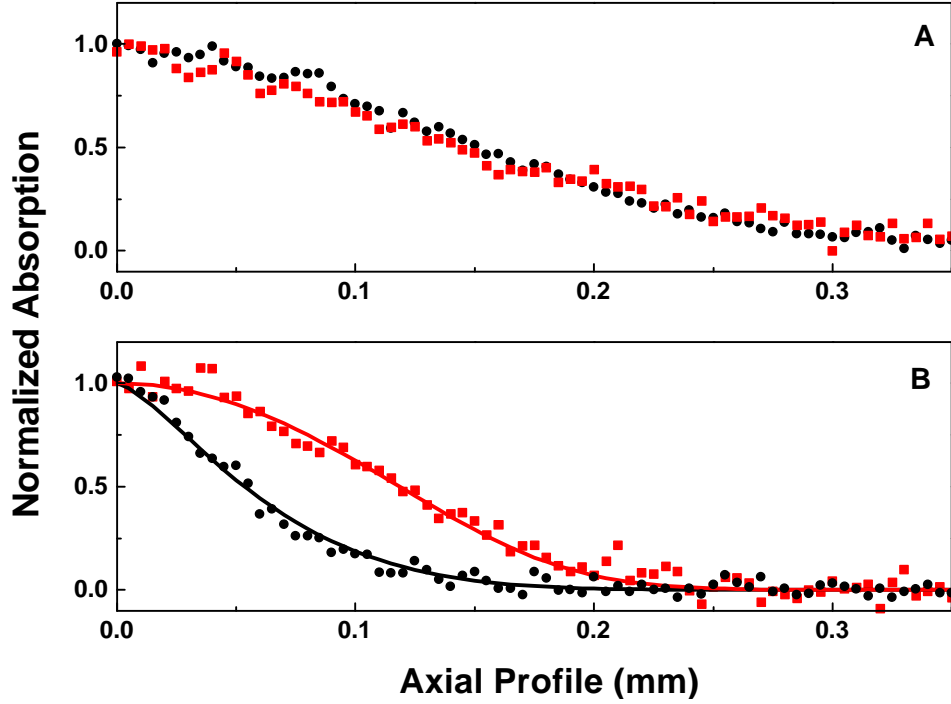


Figure 2. Comparison of ^6Li (red) and ^7Li (black) atom cloud axial profiles. (A) Data from the top image of Fig. 1, corresponding to $T/T_F = 1.0$. (B) Data from the bottom image of Fig. 1, corresponding to $T/T_F = 0.25$.

cooling cycles halted at different final temperatures. Unlike the fermions, the shape of the density distribution for bosons changes significantly as quantum degeneracy is approached. Even for temperatures somewhat above T_c , the boson distribution begins to develop a narrow central component. For this reason, the bosons prove to be a sensitive thermometer for determining the common temperature. At high temperature, where classical statistics are a good approximation, the spatial distributions should show little difference. Indeed, the upper set of images in Fig. 1, corresponding to $T/T_F = 1.0$, are nearly indistinguishable. However, in the middle set, with $T/T_F = 0.56$, the ^6Li distribution slightly broader than that of the ^7Li . In the bottom set, corresponding to $T/T_F = 0.25$, the relative broadening of the ^6Li cloud is unmistakable. In all cases, attractive interactions limit the number of ^7Li condensate atoms to a small fraction of the total number of ^7Li [4]. The ^7Li temperature, therefore, cannot go appreciably below T_c . The effect of quantum statistics on the shape and size of the clouds can readily be seen in the axial profiles for $T/T_F = 1.0$ and 0.25, respectively (Figs. 2A and B, respectively).

The square of the radius of the ^6Li clouds is plotted versus T/T_F in Fig. 3, where it can be seen that at relatively high temperatures, the radius decreases as $T^{1/2}$, as expected for a classical gas (dashed line). At a temperature near $0.5 T_F$, however, the radius is seen to deviate from the classical prediction, and at the lowest temperatures, to plateau. At $T = 0$, every trap state is singly

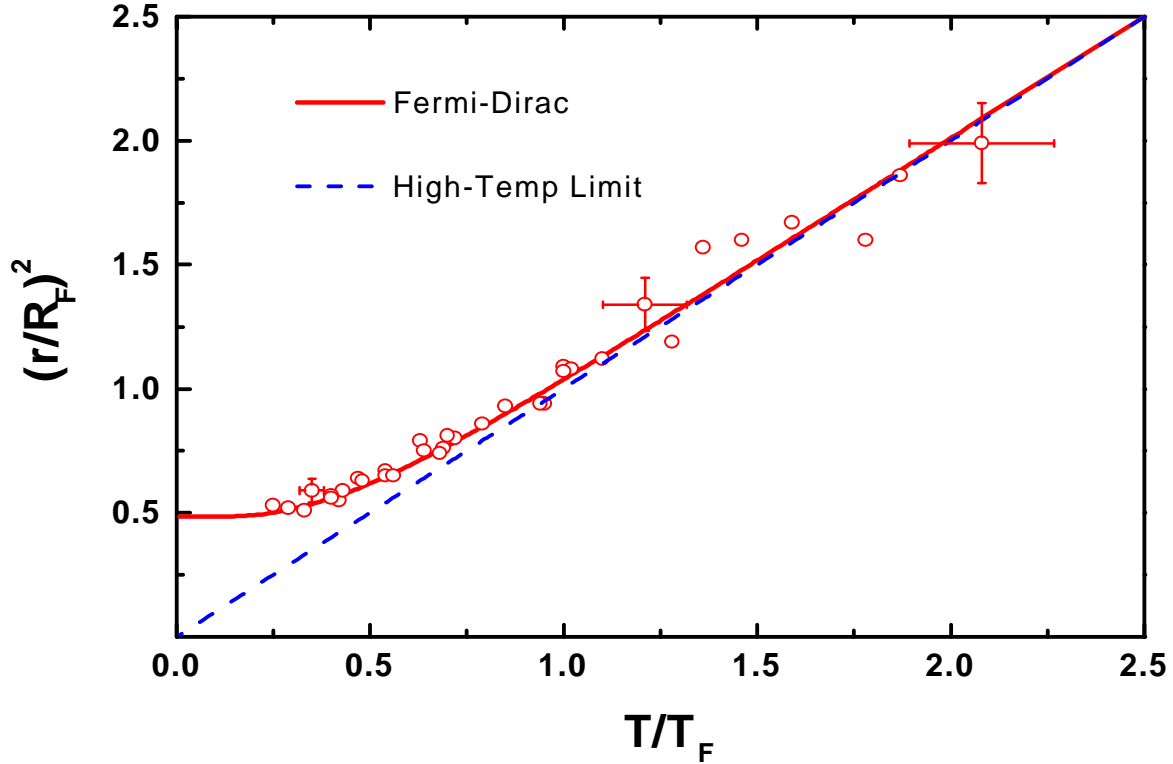


Figure 3. Square of the $1/e$ radius, r , of the ${}^6\text{Li}$ clouds vs. T/T_F . The solid line is the prediction for an ideal Fermi gas, while the dashed line is calculated assuming classical statistics. The data are shown as open circles.

occupied up to the Fermi energy, giving rise to a non-zero mean energy and a resulting Fermi pressure. Fermi pressure is responsible for the minimum radius. The same mechanism stabilizes stars made from quantum degenerate matter, white dwarf and neutron stars.

We are currently attempting to form a fermionic superfluid using ${}^6\text{Li}$ atoms. By creating a large and attractive interaction between the atoms by using a magnetically-tuned “Feshbach resonance”, we hope that the atoms will form Cooper pairs, in analogy with superfluid ${}^3\text{He}$, but in the gas phase. This would enable investigation of Cooper pairing from the weak coupling limit, where the size of the Cooper pairs is large in comparison with the mean separation between particles, to the opposite strong-coupling limit, which has yet to be achieved in any system.

Formation and Propagation of Matter Wave Soliton Trains

Bose-Einstein condensates are a manifestation of the wave property of matter and can, therefore, exhibit phenomena associated with waves. Dispersion and diffraction cause localized wave packets to spread as they propagate. Solitons are compact wave packets for which a

nonlinear interaction produces a self-focusing of the wave packet that compensates for dispersion. Such localized structures have been observed in many diverse physical systems including water waves, plasma waves, sound waves in liquid helium, particle physics and in optics. Solitons have also been previously observed in BEC's with repulsive interactions [5-7]. These “dark” solitons are localized structures, caused by the absence of atoms within a condensate. Bright solitons created from BEC's with attractive interactions, on the other hand, may propagate over much larger distances as they are themselves condensates.

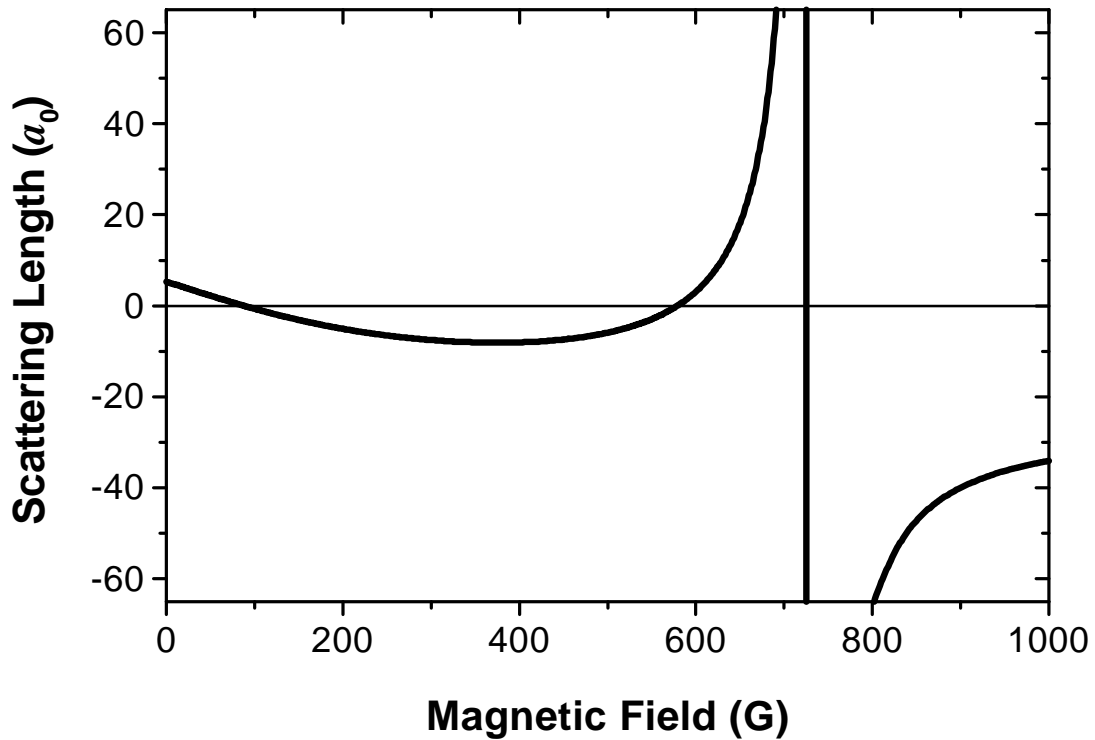


Figure 4. Calculated Feshbach resonance for ^7Li atoms in the $(1, 1)$ state.

The apparatus used in this experiment was the same as that described in the previous section and the experimental details are further described in our recent publication [8]. ^7Li atoms in the $F = 2$, $m_F = 2$ sublevel are evaporatively cooled in a magnetic trap to a temperature $T \approx 1 \mu\text{K}$. The atoms are then transferred to an optical trap made from a single focused infrared (1.06 μm) laser beam propagating in the axial direction for radial confinement, and a separated pair of cylindrically focused (532 nm) laser beams (‘end caps’) propagating in the radial plane for axial confinement. Microwave radiation is used to transfer the atoms to the $F = 1$, $m_F = 1$ sublevel.

The optical trap is necessary because atoms in this sublevel are not magnetically-trappable. Furthermore, the optical trap creates a quasi-1D confining potential with radial and axial trapping frequencies of ~ 800 Hz and ~ 4 Hz, respectively. Soliton stability requires an effective 1-D potential. The optical trap also enables a uniform magnetic field to be applied. The atoms undergo a collisional (“Feshbach”) resonance at a field of ~ 725 G, where the magnitude and sign of the collisional scattering length a can be varied (Fig. 4). A large stable condensate can be formed by tuning the field B to where a is large and positive. To form a soliton, B is reduced to where a is negative, corresponding to the required attractive interactions, but small in magnitude, in order to maximize the number of atoms that can stably form the soliton. Fig. 5 shows the inelastic losses experienced near the Feshbach resonance.

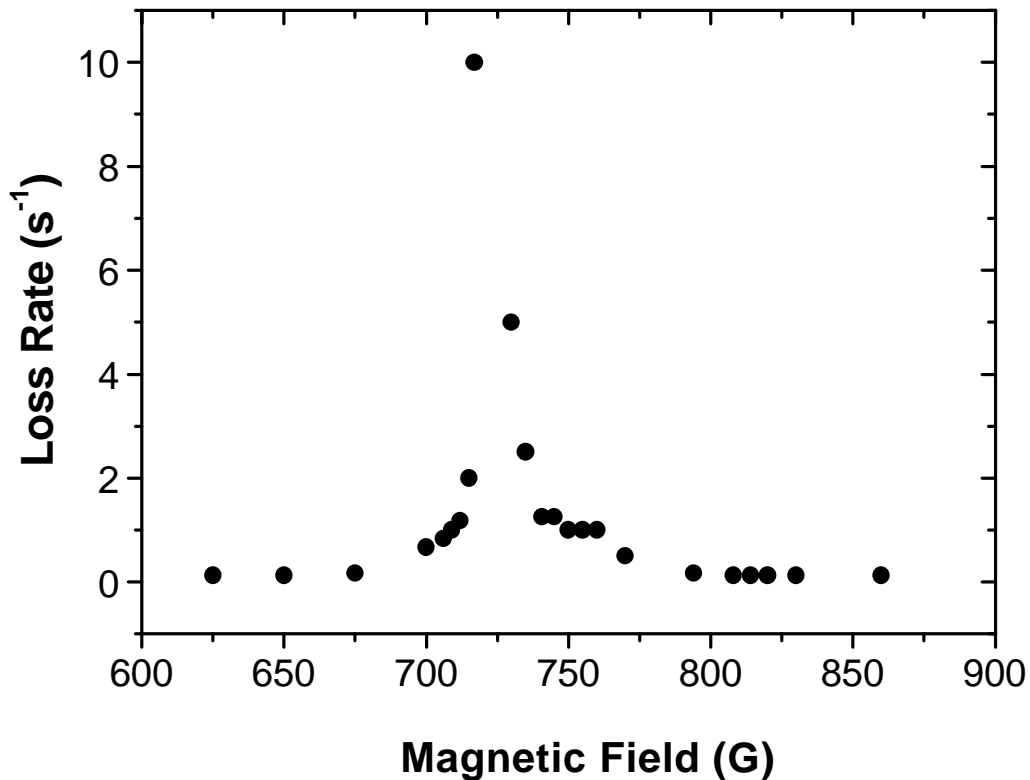


Figure 5. Measured rate of inelastic collisional loss of atoms near the Feshbach resonance.

Following the formation of the condensate, the field is ramped down to a value between 545 G and 630 G, where a is small, but either negative or positive. The condensate can be created on the side of the optical potential by axially displacing the focus of the infrared beam

relative to the centers of the magnetic trap and the box potential formed by the end caps. The end caps prevent the condensate from moving under the influence of the infrared potential until, at a certain instant, the end caps are switched off and the condensate is set in motion. The condensate is allowed to evolve for a set period of time before an image is taken. As shown in Fig. 6, the condensate spreads for $a > 0$, while for $a < 0$, non-spreading, localized structures (i.e. solitons) are formed. Solitons have been observed for times exceeding 3 s, a limitation that we believe is due to loss of atoms rather than wave-packet spreading.

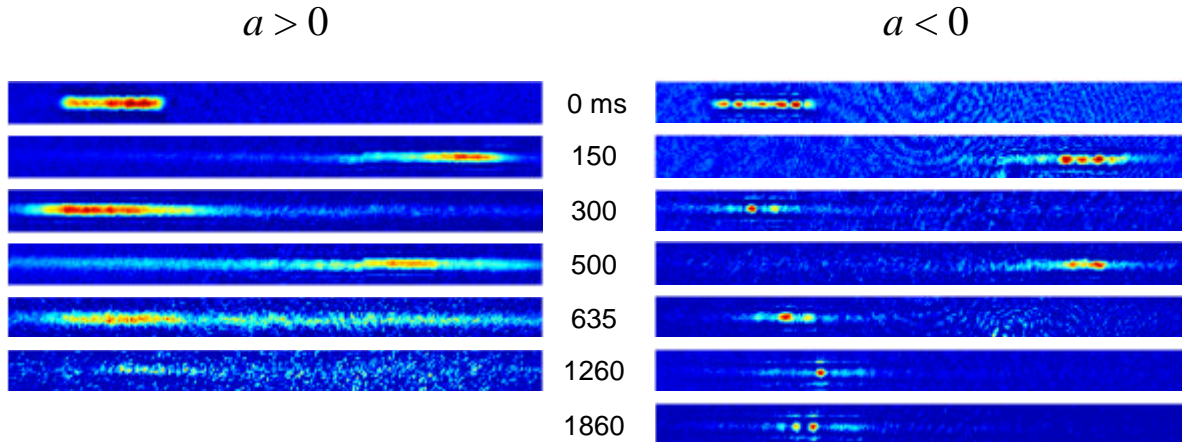


Figure 6. Comparison of propagation of repulsive condensates ($a > 0$) and atomic solitons ($a < 0$). The axial dimension of each image is 1.28 mm. The repulsive condensates quickly spread out through the potential, while the solitons propagate without spreading.

Multi-solitons (“soliton trains”) are usually observed, as is evident in Figs. 6 and 7. We find that typically 4 solitons are created from an initially stationary condensate. Although multi-soliton states with alternating phase are known to be stationary states of the nonlinear Schrödinger equation, mechanisms for their formation are diverse. It was proposed that a soliton train could be generated by a modulational instability [9], where in the case of a condensate, the maximum rate of amplitude growth occurs at a wavelength approximately equal to the condensate healing length $\xi = (8\pi n|a|)^{-1/2}$, where n is the atomic density [10]. As a and ξ are dynamically changing in the experiment, the expected number of solitons N_s is not readily estimated from a static model. Experimentally, we detect no significant difference in N_s when the time constant, τ , for changing the magnetic field is varied from 25 ms to 200 ms. The dependence of N_s on condensate velocity v is investigated by varying the interval Δt between the time the end caps are switched off to the time when a changes sign. We find that N_s increases linearly with Δt , from ~ 4

at $\Delta t = 0$ to ~ 10 at $\Delta t = 35$ ms. As the axial oscillation period is ~ 310 ms, $v \propto \Delta t$ in the range of Δt investigated.

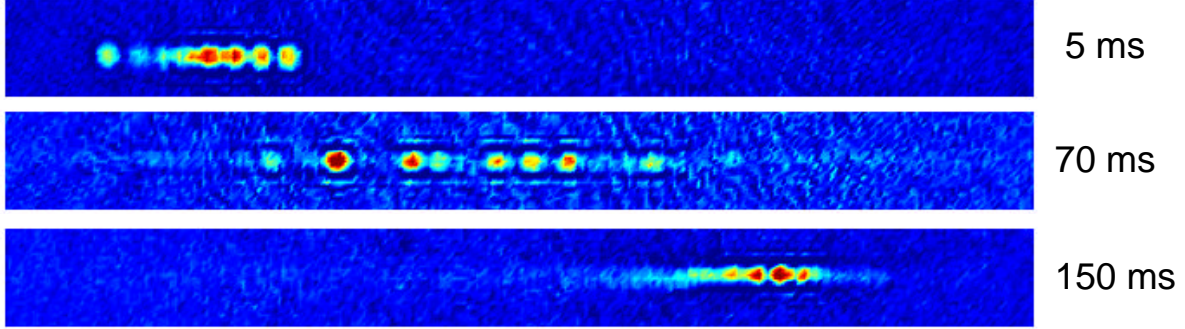


Figure 7. Repulsive interactions between solitons. The spacing between points is compressed near the turning points, and spread out near the center of oscillation.

The alternating phase structure of the soliton train can be inferred from the relative motion of the solitons. Non-interacting solitons, simultaneously released from different points in a harmonic potential, would be expected to pass through one another. However, this is not observed as can be seen from Fig. 7, which shows that the spacing between the solitons *increases* near the center of oscillation and bunches at the end points. This is evidence of a short-range repulsive force between the solitons. Interaction forces between solitons have been found to vary exponentially with the distance between them and to be attractive or repulsive depending on their relative phase [11]. Because of the effect of wave interference on the kinetic energy, solitons that differ in phase by π will repel, while those that have the same phase will attract. An alternating phase structure can be generated in the initial condensate by a phase gradient, $d\phi/dz$, across the condensate. Such a gradient may be imprinted by a condensate velocity, since $d\phi/dz = mV/\hbar$, where m is the atomic mass. If N_s is identified with ϕ/π , the model predicts $N_s \propto v$, in agreement with the observed v -dependent part of N_s . Furthermore, for the largest v and for parameters consistent with the experiment, the model gives $N_s \approx 15$, in rough agreement with observation.

For a soliton with $a = -3 a_0$, the calculated maximum number of atoms that ensures stability is only ~ 6000 per soliton [12], which accounts for far fewer atoms than the number contained in the initial repulsive condensate. Apparently, most of the atoms from the collapsing condensate are lost, while only a small fraction remain as solitons. Immediately after switching a from positive to negative we observe a diffuse background of atoms spreading out axially. This

observation is reminiscent of the jet emitted by a ^{85}Rb condensate after switching from repulsive to attractive interactions [13]. In our system, which is in the quasi-1D regime, the remnant atoms form solitons with atom number near their stability limit. Finally, a similar experiment was performed at the E.N.S. in Paris, although they observed only single solitons, rather than trains [14], presumably because the number of initial condensate atoms was more than a factor of 10 lower than used here.

The remarkable similarities between bright matter wave solitons and optical solitons in fibers underscore the intimate connection between atom optics with Bose-Einstein condensates [15] and light optics. Many issues remain to be addressed, however, including the dynamical process of soliton formation. In addition, further investigation of soliton interactions and collisions can be undertaken with this system. Finally, we speculate that an “atomic soliton laser”, based on bright matter wave solitons, may prove useful for precision measurement applications, such as atom interferometry.

Conclusions and Outlook

The opportunity to study degenerate gases is very exciting. ^6Li is particularly interesting because it is a Fermion with an enormously large attractive interaction, which may provide the means to observe a BCS phase transition to a gaseous superfluid state. Microgravity environments may be very important in ultra-cold atom experiments due to the simple fact that the gravitational potential is comparable to, or even larger than the kinetic temperature of the atoms. The effect of gravitational forces on evaporative cooling must already be considered in ground-based experiments, and may be expected to effect delicate phase transitions, such as the BCS transition of ^6Li .

The authors wish to thank the NASA Microgravity Research Division for their support of this program.

References

1. C. C. Bradley, C. A. Sackett, J. J. Tollett, and R. G. Hulet, *Phys. Rev. Lett.* **75**, 1687 (1995).
2. A. G. Truscott, K. E. Strecker, W. I. McAlexander, G. Partridge, and R. G. Hulet, *Science* **291**, 2570 (2001);
3. H. T. C. Stoof, M. Houbiers, C. A. Sackett, and R. G. Hulet, *Phys. Rev. Lett.* **76**, 10 (1996);

- M. Houbiers, R. Ferwerda, H. T. C. Stoof, W. I. McAlexander, C. A. Sackett, and R. G. Hulet, Phys. Rev. A **56**, 4864 (1997).
4. C. C. Bradley, C. A. Sackett, and R. G. Hulet, Phys. Rev. Lett. **78**, 985 (1997).
 5. S. Burger, K. Bongs, S. Dettmer, W. Ertmer, and K. Sengstock, Phys. Rev. Lett. **83**, 5198 (1999).
 6. J. Denschlag *et al.*, Science **287**, 97 (2000).
 7. B. P. Anderson *et al.*, Phys. Rev. Lett. **86**, 2926 (2001).
 8. K.E. Strecker, G.B. Partridge, A.G. Truscott, and R.G. Hulet, Nature **417**, 150 (2002).
 9. K. Tai, A. Hasegawa, and A. Tomita, Phys. Rev. Lett. **56**, 135 (1986).
 10. L. D. Carr, C. W. Clark, and W. P. Reinhardt, Phys. Rev. A **62**, 063611 (2000).
 11. J. P. Gordon, Opt. Lett. **8**, 596 (1983).
 12. V. Pérez-García, H. Michinel, and H. Herrero, Phys. Rev. A **57**, 3837 (1998).
 13. E. A. Donley *et al.*, Nature **412**, 295 (2001).
 14. L. Khaykovich *et al.*, Science **296**, 1290 (2002).
 15. G. Lenz, P. Meystre, and E. M. Wright, Phys. Rev. Lett. **71**, 3271 (1993).